Investigating Enteric Glial Cell Regulation of T-cell Directed Immune Responses During Infection and Autoimmunity

Ryan Matthew Brown
Charlottesville, VA

Bachelor of Science, University of New Mexico, 2018

A Dissertation presented to the Graduate Faculty of the University of Virginia in Candidacy for the Degree of Doctor of Philosophy

Department of Neuroscience

University of Virginia
May, 2025

Abstract

The intestine is a highly complex organ responsible for digesting and absorbing nutrients while also serving as a frontline defense against ingested pathogens and toxins. This vital function relies on a diverse array of specialized cell types working in coordination to maintain gut homeostasis. Paramount to this regulation is the enteric nervous system, a vast network of specialized neurons and glial cells that orchestrate essential physiological processes. Among these, enteric glial cells (EGCs) have emerged as key modulators of intestinal homeostasis, particularly for their critical roles in regulating immune responses.

A delicate balance in adaptive immunity is required to combat enteric infections while preventing excessive inflammatory responses that can drive autoimmunity. T cells play a pivotal role in this balance, coordinating immune responses against pathogens while also contributing to autoimmune disorders such as inflammatory bowel diseases (IBD). This underscores the need for further research into novel regulators of T cell responses in the gut.

This dissertation reviews the roles of enteric glial cells in intestinal homeostasis and disease, exploring their novel functions in adaptive immune regulation. Specifically, we investigated whether EGCs contribute to T cell activation via antigen presentation. Reanalysis of single-cell RNA sequencing datasets from IBD patients revealed an upregulation of antigen presentation machinery in EGCs during disease. Using functional antigen presentation assays with primary EGC cultures, we demonstrated their capability for MHC I-mediated antigen presentation, including antigen cross-presentation, while MHC II-mediated presentation was not observed. Additionally, employing a model of acute *Toxoplasma gondii* infection, we confirmed that EGCs upregulate MHC I expression during disease, whereas MHC II expression is limited.

Beyond enteric infections, we explored the potential role of T cell responses against EGC-derived antigens in multiple sclerosis (MS). Given that EGCs express myelin-associated antigens and that MS patients frequently experience gastrointestinal symptoms, we investigated their relevance in the experimental autoimmune encephalomyelitis (EAE) model. While we found a limited role for intestinal T cell responses in EAE, our findings suggest the potential for autoimmune targeting of ENS-derived antigens. Furthermore, we propose a novel model for selective EGC ablation to study their role in demyelinating diseases.

In summary, this dissertation highlights emerging roles for enteric glial cells in regulating adaptive immune responses within the gut. Our work provides functional evidence of EGC antigen presentation and its implications in infection and autoimmunity, raising new questions about the broader impact of enteric glial cells in intestinal immune regulation.

Acknowledgements

As I near the end of my PhD journey, I want to take a moment to reflect with a deep sense of gratitude towards all of the people who have helped get me here. It truly takes a village, and I am extremely fortunate to have encountered those who have supported me and to have been a part of such a nurturing and supportive environment in the Neuroscience Graduate Program and BIG Center over the past several years.

I want to start by thanking my PhD thesis committee, which includes Dr. Barry Condron, Dr. Tajie Harris, Dr. Ukpong Eyo, and Dr. Melanie Rutkowski. You all have provided valuable insights and feedback on my work and have always done so in a constructive and courteous manner. While I maybe didn't have as many committee meetings as I should have, I was never anxious about meeting with you all and always came out of it with a clear sense of direction and pride in my work. Dr. Eyo, you were the first lab I rotated with when I started my PhD back in 2019 and I will always appreciate the warm welcome I received from your lab and your continued support throughout my studies. Dr. Harris, I am thankful to you and your lab for helping lead my venture into the *Toxoplasma gondii* model when I felt like my project was at a crossroads. I am also thankful for all of your insightful questions and career advice, as well as gracing me with the opportunities to dog sit Hank and Jaxy. Dr. Rutkowsky, I'm thankful for your unique insights and support. And last but not least, thank you Dr. Condron for being an excellent chair. In addition to your valuable scientific and career advice, it was always great to have the company of a fellow rock climber and ultra runner.

To my PhD advisor, Dr. Alban Gaultier, thank you for your constant support and patience over the years. I've encountered plenty of hardships throughout my PhD, and you've helped me build resilience by encouraging a sense of belief in myself and pride in my work. I've grown a lot as a scientist, both in technical skills and the ability to approach a question with high level critical thinking, largely in part to mentorship I've received from you and other members of the lab. I've been grateful to always enjoy a welcoming lab environment where everyone is well integrated and eager to work as a team, and I appreciate your dedication to making sure this is the case. You've been an excellent mentor and a caring human – I will be leaving UVA with immense confidence in myself as I pursue a career as an academic scientist, and I look forward to sharing future successes with you.

To the Glab, past and present, thank you for being excellent. Becca, Courtney, and Andrea – I'm grateful to have started my PhD with such fantastic scientists and role models to look up to. It was a rocky start joining the lab right before the Covid19 pandemic, but you all did a great job getting me integrated and trained and were always available to help if I needed it. To the current generation of Tula, Stephanie, Sam, Emily, Jules, Shreyas, and Alison, thanks for providing an engaging and insightful environment. You all are a joy to be around and will be dearly missed. To my former undergraduate mentee and future med student Helen Le, it was a pleasure to have you in the lab and help guide you through your

undergraduate thesis. All of your hard work and contributions to my thesis research are deeply appreciated, as well as your kind presence in the lab.

I would be remiss not to mention my undergraduate advisor Dr. Irene Salinas, as I wouldn't be at this stage without you. After stumbling through my first couple years of college, I was looking into getting some experience doing research and you immediately took me into your lab and made me feel like I belonged. I didn't really know a career in scientific research was a possibility for me, but you showed me it was and played a tremendous part in helping me get into grad school, and I'm incredibly thankful for that. I also would like to acknowledge Dr. Aurora Kraus and Dr. Ryan Heimroth, the two of you were also monumental in getting me prepared for grad school, in addition to being amazing friends in the Salinas Lab.

To my NGP cohort – y'all are truly the best. Katriel Cho, your kindness and creativity is inspirational, and I appreciate you sharing your art with me. Kendra Liu, Kristine Zengeler, David Tyus, and Jenny Fu, I appreciate that you all are always down for tacos/margs – our venting/tea spilling sessions during Taco Tuesdays over the years were instrumental in my grad school experience. Nick Conley, our chats and chess games over the years engaged my mind on par with anything else and have helped shape the way I see myself in the world – thanks for being such a deep thinker.

David Tyus and Kristine Zengeler a.k.a. my Hash Slinging Flashers a.k.a. my Milkshake Musketeers, y'all get a second shoutout for being so awesome. You quickly became two of my closest friends and I will forever cherish all of the adventures we shared. Including (but not limited to) finding the best milkshake in Charlottesville (it was Wayside all along), Friday night climbs, and many great hikes and runs. Kristine, thank you for always being down to go explore a new bike route or share a beer and game of chess. Our newfound hobby of cycling kept me going through the pandemic and I'll always appreciate you lending an ear when I need it. David, thank you for sharing your love of music, running, and climbing with me. Some of my best memories were the trips we went on together – from my first "international" trip to Banff to running the St. Louis marathon to concerts in D.C.. The two of you kept me going when times were tough and shared so much joy all throughout grad school and I sincerely thank you for that.

To the Charlottesville running community – from all of the speedsters that show up Wednesdays at 5:30AM to run track workouts hosted by Mark Lorenzoni, to the Charlottesville Area Trail Runners (CATS), to SuperFly Run Club with Lindsey, Kristine, Nick Dunham, and Collin Dube, and everyone else I've ran with – thanks for keeping me inspired.

To my New Mexico homies, thanks for constantly uplifting me from afar and always picking back up right where we left off when I come back to visit.

To my family, thank you for all of your continued love and support. It's been tough being on the other side of the country, but I know you all are proud of the work I'm doing, and I would not be half the man I am without you all. To my mom and dad, I love you and appreciate all that you do for me. To my brothers David, Michael, and Isaiah – I'm glad I got to show you all around Charlottesville and am always thankful for a call or visit home providing the reset I need.

To my cat Jasper, you are who I do this for. Thanks for choosing me at the CASPCA on 02/15/2020 – little did I know a global pandemic was right around the corner and I couldn't have asked for a better roomie to spend lockdown with and even though you can't read this, I appreciate coming home to a warm welcome every day after lab.

Finally, thank you my PFL, Lindsey Power. The best part of grad school was meeting you and I'm so lucky to have you in my life. You always keep me grounded, and I can always count on you and Jasper to help recharge when I'm feeling low. We make a great team, and I've cherished the memories we've made, from getting momentarily lost in the wilderness from time to time, to Power family beach week at the marvelous Ocean City, Maryland, to training for (ultra)marathons together, and now frantically writing our dissertations at coffee shops around Charlottesville. Your love and support means the world to me and I'm so thrilled to continue on this journey together. Love you lots.

Table of Contents

List of Figures

Chapter 1: Introduction

1.1 Abstract

The enteric nervous system comprises an intricate network of neurons and glial cells that span the entirety of the gastrointestinal tract. Enteric glial cells are critical constituents of the enteric nervous system that work to regulate homeostatic gut function. This includes regulation of intestinal motility, epithelial barrier maintenance and repair, and sustaining neuronal health and function. Additionally, emerging roles for enteric glial cells regulating immune function are being actively investigated. This review will explore the discovery and characterization of the enteric nervous system, highlighting the essential contributions of enteric glial cells to gut function, with a focus on their immunoregulatory roles.

1.2 List of abbreviations

5-HT, 5-Hydroxytryptamine (Serotonin); 6-OHDA, 6-Hydroxydopamine; Ach, Acetylcholine; AD, Alzheimer's Disease; ASD, Autism Spectrum Disorder; ATP, Adenosine Triphosphate; CCK, Cholecystokinin; CGRP, Calcitonin Gene-Related Peptide; ChAT, Choline Acetyltransferase; CNP, 2'-3'-Cyclic Nucleotide 3'-Phosphodiesterase; CNS, Central Nervous System; Cx43, Connexin-43; DRG, Dorsal Root Ganglion; DSS, Dextran Sodium Sulfate; DTA, Diphtheria Toxin subunit A; EEC, Enteroendocrine Cell; EGC, Enteric Glial Cell; ENCC, Enteric Neural Crest Cell; ENS, Enteric Nervous System; EPSP, Excitatory Postsynaptic Potential; FACS, Fluorescence Activated Cell Sorting; FFAR, Free Fatty Acid Receptor; GDNF, Glial Derived Neurotrophic Factor; GFAP, Glial Fibrillary Acidic Protein; GFL, GDNF-Family Ligand; GI, Gastrointestinal; GLP, Glucagon-like Peptide; GSNO, S-nitrosoglutathione; IBD, Inflammatory Bowel Disease; IEC, Intestinal Epithelial Cell; IGLE, Intraganglionic Laminar Ending; ILC3, Type 3 Innate Lymphoid Cell; iNOS, Inducible Nitric Oxide Synthase; IPAN, Intrinsic Primary Afferent Neuron; ISC, Intestinal Stem Cell; MADM, Mosaic Analysis with Double Markers; MBP, Myelin Basic Protein; MIA, Maternal Immune Activation; MMC, Migrating Myoelectric Complex; MP, Myenteric Plexus; MS, Multiple Sclerosis; NANC, Non-adrenergic, Non-cholinergic; NCC, Neural Crest Cell; NO, Nitric Oxide; NOS, Nitric Oxide Synthase; NPY, Neuropeptide Y; PACAP, Pituitary Adenylate Cyclase-activating Polypeptide; PD, Parkinson's Disease; PLP1, Proteolipid Protein 1; PYY, Peptide YY; RAGE, Receptor for Advanced Glycation End-products; SMP, Submucosal Plexus; SOM, Somatostatin; TK, Tachykinin; TRP, Transient Receptor Potential; VIP, Vasoactive Intestinal Peptide; WNV, West Nile Virus

1.3 Preface

The Enteric Nervous System (ENS) is composed of a vast network of neurons and glia that work together to coordinate a variety of functions including control of gut motility[1], regulation of fluid movement between the gut lumen and body fluid compartments[2], controlling gastric acid secretion[3] and contributing to mucosal barrier immunity[4,5]. It is estimated that there are 200-600 million neurons in the human ENS[6]. The ENS is unique in the sense that intrinsic circuits are able to control gut motility without input from the Central Nervous System (CNS). In this regard, the ENS has been referred to as the "First Brain" evolutionarily, as a functional ENS is observed in Cnidarians, Echinoderms, and Hemichordates- all of which do not have a conventional CNS[7]. Still, many extrinsic circuits exist within the gastrointestinal (GI) tract to communicate with the brain, largely accomplished through the vagus nerve. These extrinsic circuits influence and are influenced by local ENS activity to facilitate bidirectional gut-brain communication.

Enteric glial cells (EGCs) are critical constituents of these bidirectional networks, as they are estimated outnumber neurons 7:1 in the human myenteric plexus (MP), whereas they are present at a 1:1 ratio in the mouse myenteric plexus[8,9]. EGCs are observed throughout the intestine where they aggregate in the ganglionated plexuses- which are the myenteric plexus and submucosal plexus (SMP) (Figure 1.1). EGCs are frequently observed covering nerve fibers adjoining ganglia, as well as in close association with nerve endings in the submucosa. These cells were initially identified as Schwann Cells, until extensive ultrastructural characterization by Giorgio Gabella showed they represent a unique cell type in the gut[10].

In the time since enteric glia were classified by Gabella, studies on the putative function of these cells have started to emerge. It is widely supported that EGCs are key players in controlling gut motility[11,12]. In addition, EGCs have been attributed to epithelial barrier maintenance[13] and regulating intestinal immunity[5,15,16], all of which will be discussed in detail further below. Together, these findings suggest that EGCs represent a key player in gut health and merit further research characterizing their functions and potential as therapeutic targets in GI disorders such as Inflammatory Bowel Diseases (IBDs), in addition to potential roles as mediators in bidirectional gut-brain communication. The goal of this review is to describe what is currently known about enteric glia, the current limitation of our knowledge, and to discuss future questions that the research community should address to complete our understanding of the function of enteric glia.

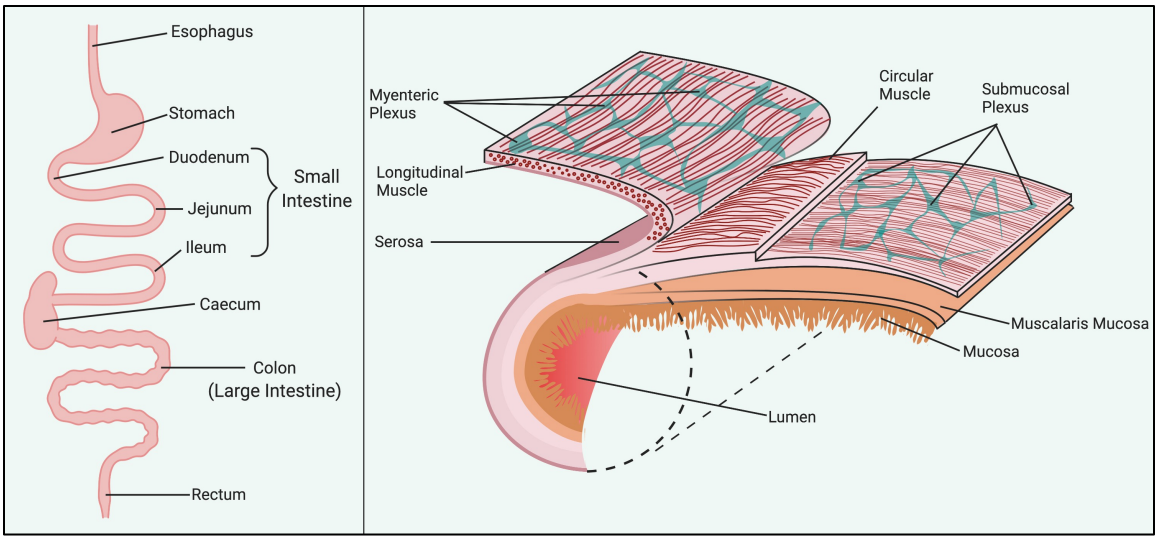

Figure 1.1 Anatomy of the gastrointestinal tract

A simplified schematic of the mouse GI tract. ***Left:*** Compartments of the GI tract from esophagus to rectum. ***Right:*** Layers of the intestinal wall, including the ganglionated plexuses where a vast majority of the ENS is located. *Created with BioRender.com*

1.4 History

The influence of the gut on health and disease has long been pondered. It was Hippocrates who is credited with the phrase "All disease begins in the gut", which has remained a prominent idea in the biomedical sciences. The notion that the gut influences the central nervous system and vice versa has long been appreciated and is now commonly referred to as the gut-brain axis. In 1765, Scottish Physician Robert Whytt published a book in which he writes on "the sympathy of the nerves", describing the connectivity of sensible parts of the body, particularly the internal organs[17]. On the stomach and intestines, he writes, "A disordered state of the stomach and intestines ... will sometimes so affect the brain." This concept was further explored by the English surgeon John Abernathy. He published a book detailing a number of medical cases he had attended to, insinuating that the gut is connected to a vast array of disease and disorders[18]. Abernathy writes on the gut-brain axis, stating "But derangement of the digestive organ arises, in many cases, from established nervous disorder: indeed, there is often reason to suppose that it is dependent on, or connected with, actual disease of the brain." Despite these speculations on the gut being implicated in "nervous disorder", little was known at the time about how these communications may occur.

In the mid 19th century, German anatomist and neuropathologist Leopold Aurbach discovered a layer of ganglion cells within the gut wall which he called the *Plexus myentericus Aurbachi*, today referred to as the myenteric plexus. Not long after, another German anatomist, Georg Meissner described ganglia within the level of the submucosa, which he called *Meissner's plexus*, though today it is commonly

referred to simply as the submucosal plexus. Near the dawn of the 20th century, interest in the ENS accrued as Bayless and Starling demonstrated that peristaltic waves can be generated in isolated dog intestine "independent of connections of the gut with the CNS." They described peristalsis in what they called the *law of the intestine* which states "Local stimulation of the gut produces excitation above and inhibition below the excited spot. These effects are dependent on activity of the local nervous mechanism."[19,20].

Around this same time, the first known description of glia in the ENS came from Russian anatomist and physician Alexander Dogiel in 1899[21]. Over the next few decades, limitations in staining methods would not allow for further characterization of this cell type (Figure 1.2). In the 1950's, Phillipp Stöhr Jr. utilized the Bielschowsky silver staining technique, an improvement on the method developed by Ramon y Cajal, to consistently label glial cells which he described as "Schwann cell nuclei"[22]. This description remained until the 1970s when Giorgio Gabella used electron microscopy to provide a detailed analysis of structures within the guinea pig myenteric ganglia[23]. Here, he describes distinguishing features of glial cells within ganglia, including irregular shape and dynamic processes, which had not been previously observed. Importantly, he also noted that no myelin sheaths were observed. In a later study, Gabella expanded his electron microscopy analysis to multiple mammalian species (rat, guinea pig, cat, rabbit, and sheep) to provide a deep ultrastructural analysis of glia in the enteric plexuses[10]. In this seminal work, Gabella coined the term Enteric Glia. He noted that enteric glia provide a partial sheath to groups of ganglionic neurons but rarely sheathed around an individual neurite. On the significance of these cells, Gabella speculated a role in protecting neurons from the "severe mechanical stresses imposed by the contractile activity of the gut wall."

Following their classification as a unique cell type, enteric glia received little attention over the next couple of decades, largely due to limitations in technology and a lack of a known unique molecular marker that defines this lineage. Several studies in the 21st century have begun to characterize enteric glia and explore their functional relevance in disease states, though this is still a nascent field that largely remains to be explored.

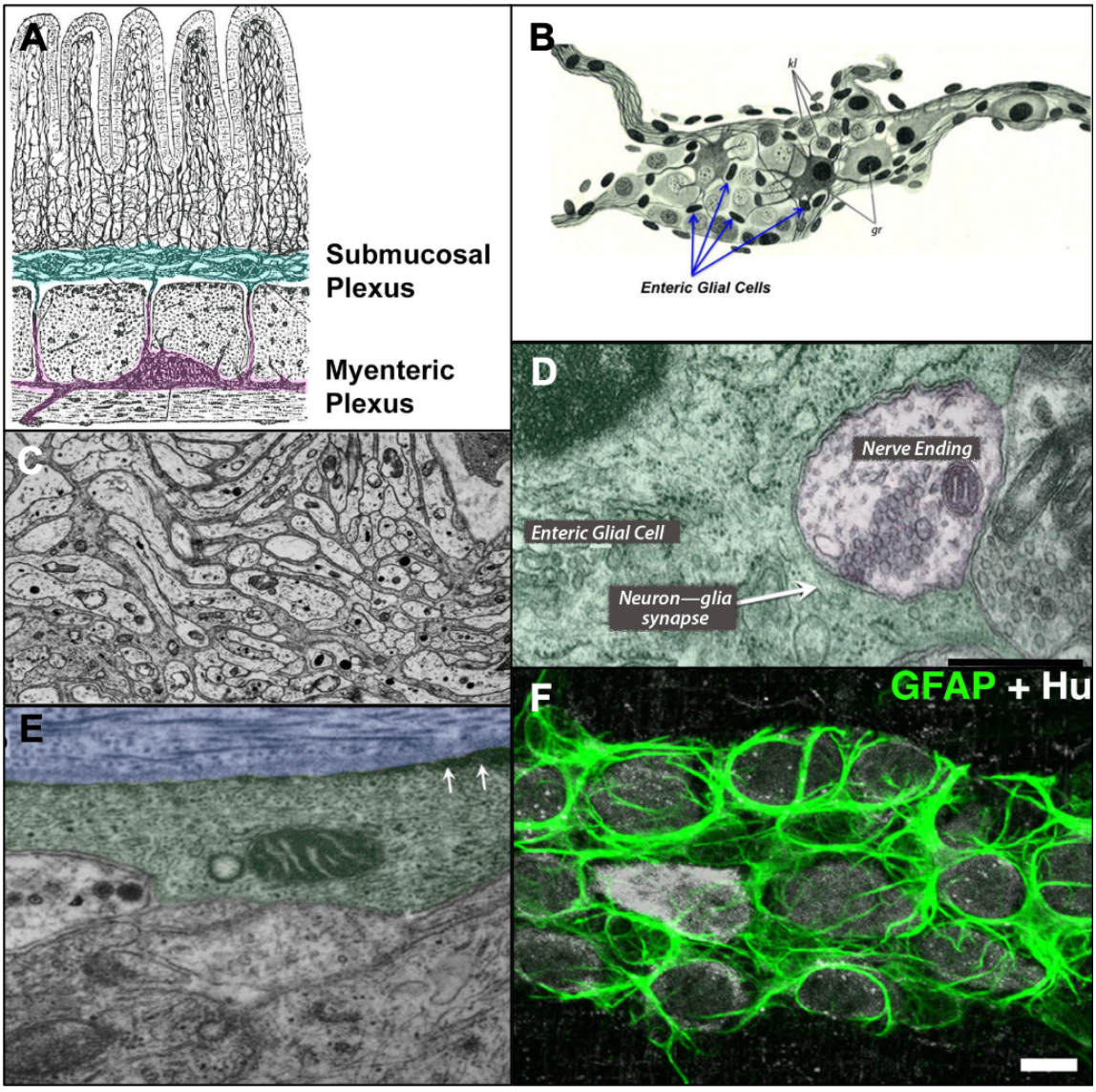

Figure 1.2 Enteric glia ultrastructural characterization

A: Drawing of intestinal cross section, with emphasis on the ganglionated plexuses. Modified from the original by Ramon y Cajal[24]. ***B:*** Beilschowsky staining method utilized by Stöhr in the rabbit small intestine[22]. This method labels cell bodies of enteric neurons, labeled 'gr' (grobe ganglienzellen "coarse/large ganglion cells") and 'kl' (kleine ganglienzellen "small ganglion cells"). However, only the nuclei of glia are labeled, which Stöhr referred to as "Schwann cell nuclei". ***C:*** Electron micrograph of ganglion in the MP of a rhesus monkey[25]. EGCs are identified by their dense cytoplasm, and do not wrap individual neurons – instead they compartmentalize large groups of unmyelinated nerve processes. ***D:*** Electron micrograph modified from Gabella[23] depicting neuron glia synapse. Scale bar = 0.5 µm. ***E:*** Electron micrograph modified from Gabella[23] depicting an EGC (green) at the outer edge of a ganglion, contacting collagen fibrils (blue) surrounding it. Arrows point to dense region where gliofilaments are attached. ***F:*** Immunofluorescence image of GFAP+ EGCs (green) ensheathing enteric neuron cell bodies (grey) in the mouse colon MP, from Gulbransen[26]. Scale bar = 20 µm.

Images from 'Enteric Glia'[26] *(original publications cited)*

1.5 Development of the Enteric Nervous System

Neurons and glia of the ENS arise from common neural crest derived progenitors. Entry of neural crest cells (NCCs) into the foregut occurs as early as 36 hours post fertilization in zebrafish[27], embryonic day 9.5 in mouse[28], and by week 4 of gestation in humans[29]. Most of the ENS is derived from neural crest cells originating from the vagal crest (somites 1-7 in mouse), while the sacral crest (caudal to somite 28 in mouse) contributes to approximately 20% of ENS cells[30–32]. Within the vagal crest, there appear to be compartments that seed specific regions of the GI tract, demonstrated by replacing segments of the vagal crest in the chick embryo with those from age matched quail embryo. These studies suggest that somites 1-2 primarily seed the esophagus while 3-7 seed the stomach and intestines[33]. Vagal derived NCCs ectopically placed in the sacral crest have been shown to colonize the gut more effectively than native sacral crest cells, demonstrating that differences in capability to seed the gut between these two cell types are cell intrinsic[34]. This is likely due to the fact that NCCs in the vagal crest do not express roundabout (ROBO) while those in the sacral crest do – as ROBO drives repulsive interactions to SLIT2, which is highly expressed in the foregut[35]. Furthermore, it has recently been established that a subset of Schwann cell precursors have been observed to migrate alongside the leading edge of vagal extrinsic nerve fibers innervating the gut where they transdifferentiate contributing to another 20% of ENS cells[36]. Whether these different sources of ENS progenitors serve to contribute to the heterogeneity observed in enteric neurons and glia remains to be studied.

Migrating NCCs are multipotent and signals within the microenvironment where they exit the neural tube largely determine their developmental potential. NCCs that go on to make up the ENS migrate ventrally into the mesoderm which locally produces retinoic acid. This signals through various retinoic acid receptors expressed by NCCs to drive expression of the receptor tyrosine kinase RET, which is critical for ENS cell development as it influences multiple facets including cell proliferation, differentiation, migration, and survival[37]. RET is activated by Glial Derived Neurotropic Factor (GDNF), which leads to its phosphorylation and activation of downstream signaling pathways including MAPK, JNK, and PI3K[38]. Upon entering the gut and gaining RET expression, these neural crest cells are then referred to as Enteric Neural Crest-derived Cells (ENCCs). The transcription factors SOX10 and PHOX2B are both required for RET activation, and their expression patterns determine ENS cell differentiation. These transcription factors both suppress one another, so that differentiation into enteric neurons requires maintaining PHOX2B (and RET), while turning off SOX10[39,40]. Conversely, differentiation into enteric glia requires maintaining SOX10 while turning off PHOX2B and RET[41].

In addition to migrating distally along the length of the GI tract, ENS cells must migrate radially extending into the submucosa. ENS development follows an outside- in pattern, where the myenteric plexus is formed before the submucosal

plexus, as demonstrated by pulse-chase experiments[42]. An elegant lineage tracing model was employed to examine the developmental potential of ENCCs[43]. In this study, the authors drove inducible expression of the *Rosa26Confetti* reporter in SOX10+ cells at E12.5 and analyzed 24 to 72 hours later. This allowed for labeling of distinctive clonal populations of ENCCs as they proliferate and differentiate into neurons and glia. They observed three distinctive types of clonal populations – those which contained only neurons (smallest fraction), those that contained both neurons and glia, and those that contained only glia (largest fraction). This suggests that ENCCs include bipotential progenitors, as well as fate-restricted neurogenic and gliogenic precursors. Importantly, clonal populations extended radially, spanning from the myenteric plexus into the mucosa and were organized into discrete columns. Interestingly, neuron-only clonal populations were restricted to the myenteric plexus, while glia-only and neuroglia clonal populations were frequently observed in both the submucosal and myenteric plexus. In the latter case, neurons/glia observed in the submucosal plexus always corresponded with clones present in the myenteric plexus, further supporting the outside-in model of development.

NCC migration, proliferation, and differentiation must be tightly regulated as to ensure functional neuronal circuits cover the entirety of the GI tract. Numerous other factors contribute to these processes which are not discussed in the current review but have been extensively reviewed elsewhere[44,45]. It is important to mention that the development of the ENS continues postnatally, with extensive neurogenesis occurring in mice up until P21[42]. Additionally, the time at which enteric neurons exit from the cell cycle influences their phenotype[45]. This contributes to the well- recognized diversity of enteric neurons, which will be discussed further in the next section.

1.6 Diversity and Function of Enteric Neurons

Neuronal control of gastrointestinal function is attributed to integration of signals from the local ENS, sympathetic inputs from the CNS, feedback loops that originate in the gut and signal through the CNS (vago-vagal reflexes), as well as entero-enteric reflexes that mediate communication between different parts of the digestive tract. The extent to which each of these neural pathways contribute to the control of gastrointestinal muscles varies by region. Most of the contractile forces in the esophagus and stomach are generated by CNS activity[46], though an extensive ENS component is still observed here and remains crucial for processes such as limiting gastric reflux through controlling the pyloric sphincter[47]. Despite this, the focus of this paper will be on functions of the small and large intestines, in which GI motility is by and large controlled by the local ENS through a diverse repertoire of neurons and glia.

1.6.1 Diversity of Enteric Neurons

Diversity among enteric neurons was observed immediately upon Dogiel's initial studies characterizing the ENS. He characterized intrinsic enteric neurons based on their morphology, separating them into three categories, which he distinguished as types I, II, and III respectively[21]. Dogiel type I neurons were described as unipolar with a single long axon which can span multiple ganglia. The cell bodies of type I neurons have a stellate morphology with numerous short, flattened dendrites, and are frequently observed within ganglia in the MP. Dogiel type II neurons are the most common type observed in the MP accounting for 10-25% of enteric neurons. These are multipolar/pseudounipolar neurons with a large cell body and multiple long axons that primarily project circumferentially, with some projections into the submucosa. Dogiel type III neurons were described as having few short dendrites that thin as they extend away from the soma. Thick axons were described, though they could not be followed to their terminals. Type III neurons were described in the Guinea Pig but have not been definitively observed in the human or mouse intestine.

More recently, the classification of enteric neurons and the circuits they make up have been expanded upon. Generally speaking, enteric neurons can be distinguished as Intrinsic Primary Afferent Neurons (IPANs), excitatory/inhibitory motor neurons, ascending/descending interneurons, and intestinofugal neurons. Dogiel type I neurons can fall into either of the first three categories, while type II neurons are largely IPANs. These divisions have been characterized based on cell morphology, neurotransmitter content, and functional properties (Table 1).

Type of neuron	Primary transmitter	Secondary transmitters, modulators	Functional properties
Intrinsic Primary Afferent Neuron	ACh, TK, CGRP	ND	Mechanosensitive, fast EPSPs to second order neurons, slow EPSPs to other IPANs
Ascending Interneuron	ACh	ATP, TK	Distal to proximal transmission from IPANs to motor neurons
ChAT/NOS Descending Interneuron	ACh, ATP	Nitric Oxide	Proximal to distal transmission from IPANs to inhibitory motor neurons
ChAT/5-HT Descending Interneuron	ACh	5-HT, ATP	Proximal to distal transmission from IPANs to excitatory motor neurons
ChAT/SOM Descending Interneuron	ACh	Somatostatin	Involved in generating the migrating myoelectric complex
Excitatory Motor Neuron	ACh	TK, enkephalin	Control gut motility
Inhibitory Motor Neuron	Nitric Oxide	VIP, ATP	Control gut motility
Noncholinergic Secretomotor Neuron	VIP	PACAP, NPY	Regulate fluid secretion into intestines, vasodilation
Cholinergic Secretomotor Neuron	ACh	ND	Regulate fluid secretion into intestines, vasodilation
Intestinofugal Neuron	ACh	VIP	Relay sensory information from gut to prevertebral ganglia

Table 1.1 Diversity of enteric neurons

The major defined classes of intrinsic enteric-associated neurons within the ENS, the neurotransmitters each is known to express, and a brief description of their function.

Table modified from 'The enteric nervous system and neurogastroenterology'[2]

Intrinsic Primary Afferent Neurons

IPANs are a class of neurons that monitor the state of the tissue they innervate by detecting chemical and mechanical stimuli and conveying this information to enteric circuits that work to maintain proper functional states. Though these are sometimes referred to as intrinsic 'sensory' neurons, it is important to note that their activation does not actually evoke sensation – thus they were described as afferents as they are the first neurons in enteric reflex circuits. It has been long been postulated that IPANs exist in the intestine, as early studies demonstrated reflexes to stimuli in the absence of any CNS connections[19,20]`. In fact, when Dogiel described type II neurons, he speculated that they are 'sensory' neurons, though their characterization wouldn't be realized until nearly a century later.

IPANs were first discovered through retrograde tracing experiments showing neurons in the SMP contain projections into the MP[48]. Submucosal IPANs are activated in response to mechanical distortion of the mucosa as well as a variety of chemical stimuli including but not limited to changes in pH, short-chain fatty acids, cholera toxin, and serotonin[49–51]. IPANs form excitatory synaptic connections with interneurons and motor neurons, as well as other IPANs[52,53]. Synaptic connections with second order neurons are descending and elicit fast EPSPs, which have been shown to be mediated by acetylcholine as well as ATP[54,55]. Meanwhile, self-reinforcing networks with other IPANs are mediated by slow G-protein coupled transmission through the release of tachykinins and acetylcholine[56,57]. Importantly, IPANs have been shown to be affected by a variety of inflammatory mediators, all of which increase excitability[58]. This suggests that IPANs might provide a therapeutic target for neuropathies such as IBDs.

Interneurons

Interneurons form connected chains in the MP directed both anally (descending) and orally (ascending). In the guinea pig small intestine, there are three classes of descending interneurons and one class of ascending interneurons[59]. The ascending interneurons are cholinergic, as they express Choline Acetyltransferase (ChAT). They also express calretinin which can be used as an identifying marker[60]. Ascending interneurons are involved in local motility reflexes, as they receive input from IPANs as well as other interneurons and synapse onto motor neurons[61,62]. The descending interneurons are also cholinergic, though blocking cholinergic signaling only partially blocks synaptic transmission, suggesting other mediators, particularly ATP, are involved[63]. In the guinea pig small intestine, the classes of descending interneurons are those immunoreactive for ChAT and nitric oxide synthase (ChAT/NOS), those reactive for ChAT and serotonin (ChAT/5-HT), and those reactive for ChAT and somatostatin (ChAT/SOM). ChAT/NOS neurons are likely to be involved in local inhibitory reflexes, as they synapse onto inhibitory motor neurons[64]. Meanwhile, ChAT/5-HT neurons are involved in the descending excitatory reflex pathway[65]. The ChAT/SOM population is thought to be involved in the

Migrating Myoelectric Complex (MMC), which is a cyclical pattern of neuronal activity that traverses the stomach and small intestine which facilitates peristalsis[66].

Motor Neurons

Excitatory and inhibitory motor neurons project to the circular and longitudinal muscle throughout the gastrointestinal tract. These are Dogiel Type I neurons primarily residing in the MP, though some contribution from neurons in the outer SMP is observed in larger mammals[67]. Excitatory motor neurons signal through choline as well as tachykinins[60,68]. Inhibitory motor neurons use multiple neurotransmitters including NOS, vasoactive intestinal peptide (VIP), and ATP[69,70]. Innervation of the circular muscle occurs locally throughout the length of the intestine. Excitatory motor neurons generally project a few millimeters orally while inhibitory motor neurons project a few millimeters anally, in accordance with the law of the intestine[71]. Motor neurons receive signals from IPANs and interneurons to coordinate local reflex circuits.

While motor neurons in the musculature account for generating motility patterns, those in the submucosa serve other key functions in the gut including controlling fluid exchange and vasodilation. Fluid movement across the intestinal epithelium must be tightly regulated as toxic molecules traversing the epithelium pose the risk of septic shock. Nutrient absorption is coupled to water movement across the epithelium into the interstitium – the absorption of carbohydrates and amino acids occurs through cation-coupled transporters, which cotransport Na+ and H_2O, account for the majority of water absorption[72]. In addition to absorption, large amounts of water and electrolytes are secreted into the intestine to maintain ionic balance and aide in digestion, and secretion is largely influenced by secretomotor neurons in the SMP. Water and electrolytes secreted into the lumen are drawn from the interstitium which in itself is derived from absorbed and circulatory fluids. As such, secretomotor neurons also influence local blood pressure to aide in secretion. Multiple classes of secretomotor/vasodilator neurons have been identified in the guinea pig, distinguished by their neurotransmitter content[73]. Two subsets of SMP motor neurons innervate both mucosal glands and submucosal arterioles and thus likely function in regulating secretion and blood vessel contractility. One of these subsets are non-cholinergic, VIP containing neurons, while the other subset is cholinergic and expresses calretinin. An additional subset has been observed which is also cholinergic and expresses neuropeptide Y (NPY). Secretomotor/vasodilator neurons act locally, with retrograde tracing studies demonstrating they project less than 1 mm along the gut in the guinea pig and 3-4 mm in human[74,75].

Intestinofugal Neurons

Intestinofugal neurons are those which have cell bodies in the gut wall (mostly MP) sending projections to prevertebral ganglia where they synapse onto inhibitory motor neurons. These neurons are cholinergic expressing ChAT as well as VIP and are responsible for entero-enteric reflexes. Intestinofugal neurons respond to distention of the intestine, resulting in fast EPSPs in prevertebral ganglia neurons and inhibition of more proximal regions[76]. Spontaneous activation of prevertebral ganglia neurons by intestinofugal neurons has been observed, which is lost upon blocking synaptic transmission in the gut[76–78]. This suggests that intestinofugal neurons are second order, likely excited by IPANs. However, upon intestinal distention EPSPs in prevertebral ganglia are reduced but not entirely eliminated with blocking synaptic transmission in the gut[76,78], suggesting intestinofugal neurons can also be independently activated by mechanical distortion. Considering all intestinofugal neurons have similar properties and receive fast EPSPs[79], it is suggested that one population exists that has first and second order properties. Recently, it has been demonstrated that intestinofugal neurons sense the presence of a microbiota and communicate this information to other visceral organs via monosynaptic connections through prevertebral ganglia in order to regulate blood glucose[80].

Interstitial Cells of Cajal

Interstitial Cells of Cajal (ICC), originally identified by Ramon y Cajal, are non-neuronal excitable cells that are imposed between the endings of motor neurons and muscle within the GI tract[81]. These serve important roles in transducing excitatory and inhibitory electrical signals from motor neurons to smooth muscle cells. ICC receive input from motor neurons through receptors for excitatory and inhibitory neurotransmitters used by motor neurons, generating an electric potential that is propagated to smooth muscle cells (and other ICC) through gap junctions. ICC have been shown to act as pacemakers as, unlike smooth muscle cells, they are able to generate spontaneous depolarizing events to control rhythmic activity in the jejunum, ileum, and proximal colon[82].

1.6.2 Extrinsic Nerve Endings in the Gut

As mentioned, there are numerous extrinsic nerve endings in the gut that act to convey motor and sensory information between the CNS and ENS. While the ENS can independently control intestinal motility, input from the CNS provides an additional layer of gut function regulation. These include sympathetic and parasympathetic efferent nerve fibers that modulate gut reflexes, as well as afferents that integrate sensory information to the brain and spinal cord. The major extrinsic pathways connecting the CNS and ENS are detailed in Figure 1.3 (adapted from Spencer and Hu, 2020[83]). The sympathetic nervous system enacts inhibitory effects on GI muscle, while also influencing gut blood flow, epithelial transport, and

endocrine signaling. Meanwhile, the parasympathetic nervous systems enacts both excitatory and inhibitory control over intestinal tone and motility[84]

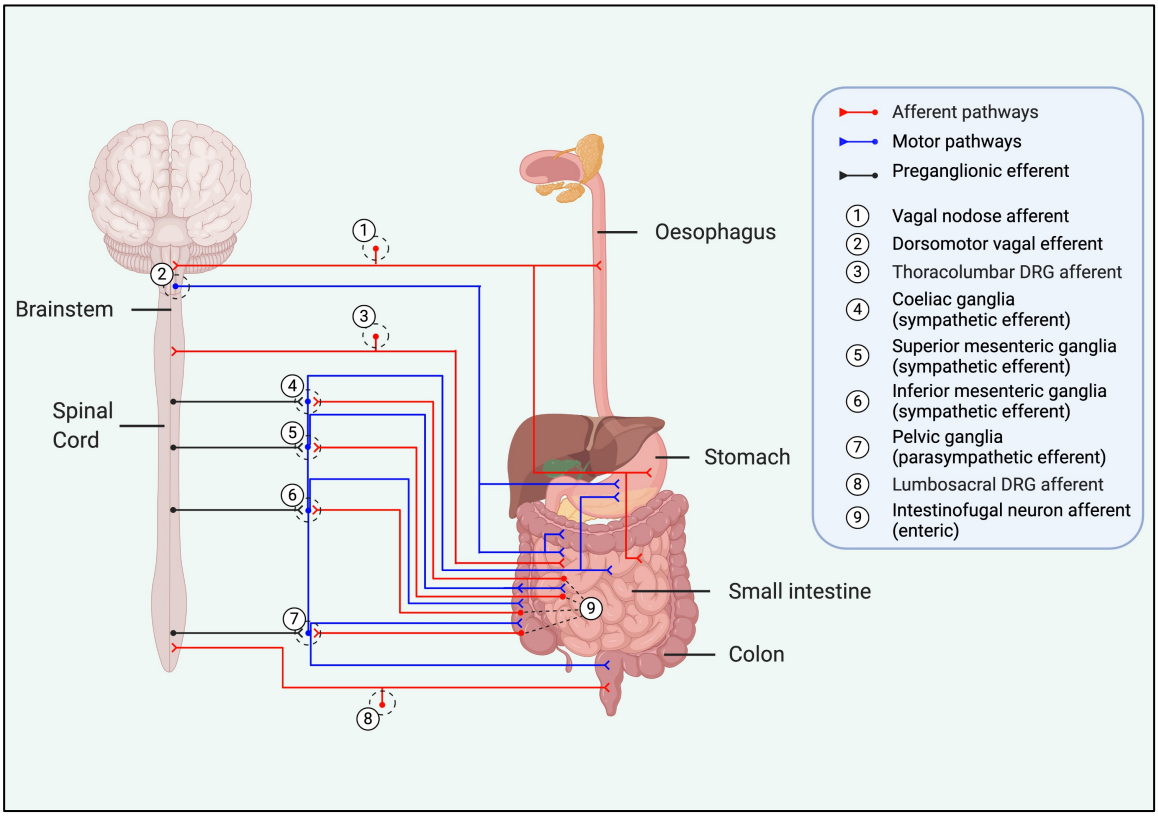

Figure 1.3 Gut-brain connections

The major neural pathways between the gut and CNS. These include extrinsic (cell bodies outside of the gut) afferent and efferent pathways as well as intrinsic (cell bodies in gut wall) intestinofugal projections. Extrinsic associated nerve endings closely associate with enteric neurons and glia.

Figure adapted from 'Enteric nervous system: sensory transduction, neural circuits and gastrointestinal motility'[83]. Created with BioRender.com

Parasympathetic Innervation of the Gut

A large portion of parasympathetic innervation of the GI tract originates from the vagus nerve, spanning from the stomach to the proximal colon. The cell bodies are located within dorsal motor nucleus of the vagus (DMV) as supported by numerous tracing studies. Vagal efferent motoneurons densely populate the stomach, decreasing in density as you move distally along the small and large intestines[85]. These synapse onto ICCs and intrinsic enteric neurons in the MP to modulate gut motility patterns[86]. Acetylcholine is the primary neurotransmitter used by vagal efferent motoneurons, though catecholamines and nitric oxide have been identified in this population as well[87,88]. This results in two distinctive pathways: an excitatory cholinergic pathway resulting in smooth muscle contraction and an inhibitory non-adrenergic non-cholinergic (NANC) pathway resulting in smooth muscle

relaxation[89]. Parasympathetic innervation of the colon is drawn from the pelvic ganglia. The same pattern presents here where a cholinergic pathway increases colonic motility while a NANC pathway inhibits motility.

Sympathetic Innervation of the Gut

Sympathetic innervation of the GI tract initiates from prevertebral ganglia, including the coeliac ganglia (stomach and small intestine), superior mesenteric ganglia (small intestine and colon), inferior mesenteric ganglia (colon), and pelvic ganglia (colon)[84]. It is established that sympathetic activity results in decreased gut motility. This is achieved by norepinephrine (NE) release acting on enteric neurons in the MP and SMP. Sympathetic fibers also innervate the vascular bed and provide regulation of vascular tone/blood pressure in the GI tract. Finally, sympathetic activity plays an important role in immune function which will be further discussed later on. Sympathetic fibers closely associate with Peyer's patches[90], muscularis macrophages[91], and enteric glia[92].

Afferent Projections from the Gut

The gut is a barrier surface which lies in direct content with the external environment, and as such, cells associated with the gut epithelium must be able to differentiate between nutrients and noxious stimuli. Different sets of stimuli sensed by the gut include but aren't limited to nutrients, microbial products/antigens, toxins, mechanical distortion, and physiochemical attributes such as temperature and pH. Afferent nerve endings are present throughout the GI tract to relay this sensory information to the CNS. There are four sensory pathways from the gut to CNS: the vagal nodose, thoracolumbar dorsal root ganglia (DRG), lumbosacral DRG, and intestinofugal neurons[93]. Each region of the gut receives dual sensory innervation from vagal and spinal pathways. Extrinsic sensory nerve endings (vagal, thoracolumbar, and lumbosacral) have been binned into five distinct subsets based on structure and location: these are referred to as intraganglionic laminar, mucosal, muscular-mucosal, intramuscular, and vascular[93].

Intraganglionic laminar endings (IGLEs) arise from the vagus nerve as well as the lumbosacral DRG. IGLEs terminate in myenteric ganglia and respond to low-threshold contractile forces through stretch-activated ion channels as well as ATP release[94,95]. Mucosal afferents are also observed from the vagus and spinal cord and terminate in the mucosa. These do not respond to distention but instead are strongly activated by signaling molecules derived from enteroendocrine cells, including 5-HT from enterochromaffin cells and cholecystokinin (CCK), which signals satiety. Muscular-mucosal afferents terminate in the submucosa and respond both to distention and light stroking of the mucosa – displaying a hybrid phenotype between the first two types discussed. Though the significance of this subset of afferents is not fully understood, it is suggested they may detect movement of content through the GI tract[93]. Intramuscular afferents arise from the

vagus nerve and spinal cord and contain branching fibers that terminate within the circular and longitudinal muscle. These 'intramuscular arrays' closely associate with ICCs, suggesting they might form complexes analogous to striated muscle spindles. Vagal intramuscular afferents largely innervate the esophagus and stomach[96,97], while spinal intramuscular afferent innervate the intestines[98,99]. In both cases, intramuscular afferents display mechanosensitive properties, but unlike IGLEs, these express the capsaicin-sensitive cation channel TRPV1[98,100]. Intravascular afferents arise only from the thoracolumbar and lumbosacral DRGs, accounting for a substantial portion of spinal afferents in the gut. These are a complex population of afferents characterized by peri-vascular axons that branch preferentially alongside arterial branch points. Transduction sites are observed on or near extramural mesenteric vessels, as well as intramural arteries and second-order arterioles within the submucosa[101]. Vascular afferents possess high-threshold mechanosensitive properties and nociceptive properties, as they express multiple TRP channels including TRPV1, TRPV4, and TRPA1. Collateral branches are also observed that terminate in the MP and SMP – these are not mechanosensitive but instead provide capsaicin-induced excitatory synaptic input on enteric neurons mediated by the neuropeptide Substance P[102,103]. The release of neuropeptides by vascular afferents couples their sensory roles to efferent roles on visceral vasculature resulting in increased vasodilation and plasma extravasation – otherwise known as neurogenic inflammation[104,105]. Vascular afferents provide an intriguing source for neuro-immune crosstalk as they are directly activated by an array of inflammatory mediators/cytokines including IL-1β, IL-6, and TNFα[106–108].

1.6.3 Enteroendocrine Cells

A vast majority of nutrient sensing occurs through enteroendocrine cells (EECs), which are sensory epithelial cells located in the intestinal epithelium, as well as lining the stomach and pancreas. EECs act in close concert with enteric neurons and glia to play critical roles in gastrointestinal function. EECs are derived from $Lgr5^+$ stem cells in the intestine and all intestinal EECs arise from a common $Neurogenin3^+$ progenitor[109,110]. These cells were initially characterized based on endocrine functions, as they can secrete more than 30 different hormones in response to distinctive stimuli, making the gut the largest endocrine organ in the body[111]. Multiple subtypes of EECs have been described, which have traditionally been differentiated by the principal hormone they produce, though it is now well established that many EECs express multiple signaling molecules[112]. EECs can also be divided into open and closed types: open types have a bottleneck shape with microvilli at the apical surface directly exposed to luminal contents, while closed types are located near the basal side of the epithelium and do not reach the luminal surface. EECs are equipped to respond to numerous stimuli as they possess a variety of sensory receptors that distinguish between different nutrient sources, such as the classic taste receptors and free fatty acid receptors (FFARs).

The ability of EECs to instigate neuronal activation has become a focal point in research on their function. EECs have been shown to produce a variety of hormones involved in regulating appetite and gut function, including but not limited to 5-HT, somatostatin, ghrelin, glucagon-like peptides (GLP 1/2), peptide YY (PYY), and CCK[113]. These can act locally within the gut and other visceral organs to aide in digestion and barrier function and can also act on the CNS to influence appetite and satiety. Influences on the CNS are derived either indirectly largely through peripheral immune cells, or directly which is highly dependent on the vagus nerve. Extrinsic sensory nerve endings possess receptors for numerous enteroendocrine-derived hormones, including CCK, GLP-1/2, 5-HT, ghrelin, and PYY[114]. Fatty acids have been shown to act on intrinsic enteric neurons and extrinsic nerve endings through distinct subsets of EECs. Fatty acid binding promotes the release of PYY and GLP-1 from L cells – where PYY acts on intestinofugal neurons to activate the 'ileal brake' which ultimately inhibits propulsive activity[115]. In addition, short- and medium-chain fatty acids promote the release of the primary satiety signaling hormone cholecystokinin (CCK) from EECs in the small intestine, which excites vagal afferent nerve endings[116]. CCK is however slow acting, as CCK levels often peak after a meal has ended, prompting the search for quicker acting mechanisms. Recently, a subset of CCK^{+} enteroendocrine cells dubbed the 'neuropod' has been identified and described to form synaptic connection with vagal nodose neurons in the small intestine to rapidly relay sensory nutrient information to the CNS[117]. These gut-innervating sensory vagal neurons induce dopamine release in brain reward pathways[87]. Neuropods differentiate between caloric/non-caloric sugars and convey this information to vagal neurons utilizing distinctive neurotransmitters – glutamate for caloric (sucrose) and ATP for non-caloric (sucralose)[118]. Importantly, EGCs are tightly coupled to this system as they come in direct contact with neuropods and contain secretory vesicles, strongly suggesting they are capable of modulating neuropod function[119]. Future studies will need to address the means by which enteric glia act on this system to better understand their functional relevance in nutrient sensing.

1.7 Diversity and Function of Enteric Glial Cells

Enteric glial cells are an emerging area of interest in improving our understanding of how they contribute to homeostatic gut function as well as determining how these cells might be implicated in a myriad of disease states. Research on glial cells in the CNS has demonstrated tremendous complexity and heterogeneity in how these cells assemble and pilot a nervous system[120]. Importantly, it is known that despite different origins – as peripheral glial cells are neural crest-derived[121] – central and peripheral glia share expression of some core lineage genes and functional characteristics. Study of EGCs has brought useful description of markers, plasticity, and functional properties, making some striking comparisons to CNS glia. These comparisons are useful but limited in that the compartments each exist within are drastically different, as the gut is uniquely tasked with coupling nutrient sensing and

absorption with pathogen recognition and immunity. Furthermore, the mucosal immune system harbored in the gut is critical in the regulation of bidirectional gut-brain communications[122]. Here, we will review what is currently known about the diversity of EGC functions in health and disease and pose their putative roles in bridging gut-brain communication by means of contributing to the numerous systems that integrate sensory information from the gut (Figure 1.4).

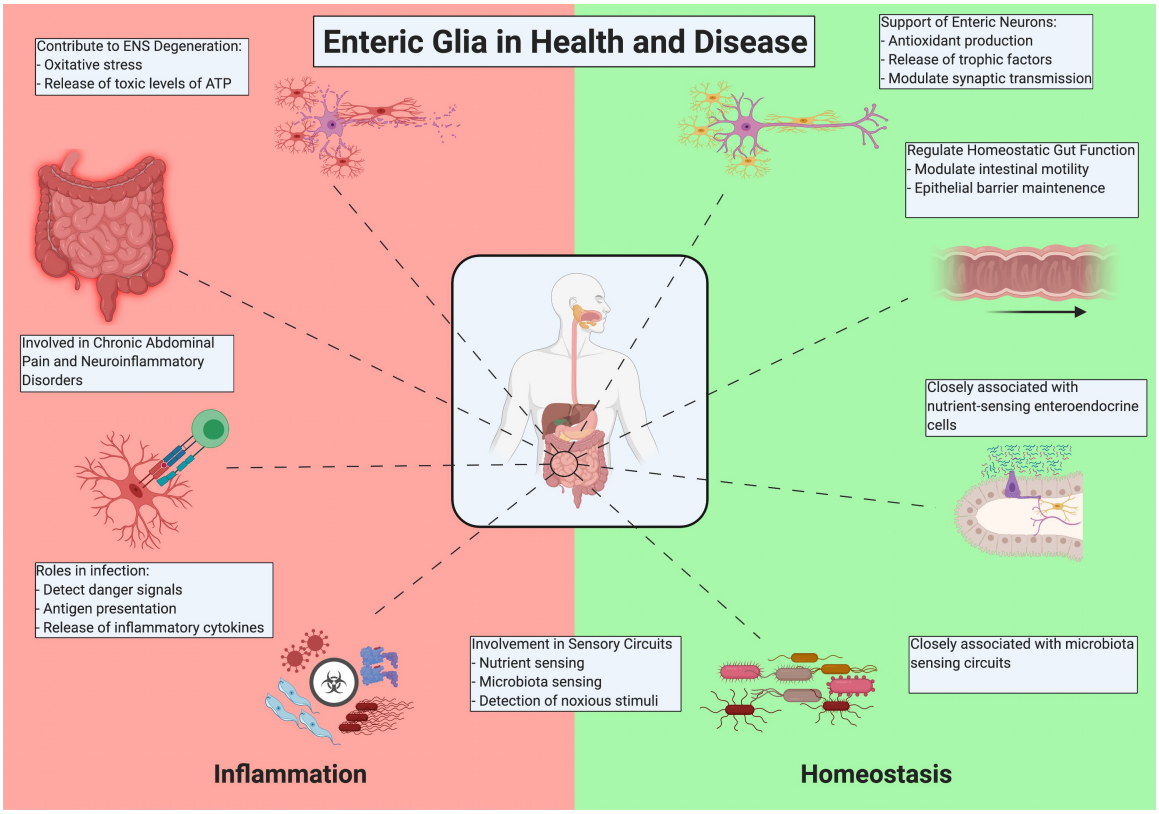

Figure 1.4 Enteric glia in health and disease

EGCs are supported to be involved in a number of processes that affect gut function and communication with the CNS. Some key processes in homeostasis and inflammation are shown here.

Created with Biorender.com

1.7.1 Molecular composition of Enteric Glial Cells

Intriguingly, EGCs share core identity markers with two distinctive types of CNS glia: these include Glial Fibrillary Acidic Protein (GFAP) – expressed by astrocytes in the CNS – and Proteolipid protein 1 (PLP1) – a myelin protein expressed by oligodendrocytes as well as Schwann cells in the periphery[123]. It has been further determined that murine EGCs preferentially express the DM20 isoform of PLP1 similar to Schwann cells, while expression of full length PLP (the most abundant CNS myelin protein) is undetected at the protein level[124]. Furthermore, DM20 expression appears to peak during early development in the mouse (~P9) and

declines into adulthood (P88)[124]. Other core EGC marker genes identified are S100B (also expressed by Astrocytes) and Sox10 (expressed by Oligodendrocyte-lineage cells and Schwann cells). At the transcriptional level, RNA-sequencing reads from sorted EGCs were compared to available microarray datasets from other CNS and peripheral glia[123]. Here, EGCs clearly represented a unique cell type which share gene expression patterns most strongly with Oligodendrocytes and Schwann cells, as well as Astrocytes to a lesser extent. Interestingly, despite a lack of compact myelin in the ENS, EGCs express transcripts for several other myelin-related proteins including Myelin Basic Protein (MBP), Myelin Protein Zero (MPZ), and 2'-3' Cyclic Nucleotide 3' Phosphodiesterase (CNP). However, it remains unclear if these myelin-related genes are translated into protein and if so, what is their functional relevance.

It is known that there is variation in the expression of marker genes across ECG subsets. SOX10, PLP1, and S100B are all considered 'core' EGC markers that are reliably expressed by a majority of EGCs throughout the intestine. Of these, SOX10 offers the most complete coverage across glial subtypes as it encodes a transcription factor necessary for EGC differentiation[41]. However, as SOX10 may be expressed by pools of ENS progenitor populations, the faithfulness of this marker should be considered when using it to target EGCs. In addition, a small population of $Sox10^-$, $GFAP^+$ cells have been observed in adult mice in homeostatic conditions – furthermore, these cells were determined to be derived from $Sox10^+$ progenitors, suggesting Sox10 expression may be dynamic[125]. S100B is reported to be co-expressed with the majority (>90%) of Sox10+ cells in the ileum[125] and >80% of PLP1 positive cells throughout the intestine[123]. PLP1 is not observed in other cell types and appears to be expressed by a majority of EGCs throughout the intestine, though a small population of $GFAP^+$, $PLP1^-$ cells has been reported[123]. Expression of PLP1 may be dynamic in EGC subsets upon challenge, as a population of $GFAP^+$, $PLP1^-$ EGCs have been demonstrated to contribute to intestinal epithelial repair following injury[14]. The DM20 transcript appears to decrease from P9 to P21 and is scarcely detected in intestinal tissue at P88 in mice[124] – however PLP1 promoter activity demonstrated by PLP-EGFP reporter mice is reliably observed across EGC subsets at P56[123] and remains constant throughout adulthood (unpublished observations). GFAP is another common marker that has been utilized to target EGCs - it should be considered that this marker presents with incomplete coverage as it is reported to be expressed 35-54% of $PLP1^+$ cells[123]. GFAP also presents with much more dynamic expression compared to the aforementioned 'core' markers, as it's upregulation is associated with 'enteric gliosis'[14,126,127] – a term broadly describing EGC responses to tissue damage and inflammation which will be further described later in this review.

1.7.2 Enteric Glial Cell Heterogeneity

Upon his early characterization of enteric glia, Gabella noted on the heterogeneity of these cells. He wrote, "In spite of obvious structural differences among the

numerous glial cells of the intramural plexuses, these cells have not yet been classified in different types. Some glial cells are, so to speak, wrapped around a nerve cell and cover a large part of its surface. Other glial cells have so many processes (particularly rich in gliofilaments) that the shape of the cell body is ill-defined."[128]. A study by Boesmans et. al. used Mosaic Analysis with Double Markers (MADM) driven by a Sox10 Cre to sparsely label EGCs and determined a classification scheme based on morphology and location which splits enteric glia into four distinctive subtypes[125] (Figure 1.5). Type I enteric glia (or protoplasmic glia) are intraganglionic with a star shaped morphology. Type II enteric glia (fibrous glia) have an elongated profile and are interganglionic as they adjoin adjacent ganglia. Type III enteric glia (subepithelial glia) are those observed extraganglionically in the MP and in the mucosa which possess several long-branched processes. Finally, Type IV enteric glia (intramuscular glia) also have an elongated profile and are observed alongside nerve fibers in the muscle layers.

Studies have also observed variation in marker expression between subsets in the MP (types I-III) upon labeling for Sox10, GFAP, and S100B. Most EGCs are Sox10+/ S100B+ within all subsets, while GFAP is more frequently detected in type I, followed by types II and III. It is currently believed that only a single EGC progenitor pool exists, suggesting expression of these markers is driven by the environment. Functional heterogeneity between enteric glial subtypes has been demonstrated by calcium imaging studies to measure the response of EGCs in isolated MP segments to ATP, as enteric glia are known to respond to purinergic signaling[129]. The majority of type I and II EGCs responded to ATP (86.8% and 73.9% respectively), though the amplitude of the response was much lower in the type II population. Meanwhile, only 34.6% of type III EGCs displayed Ca2+ transients in response to ATP, also with a low amplitude. These data suggest that populations of EGCs in the MP can be distinguished based on their response to neurotransmitters. Further description of the diversity of enteric glial cell function will be discussed later in this review.

In addition to delineations of morphological and regional heterogeneity, several studies have described diversity of enteric glial cells at the transcriptomic level in humans and mice through the use of single cell RNA sequencing[130–135]. The number of enteric glial cell clusters observed varies slightly from study to study, which can be affected by a number of factors including sample collection and clustering parameters. Nonetheless, these datasets can be used to further characterize subpopulations of enteric glial cells based on *a priori* knowledge and validation by other techniques (immunofluorescence, RNAscope, etc.). For example, in a study by Drokhlyansky et al. the authors separately sequenced myenteric- and mucosal-derived human colon tissue samples and identified unique gene signatures expressed by enteric glial cell clusters in each[130]. Mucosal-associated enteric glial cells were enriched for ferritin genes while Myenteric-associated enteric glial cells were enriched for cell adhesion molecules – though this needs to be validated experimentally. Another study by Fawkner-Corbett et al. leveraged scRNAseq and

spatial transcriptomics in human embryonic intestinal tissues to map the transcriptomic landscape of the developing intestine[132]. They identified 5 unique enteric glial cell clusters – glial progenitors marked by *PHOX2B* and low expression of mature enteric glial cell markers; intra-ganglionic glia marked by *ENTPD2* expression; submucosal glia marked by *TGFB1* expression; submucosal precursors marked by coexpression of *TGFB1* and *HAND2*; and lymphoid-associated glia marked by expression of genes involved in lymphoid structure formation as well as Retinoic Acid Receptor signaling. Future studies should further characterize unique enteric glial cell subsets with the goal of developing novel tools to selectively target individual subsets.

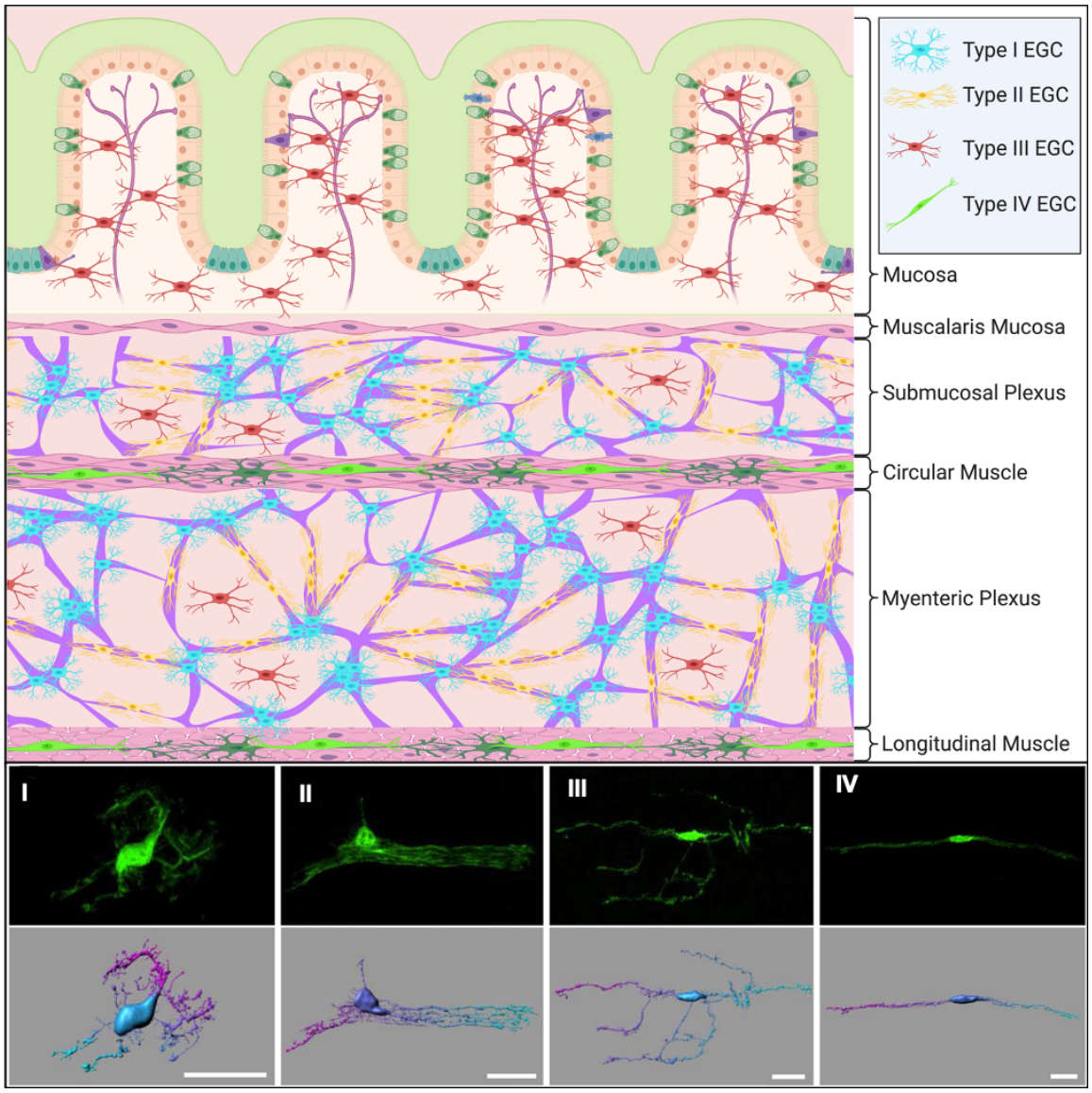

Figure 1.5 Diversity of enteric glia

Top: Schematic depicting an intestinal cross section. Different types of EGCs are shown in the compartments they reside in. ***Bottom:*** Immunofluorescence images and 3-D reconstructions of each EGC type. Scale bar = 50 µm.

Immunofluorescence images and 3-D reconstructions from 'Heterogeneity and Phenotypic Plasticity of Glial Cells in the Mammalian ENS'[125]*. Schematic created with BioRender.com*

1.7.3 Neurogenic potential of Enteric Glial Cells

The regenerative capacity of the enteric nervous system is a major field of ENS research as reduced enteric neuron density is observed in a variety of pathologies including congenital disorders such as Hirschsprung disease as well as in aging[136] and enteric infection[137,138]. Neurogenesis has been shown to occur at a modest rate in adult mice at steady state[139], and this is impacted by the microbiome[140].

However, a limited regenerative capacity is observed in many disease/injury models[141]. Lineage tracing studies have suggested that enteric glial cell trans-differentiation into enteric neurons occurs following injury[142,143]. In addition, several studies have demonstrated that primary enteric glial cell cultures differentiate into neurons – a process that begins as early as four days *in vitro*[135] and is observed using primary cultured FACS-isolated EGCs from Sox10 and PLP1 reporter mice[134,143]. These studies beg the question whether all EGCs are capable of neuronal differentiation or if there is a progenitor pool that exists throughout life. The latter is supported by several scRNAseq studies performed throughout development in mice and humans which have highlighted the existence of a progenitor-like enteric glial cell cluster[131,132,134,135]. A study by Guyer et al. utilized scMulti-seq to analyze gene expression and chromatin accessibility (ATACseq) of GFP^+ cells isolated from the small intestine longitudinal muscle/myenteric plexus of PLP-EGFP reporter mice around P14[134]. These studies indicated diverse populations of EGCs based on gene expression which included two clusters of proliferating cells (clusters 1 and 4) with enrichment of genes associated with neurogenesis. Most EGC clusters displayed similar levels of global chromatin accessibility with the exception of one cluster (cluster 8). Furthermore, cluster 4 (and to a lesser extent cluster 1) showed an enrichment of motifs associated with genes involved in neuronal differentiation (PHOX2A, PHOX2B, HAND2) – meanwhile cluster 8 showed an inverse relationship to cluster 4 for these neurogenerative motifs and lower levels of global chromatin accessibility. These authors also utilized RNAscope to probe for expression of RNA transcripts associated with neurogenic potential uncovered by their scMulti-seq (GFAP, SOX2, SLC18A2, RAMP1,CPE) and observed a robust population of intraganglionic EGCs that express these markers which remains into adulthood. Conversely, a majority of extraganglionic EGCs do not express these markers. A study by Laddach et al. similarly performed multiomic sequencing of $Sox10^+$ cells across timepoints paired with pseudotime analysis to model the differentiation trajectories of ENS progenitor cells[135]. This model suggests neuronal differentiation branches off from a default progenitor to glial differentiation trajectory. Transcriptomic profiling shows that cells gradually decrease gene expression modules associated with neurogenesis along this axis and upregulate known markers and regulators of gliogenesis and maturation as well as an array of genes associated with immune function and IFNγ signaling. While neuronal differentiation is infrequent upon adulthood at steady state, glial cells largely retain chromatin accessibility at motifs associated with neurogenesis. Together these data support the hypothesis that there is a progenitor-like pool of EGCs that persists throughout life and suggests there is spaciotemporal heterogeneity in the neurogenerative capacity of EGCs that is likely influenced by the cellular and molecular environment. This supports ongoing work aiming to utilize the neurogenic capacity of EGCs as a therapeutic treatment is ENS disorders[144–146]. Future studies should aim to further explore signals that regulate neurogenesis.

1.7.4 Enteric glia regulate intestinal motility circuits

Inter/Intraganglionic EGCs are critical components of neural networks in the myenteric and submucosal plexuses responsible for driving peristalsis. The capacity of EGC-mediated regulation of peristalsis is well studied. EGC ablation studies using the PLP1^{CreER};Rosa26^{DTA} mouse model results in increased intestinal transit time in female but not in male mice, suggesting sex differences in EGC regulation of intestinal motility[147]. Networks of EGCs communicate via Ca^{2+} signaling mediated by the gap junction hemichannel Connexin 43 (Cx43), and this is tightly coupled with neuronal signaling as Cx43-dependent Ca^{2+} waves occur in response to neuronal purinergic signaling[129]. This axis is implicated in EGC regulation of peristalsis, as genetic ablation of EGC Cx43 using hGFAP::*Cre*ER$^{T2+/-}$;Cx43$^{fl/fl}$ mice (as well as pharmacological blockade) results in reduced smooth muscle contractions in *ex vivo* colon preparations and increased intestinal transit time *in vivo*[11]. In agreement with this notion, chemogenetic activation of EGC Ca^{2+} responses with GFAP::*hM3Dq* mice results in increased smooth muscle contractions and decreased intestinal transit time[12]. Meanwhile, inhibiting Ca^{2+} responses by disrupting SNARE mediated exocytosis or inhibiting inositol triphosphate (IP3) has no effect on intestinal transit time, though both of these (along with Cx43 knockdown) alter the migrating myoelectric complex[148].

As described by the *law of the intestine*, peristalsis is facilitated by ascending interneurons activating motor neurons upstream of a point of stimulus concordant with descending interneurons inhibiting motor neurons downstream – this results in contraction above and inhibition below the excited spot. This response is largely driven by functional coupling of cholinergic, nitrergic, and purinergic signaling pathways[149]. This is supported by pharmacological or genetic inhibition of these neurotransmitters showing that inhibition of cholinergic signaling impairs upstream contraction[61], while inhibition of neuronal nitrergic signaling impairs downstream relaxation[150]. A study by Ahmadzai et al. investigated circuit specific EGC responses in the proximal colon by combining glial chemogenetic activation with calcium imaging in neurons and glia through the use of GFAP-hm3Dq$^{+/-}$;Wnt1-GCAMP$^{+/+}$ mice[151]. The authors performed focal tract stimulation to independently activate ascending or descending pathways and measure neuronal and glial calcium responses in individual myenteric ganglia – they determined that while most EGCs within a ganglia respond to both stimuli, there are modest subpopulations that preferentially respond to either ascending or descending stimuli. DREADD-induced activation of EGCs impaired neuronal calcium responses in response to both stimuli, though this was more pronounced in response to ascending activation. In turn, pairing chemogenic activation of EGCs with pharmacological blockade of cholinergic signaling prevented a change of neuronal calcium flux only upon descending activation suggesting that the repressive effects of EGCs on the descending pathway are in part mediated by cholinergic signaling. Pharmacological blockade of purinergic signaling significantly reduced neuronal signaling upon

ascending activation regardless of glial activation. Ongoing work by Scavuzzo et al. has utilized high-throughput snRNAseq of myenteric plexus-derived EGCs to identify a subcluster of EGCs that are functionally specialized for biosensing which they term as “hub cells”, which show enriched expression GFAP and the mechanoreceptor Piezo2[152]. Deletion of Piezo2 from the GFAP$^+$ subset results in reduced intestinal transit time and phenocopies pan-EGC Piezo2 deletion driven by Sox10. These studies demonstrate the capacity for EGCs to regulate motor neurocircuits and suggest circuit-specific functional heterogeneity. Advancement in platforms to generate high quality multi-omic analysis of EGCs will continue to describe the mechanisms underlying this functional heterogeneity.

1.7.5 Enteric glia regulate gut barrier integrity

Support for EGCs contributing to gut barrier integrity comes from the fact that they express several releasable factors that influence intestinal epithelial cell (IEC) differentiation, which include Glial-derived S-nitrosoglutothion (GSNO)[13], 15d-PGJ2[153], TGF-β[154], and proEGF[155]. One study performed microarray analysis in Caco2 cells (Colorectal Adenocarcinoma derived IECs) to screen for genes/pathways that are differentially expressed upon coculture with EGCs[156]. Here, the authors identified pathways involved with differentiation and adhesion were upregulated in IECs the presence of EGCs, suggesting glia might affect barrier integrity. However, *in vivo* support for this notion is contradictory. Initial studies provided support for EGCs influencing barrier integrity by ablating EGCs by expressing herpes simplex virus thymidine kinase in GFAP$^+$ cells, where they observed severe necrosis and inflammation of the small intestine that resulted in fatality[157]. Several issues with this model have since come to light, mainly in that this method of ablation produces inflammation on its own which severely confounds the results. Meanwhile, methods of ablation that do not result in inflammation, including chemical ablation with fluorocitrate and genetic ablation by expressing diptheria toxin subunit A (DTA) in PLP-expressing cells, were not associated with any major changes in barrier integrity as permeability and epithelial proliferation were unchanged[147,158]. However, more nuanced effects of PLP$^+$ EGC ablation on the epithelial layer have been described. Prochera et. al demonstrated genetic inducible EGC ablation in Plp1^{CreER};Rosa26$^{DTA/+}$ mice results in impaired paneth cell secretory activity and is associated with an altered gut microbiota composition, though the mechanisms influencing EGC-Paneth cell crosstalk are yet to be determined[159].

A study by Baghdadi et al. examined the effects of genetic ablation of PLP$^+$ and GFAP$^+$ EGCs using Plp1^{CreER} Rosa26$^{DTA/+}$ and GFAP^{CreER} Rosa26$^{DTA/+}$ mice, providing more insights into the heterogeneity of EGC regulation of the gut epithelial barrier[14] – though it should be noted that a limitation of this method of ablation is that it is not restricted to the intestinal compartment as ablation of CNS astrocytes and oligodendrocytes as well as other peripheral glial cells will also be ablated. They showed that ablation of PLP$^+$ EGCs has no effect on intestinal stem cell (ISC) proliferation, consistent with previous studies. Meanwhile, ablation of GFAP$^+$ EGCs

resulted in a transient reduction in ISCs, suggesting compensatory effects by the PLP^+ subset. Ablation of both PLP^+ and $GFAP^+$ EGCs resulted in collapse of the intestine and lethality within 5-9 days. Ablation of $GFAP^+$ EGCs also resulted in a blunted repair of the epithelium following radiation or chemical induced injury. Comparison of gene expression profiles of PLP^+, $GFAP^-$ and PLP^-, $GFAP^+$ EGCs showed enrichment of WNT niche ligands in the $GFAP^+$ subset. Furthermore, deletion of these ligands using $GFAP^{CreER}$;$WNTless^{fl/fl}$ mice also resulted in a blunted injury repair response, whereas no effect was observed in $PLP1^{CreER}$;$WNTless^{fl/fl}$ mice. These results provide support for a subset of EGCs contributing to epithelial barrier maintenance and repair, and further characterization of this subset may have important implications in the context of GI disease or infection.

1.7.6 Reactivity of Enteric Glia

Intraganglionic EGCs (type I) resemble CNS astrocytes, both in morphology and marker gene expression. Type I EGCs express GFAP more robustly than any other subset, and bulk RNA-seq has shown EGC expression of other core astrocyte genes ENTPD2 and DIO2[123]. Groundbreaking work from the Barres lab in the study of the 'reactive' properties of CNS astrocytes has further contributed to the understanding of glia[160]. This has led to the profiling of astrocytes as "A1" or "A2" based on two opposing observable states. An A1 phenotype is observable upon inflammation resulting in production of neurotoxic molecules which include ROS and ultimately promotes neuronal death. Meanwhile, an A2 phenotype is observable upon ischemia which promotes neuronal survival by the upregulation of neuroprotective genes, including neurotrophic factors and thrombospondins. This nomenclature does not reflect a binary system, but rather two extremes that heterogenous populations of astrocytes appear to polarize towards in accordance with environmental signals. Astrocyte reactivity (A1) is classically associated with increased GFAP expression, which has also been observed in EGCs in a variety of inflammatory conditions, including in patients with Multiple Sclerosis (MS), Parkinson's, Crohn's disease, as well as after traumatic brain injury[161–167]. While GFAP expression certainly has its limits as an indicator of cell function, a more detailed analysis of EGC reactivity will provide useful insights into their putative roles in IBDs and other neuroinflammatory disorders that affect the gut.

As mentioned above, a key feature of reactive glia in the CNS is increased ROS production. Nitric Oxide (NO) production by EGCs is tightly coupled to elevated S100B expression, both of which are observed under inflammatory conditions such as exposure to pathogenic bacteria[168], DSS-induced colitis[169], as well as in human patients with Celiac Disease and Ulcerative Colitis[170,171]. S100B is a Ca^{2+}/Zn^{2+} binding protein also shared with CNS astrocytes, though it is selectively expressed by EGCs in the gut. S100B likely promotes NO production by interacting with the Receptor for Advanced Glycation End products (RAGE), which ultimately results in the activation of nuclear factor kappa B (NF-kB) – a major immune transcription factor that promotes transcription of inflammatory genes including iNOS, IL-1β, and

TNF-α[172]. As S100B can be secreted, EGCs can likely act in paracrine to promote inflammation in other RAGE expressing cells.

A role for ROS production by EGCs in mediating neuronal death in the dinitrobenzyne sulfonic acid (DNBS) mouse model of colitis has been eloquently demonstrated[173]. Here, a purinergic signaling feedback loop is described in which ATP released by enteric neurons through pannexin 1 upon inflammation is readily hydrolyzed to ADP by eNTPDase expressed by EGCs. ADP then acts on the EGC P2Y1Rs resulting in increased intracellular [Ca^{2+}] and inducible Nitric Oxide Synthase (iNOS) activation. Finally, NO potentiates ATP release by EGCs through Cx43 hemichannels, which acts on neuronal P2X7Rs resulting in more neuronal ATP release through pannexin 1 and ultimately neuronal death[174]. Importantly both ablating glial iNOS and Cx43 prevented neuronal death in this model. This work describes an active role for EGCs in contributing to neuronal death upon inflammation which deeply contrasts the neuroprotective properties observed under homeostatic conditions, which is similarly seen in CNS astrocytes. Importantly, Cx43 has also been shown to be crucially involved in an inflammatory feedback loop between EGCs and enteric neurons which drives purinergic release from both[173]. Here, ATP released by EGCs through Cx43 acts on neuronal P2X7Rs, contributing to neuronal death in colitis. As ATP is a major neuroactive compound in the ENS, the importance of its release (and potentially other neurotransmitters) by EGCs under homeostatic conditions is intriguing.

1.7.7 Enteric glia regulate intestinal immunity

The intestine is tasked with allowing nutrients across the epithelial barrier to distribute energy sources throughout the body, while at the same time standing guard to deter any noxious stimuli. As such, the intestine contains the largest immune cell population of any tissue in the body, with diverse regional specificity of numerous effector immune cell subsets[175]. An emerging role for EGCs in regulating immune functions in the gut has developed as they express several immune related molecules and are in close proximity to a myriad of effector immune cells throughout the intestine.

EGC ILC3 interactions

EGCs have been shown to orchestrate IL-22 production by Group 3 Innate Lymphoid Cells (ILC3s) as demonstrated by Ibiza et al[176]. ILC3s generally work in concert with Th17 cells – both of which are specialized to act against extracellular pathogens. Interestingly, ILC3s are dependent on the GDNF family ligand (GFL) receptor RET for optimal tissue defense, which is a crucial receptor expressed in Neural Crest derived cells throughout ENS development. Ibiza et al. identified a population of $GFAP^+$ EGCs that are in close proximity to ILC3s in mucosal lymphoid aggregates known as cryptopatches. These authors also showed that EGCs

upregulate GFL production when stimulated with TLR2/4 agonists as well as IL-1β and IL-33, all of which signal through MYD88. Further, deletion of MYD88 in GFAP+ EGCs resulted in a blunted ILC3 response coupled with worsened outcomes in DSS colitis and *Citrobacter rodentium* infection, which phenocopied outcomes following RET deletion in ILC3s. Together, these data support that ILC3 function is tightly coupled to PAMP/DAMP recognition by EGCs. Intriguingly, Fawkner-Corbett et al. identified an EGC subcluster in their scRNAseq dataset of the developing human intestine that was characterized by expression of GFLs as well as genes involved in immune infiltrate formation[132], suggesting a unique EGC subset may be responsible for regulating immunity at mucosal lymphoid aggregates.

EGC interactions with monocytes/macrophages

Crosstalk between EGCs and macrophages has been demonstrated in a variety of inflammatory conditions. One study demonstrated that EGCs activate muscularis macrophages through Cx43-dependent M-CSF production during DSS colitis[15]. In this study by Grubišic et al., the authors demonstrated that deleting Cx43 in EGCs using $Sox10^{CreERT2}$;$Cx43^{fl/fl}$ mice attenuated visceral hypersensitivity during DSS colitis, although other hallmarks of disease severity remained unchanged. Cx43 ablation in EGCs resulted in decreased M-CSF expression coupled with reduced macrophage activation denoted by a reduction in CD68 positivity. Using primary EGC cultures, the authors showed that Cx43 is required for upregulating PKC and TACE activity following inflammation, where TACE is responsible for cleaving membrane bound M-CSF to its active form. A subset of enteric glial cells has also been implicated in monocyte recruitment in a model of psychological stress-driven colitis exacerbation[16]. In this study by Schneider et al., the authors performed scRNAseq of Sox10+ cells in a mouse model of restraint-induced stress and identified a subset of EGCs that was unique to the stress group and was marked by heightened expression of genes involved in glucocorticoid signaling as well as immune signaling including the chemokine CSF1. The authors also observed that stressed mice were sensitized to DSS colitis which was marked by heightened inflammation driven by TNF-producing monocytes. The authors ablated EGCs in this model by delivery of a blood-brain-barrier-impermeable PEGylated diphtheria toxin to PLPCreERT2;ROSA26iDTR mice, which demonstrated protection against stress-driven colitis exacerbation and prevented accumulation of inflammatory monocytes. This supports a role for EGC-monocyte interactions is crucial for driving stress induced colitis exacerbation. EGC-macrophage interactions have also been implicated in colorectal cancer[177]. In this study by van Barle et al., the authors demonstrated that local ablation of EGCs by colonoscopy-guided injections of diphtheria toxin into the colon wall of PLPCreERT2;ROSA26iDTR mice resulted in reduced tumor growth in a colorectal cancer model driven by MC38 tumor cell injection. Furthermore, injecting neurosphere-derived EGCs in tandem with MC38 cells resulted in increased tumor growth, suggesting EGCs promote tumorigenesis. The authors then leveraged *in vitro* tumor EGC models and single cell

transcriptomics to identify signaling cascades responsible for EGC tumor promotion. The authors identified a neuroinflammatory feedback loop where monocyte-derived IL-1α/IL-1β signals onto EGCs resulting in cytokine release from EGCs – notably including IL-6 which then favors differentiation of SPP+ Tumor-associated macrophage differentiation which is associated with worsened outcomes. Notably, deleting both IL-6 and IL-1R in EGCs resulted in reduced tumor growth. The authors also provided evidence that this EGC-macrophage signaling axis may be implicated in human colorectal cancer patients by analyzing datasets from The Cancer Genome Atlas – this analysis showed that patients with higher enteric glia transcriptomic signatures presented with decreased survival probability and furthermore the EGC transcriptomic signature observed in colorectal cancer patients largely overlapped with that observed in the MC38 mouse model.

EGC Interferon gamma response

EGCs have also been demonstrated to play a crucial role in regulating IFNγ-mediated immunity in the context of *Heligmosomoides polygyrus* infection as demonstrated by Progatzky et al[5]. *H. polygyrus* is a helminth that establishes infection in the outer smooth muscle regions of the proximal small intestine and thus is in close contact with multiple subsets of EGCs in the myenteric and submucosal plexuses. Progatzky et al. showed that infection with this helminth drives a robust IFNγ response signature in EGCs marked by upregulation of CXCL10, CCL2, and STAT1 amongst other genes involved in IFNγ signaling. Disrupting this axis by deleting the IFNγ receptor in EGCs (using *Sox10CreER^{T2};Ifngr2$^{fl/fl}$* mice) resulted increased recruitment of granulocytes and monocytes coupled with increased granuloma formation, though there were no differences in parasite load. There were also no changes in NK cell or CD4+ T cell number, though CD8+ T cell numbers were decreased. This phenotype was similar when deleting CXCL10 in EGCs (using *Sox10CreER^{T2};Cxcl10$^{fl/fl}$* mice), suggesting EGCs play a critical role in regulating the immune response to *H. polygyrus* though the exact effector mechanism is not fully determined.

EGC T cell interactions

A highly speculated putative role of EGCs in inflammation is that of antigen presentation. In support of this notion, directing CD8+ T cell responses to EGCs in mice results in fulminant jejuno-ileo-colitis and premature death[165]. While this is a severe example, it shows that EGC antigen presentation on MHC I has the capacity to drive gut inflammation. T cells have also been shown to cause damage to enteric glial and neuronal cells in a murine model of West Nile Virus (WNV) infection[138]. In this study by Janova et al, the authors showed that WNV infection resulted in persistent reductions in enteric glial and neuronal coverage in the myenteric plexus, which was worsened upon depletion of tissue resident muscularis macrophages. The reduction in enteric glial and neuronal coverage was dependent on antigen

specific CD4+ and CD8+ T cells. This was also dependent on Perforin and FasL, suggesting cytolytic targeting of enteric glial and neuronal cells, though this was not directly shown, nor was expression of MHC I/II interrogated in ENS cells. While the ability of EGCs to present antigen on MHC I should be expected, the capacity to present antigen on MHC II would be more surprising and would define them as nonconventional antigen presenting cells. MHC II antigen presentation by non-professional antigen presenting cells has been described in few subsets of cells including sinusoidal endothelial cells and hepatocytes in the liver[178]. EGCs have been reported to express MHC II and costimulatory receptors CD80/86 in Chagas disease, which is the infection caused by the parasite *Trypanosoma cruzi*, resulting in robust intestinal immunity and ENS damage[179]. EGCs have also been reported to express MHC II in mice following administration of LPS and IFNγ[180]. In this study, Chow et al. deleted MHC II in EGCs using $Sox10^{CreERT2}$;$IAB^{fl/fl}$ mice and showed this resulted in reduced CD4+ T cell activation following LPS/IFNγ delivery. However, limitations of these studies include a lack of quantification of EGC/MHC II colocalization by immunostaining and no colabeling of muscularis macrophages, as well as nonselective targeting of EGCs as several other cell types will be targeting in the $Sox10^{CreERT2}$;$IAB^{fl/fl}$ system. My thesis work further explored the functional capacity of EGCs to act as antigen presenting cells and will be described in detail in the following chapter.

1.7.8 Enteric glia in the etiology and pathogenesis of neuroinflammatory disorders

So far, we have described roles for EGCs in actively regulating gut inflammation in a variety of settings, suggesting clinical relevance as potential therapeutic targets in neuroinflammatory disorders which affect the gut. These include inflammatory bowel disorders and extend to disorders which are often thought to primarily affect the CNS. Perturbations to the intestinal microbiome are observed in (but are not limited to) Ulcerative Colitis, Crohn's Disease, Parkinson's Disease (PD), Alzheimer's Disease (AD), Multiple Sclerosis (MS), and autism spectrum disorder (ASD)[181]. Of course, the gut microbiome does not exist in a vacuum, as dysbiosis can be viewed as a reflection of substantial changes to the cellular environment in these disease states, often coinciding with drastic alterations to the intestinal immune landscape. Enteric glial cell activation as determined by elevated GFAP expression is observed in patients with Inflammatory Bowel Disorders[165,182] and several mechanisms of EGC-mediated immune regulation in murine models of IBD were described in the previous section.

An enteric origin for Parkinson's Disease has long been postulated, as famously hypothesized by the researcher Heiko Braak. Braak was among the first to observe α-synuclein aggregates in Enteric Neurons throughout the intestine in postmortem patient samples, which included patients at the end stages of disease as well as in non-symptomatic individuals that presented with PD-related brain lesions limited to the lower brainstem[183]. Possible EGC activation in PD is indicated by increased

GFAP expression[163]. A putative gut origin of PD is also supported by a study by Challis et al., demonstrating that delivery of α-synuclein fibrils to the duodenum of aged mice results in progression of α-synuclein histopathology to the midbrain and presentation with motor deficits, in addition to elevated GFAP coverage in the myenteric plexus[184]. Elevated GFAP expression has also been reported in rats using the 6-OHDA PD model, which also present with elevated detection of substance P, the tachykinergic receptor $NK_{1,}$, lipid peroxidation, and inflammatory cytokines within the outer gut wall[185]. Involvement of the enteric nervous system is also considered in the case of Alzheimer's Disease, as amyloid plaque pathology has been observed in the intestine on postmortem AD patient samples[186,187]. Amyloid plaque accumulation is also reported in the intestines of the 5XFAD mouse model of AD which coincides with low grade intestinal inflammation and accelerated intestinal transit time – though no differences in enteric neuron cell count and S100B/GFAP expression by EGCs were observed[188]. Future studies should further investigate how EGCs are impacted in PD and AD to explore if they could be potential therapeutic targets.

EGC activation may also be indicated in MS as indicated by an upregulation in GFAP expression[167]. In the animal model of MS, Experimental Autoimmune Encephalomyelitis (EAE), mucosal immune responses are critical as the presence of SFB-induced Th17 cells is necessary for disease onset[189]. Furthermore, a study by Wunsch et al. described potential autoimmune targeting of the ENS in an EAE model driven by a PLP-MBP fusion peptide[167]. The necessity of SFB-induced Th17 cells is also true in the Maternal Immune Activation (MIA) model of ASD[190]. Patients with MS and ASD also frequently report GI issues, as one study showed that two-thirds of MS patients present with gastrointestinal symptoms[191] and another study reporting at least one functional gastrointestinal disorder is present in 30.5% of ASD patients[192]. Though the ENS has not been extensively characterized in ASD models, intestinal dysfunction has been observed in several genetic models of ASD[193–195]. Future studies should further interrogate a putative roles for EGCs in the onset and pathology of neuroinflammatory disorders.

1.8 Conclusions

As our understanding of the gut-brain connection continues to evolve, the roles of enteric glial cells in these complex systems are likely to become even more distinct. EGCs serve as dynamic mediators, actively interacting with the intestinal microbiota, epithelial barrier, immune system, and enteric neurons – all of which work in concert to relay critical information to the central nervous system. Through these intricate interactions, EGCs not only support gut homeostasis but also influence broader neuroimmune and neuroinflammatory processes. Given their pivotal role in modulating intestinal and neural functions, enteric glial cells have emerged as promising therapeutic targets for neuroinflammatory disorders, offering new avenues for intervention in conditions that bridge the gut and the brain.

Chapter 2: Functional analysis of antigen presentation by enteric glial cells during intestinal inflammation

2.1 Abstract

The Enteric Nervous System is composed of a vastly interconnected network of neurons and glial cells that coordinate to regulate homeostatic gut function including intestinal motility, nutrient sensing, and mucosal barrier immunity. Enteric Glial Cells (EGCs) are a heterogenous cell population located throughout the gastrointestinal tract and have well described roles in regulating intestinal immune responses. EGCs have been suggested to act as nonconventional antigen presenting cells via the Major Histocompatibility Complex II (MHC II), though this has not been confirmed functionally. Here, we investigate the capability of EGCs to present antigen on MHC I and MHC II using *in vitro* antigen presentation assays performed with primary murine EGC cultures. We found that EGCs are capable of functional antigen presentation on MHC I, including antigen cross-presentation, but are not capable of functional antigen presentation on MHC II. We also determined EGC cell surface MHC I and MHC II expression levels by flow cytometry during intestinal inflammation during Dextran Sodium Sulfate-induced colitis or acute *Toxoplasma gondii* infection. We found that EGCs upregulate MHC I during acute *T. gondii* infection and induce low-level MHC II expression. These findings suggest that EGCs may be important in the regulation of $CD8^+$ T cell responses via MHC I mediated antigen (cross) presentation but may not be relevant for MHC II-mediated antigen presentation.

Ryan M. Brown (rmb5kk@virginia.edu, ORCID: 0000-0002-7513-915X)[1,2,3*], Helen H. Le (hhl4tx@virginia.edu, ORCID: 0009-0002-2144-4113)[1,2], Isaac W. Babcock (iwb6v@virginia.edu, ORCID: 0000-0003-0360-0821)[1,2,3], Tajie H. Harris (thh9t@virginia.edu, ORCID: 0000-0002-1355-2109)[1,2], and Alban Gaultier (ag7h@virginia.edu, ORCID: 0000-0002-4175-6053)[1,2*]

[1]Center for Brain Immunology and Glia, University of Virginia School of Medicine, Charlottesville, VA 22908, USA, [2]Department of Neuroscience, University of Virginia School of Medicine, Charlottesville, VA 22908, USA, [3]Neuroscience Graduate Program, University of Virginia School of Medicine, Charlottesville, VA 22908, USA.

*Corresponding authors.
Ryan Brown: rmb5kk@virginia.edu and Alban Gaultier: ag7h@virginia.edu, Department of Neuroscience, University of Virginia, 409 Lane Road, MR4 Rm 5126, Charlottesville, VA, USA, 22908

Glia. 2024 Nov 4;73(2):291–308. doi: 10.1002/glia.24632

2.2 List of abbreviations

BMDC, Bone Marrow-derived Dendritic Cell; DIV, Days *in vitro*; DSS, Dextran Sodium Sulfate; EGC, Enteric Glial Cell; EGFP, Enhanced Green Fluorescent Protein; FMO, Fluorescence Minus One; GDNF, Glial-derived Neurotrophic Factor; GFP, Green Fluorescent Protein; HLA, Human Leukocyte Antigen; IBD, Inflammatory Bowel Disease; IFNγR, Interferon-gamma receptor; IFNg, Interferon-gamma; IL17a, Interleukin 17a; IL33, Interleukin 33; IL6, Interleukin 6; ILC3, Type 3 Innate Lymphoid Cell; LMMP, Longitudinal Muscle and Myenteric Plexus; LPS, Lipopolysaccharide; MFI, Mean Fluorescence Intensity; MHC, Major Histocompatibility Complex; TLR, Toll Like Receptor; TNF, Tumor Necrosis Factor

2.3 Introduction

Enteric Glial Cells (EGCs) are critical components of the Enteric Nervous System as they are attributed to be involved in a variety of homeostatic gut functions including regulation of intestinal motility [11,12,147], regulation and repair of gut epithelial barriers [13,14,196], and regulation of intestinal immunity [5,176,197]. EGCs are observed throughout the gastrointestinal tract – this includes dense aggregation within the ganglionated plexuses (myenteric and submucosal), in close proximity to nerve fibers within the longitudinal and circular muscle layers, and throughout the mucosa. Based on location, morphology, and transcriptional analysis, EGCs are heterogeneous and categorized into four distinctive subtypes [125,134].

EGCs are emerging as critical contributors to the regulation of intestinal immunity. EGCs are capable of detecting pathogens and noxious stimuli as they express several pathogen recognition receptors including TLR2 and TLR4 [169,198]. Furthermore, EGCs are evidenced to relay these signals to immune cells, as it has been demonstrated that EGCs provide GDNF-family ligands to activate ILC3s in a MyD88-dependent manner, and disrupting this axis heightens inflammation during Dextran Sodium Sulfate (DSS) induced colitis and *Citrobacter rodentium* infection [176]. In addition to regulation of type 3 immune responses, EGCs have been described in the regulation of type 1 immunity through their expression of the Interferon-gamma receptor (IFNγR). In a model of helminth infection driven by *Heligmosmoides polygyrus,* EGC IFNγR signaling drives CXCL10 expression and promotes pathogen clearance and tissue repair [5]. EGCs have also been proposed to modulate adaptive immune responses by acting as antigen presenting cells. EGCs have been described to express MHC II in humans in Chagas disease [179], Crohn's Disease [199], and in mice following LPS/IFNγ administration [180]. However, these studies are limited to immunohistochemical detection of MHC II expression by EGCs and do not provide sufficient evidence for functional antigen presentation on MHC II.

In the present study, we investigate the ability of EGCs to act as antigen presenting cells via MHC I and MHC II. We utilize *in vitro* antigen presentation assays with primary murine EGCs, as well as *in vivo* models of intestinal inflammation driven by

DSS colitis or acute *Toxoplasma gondii* infection paired with spectral flow cytometry and confocal microscopy. Our results indicate a putative role for EGC antigen presentation on MHC I during *T. gondii* infection but do not support a role for EGC antigen presentation on MHC II. Furthermore, *in vitro* studies performed with primary cultures suggest EGCs are not capable of mediating functional antigen presentation via MHC II.

2.4 Results

2.4.1 Enteric glial cells upregulate genes associated with antigen processing and presentation in Inflammatory Bowel Disease

To explore how EGCs respond to inflammation, we reanalyzed available scRNAseq datasets containing EGCs derived from colonic biopsies of human patients with either Ulcerative Colitis (Kinchen et al., 2018) or Crohn's Disease (Kong et al., 2023) compared to healthy controls. In these studies, Colonic tissue samples were collected by endoscopy and thus will be enriched for mucosal tissue. The study by Kinchen et al depleted epithelial and immune cells by magnetic-activated cell sorting [200], while the study by Kong et al depleted epithelial cells by vigorous shaking in PBS/EDTA and analyzed non-immune and immune cell subsets individually [201]. We adjusted the clustering parameters to closely match the cell populations observed in the original studies (2.1a,e). We subsetted EGCs by cluster as well as coexpression of core markers *S100B* and *PLP1* in order to further validate cell identity (Figure 2.2a). We observed modest downregulation of these core markers in Ulcerative Colitis (Figure 2.1b) while there was no apparent change in Crohn's Disease (Figure 2.1g). Upon subsetting EGCs, we then looked at genes that were significantly differentially expressed in each condition compared to healthy controls (Figure 2.1c,h). In either condition, several HLA genes were significantly upregulated as well as other genes associated with antigen processing and presentation such as *PSMB8*, *CD74*, and *TAP1*. Furthermore, Gene Ontology analysis identified several terms implicating antigen processing and presentation as the most significantly enriched biological process by EGCs in either disease state (Figure 2.1d,i). To get a better representation of which antigen presentation pathways might be utilized by EGCs in IBD, we plotted all significantly upregulated genes in the KEGG antigen processing and presentation gene set (Figure 2.1e,j). EGCs showed robust upregulation of genes involved in MHC I presentation including every MHC I allele (*HLA-A-F*), subunits of the immunoproteasome (*PSME 1,2*), and the Transporter associated with Antigen Processing (*TAP 1,2)*. EGCs also showed significant upregulation of genes involved in MHC II presentation including the Class II Major Histocompatibility Complex Transactivator (*CIITA*), Cathepsin S (*CTSS*), CD74, and several MHC II alleles (*HLA-DP, HLA-DM, HLA-DOA, HLA-DQ, HLA-DR*). Notably, upregulation of both MHC I and MHC II associated genes was more pronounced in Ulcerative Colitis than Crohn's Disease. We repeated these analyses subsetting the *S100B*$^{+}$*/PLP1*$^{low/negative}$ cells in the EGC cluster, as it has been reported that

GFAP^{High}/*PLP1*^{Low} EGCs expand during intestinal injury and are important for epithelial barrier repair [14] – although *GFAP* was largely not detected in either dataset (data not shown). Antigen processing and presentation gene sets were similarly enriched in the *S100B*$^{+}$/*PLP1*$^{low/negative}$ EGCs during Ulcerative Colitis (Figure 2.2b-e) and Crohn's Disease (Figure 2.2g-j). Furthermore, we assessed MHC II allele expression across cell types observed in both datasets (Figure 2.2k.l). We observed consistent expression of MHC II alleles in Endothelial Cells and Lymphatic Endothelial Cells, both of which have been previously reported to express MHC II [202,203]. Meanwhile, we did not observe robust induction of MHC II in Stromal Cells, Fibroblasts, Myofibroblasts, and Pericytes indicating that the upregulation of MHC II we observed in EGCs is not linked to ambient RNAs present across cell types. This data shows that EGCs express the transcripts necessary for MHC Class I- and Class II-antigen presentation and may act as nonconventional antigen presenting cells during Inflammatory Bowel Disease

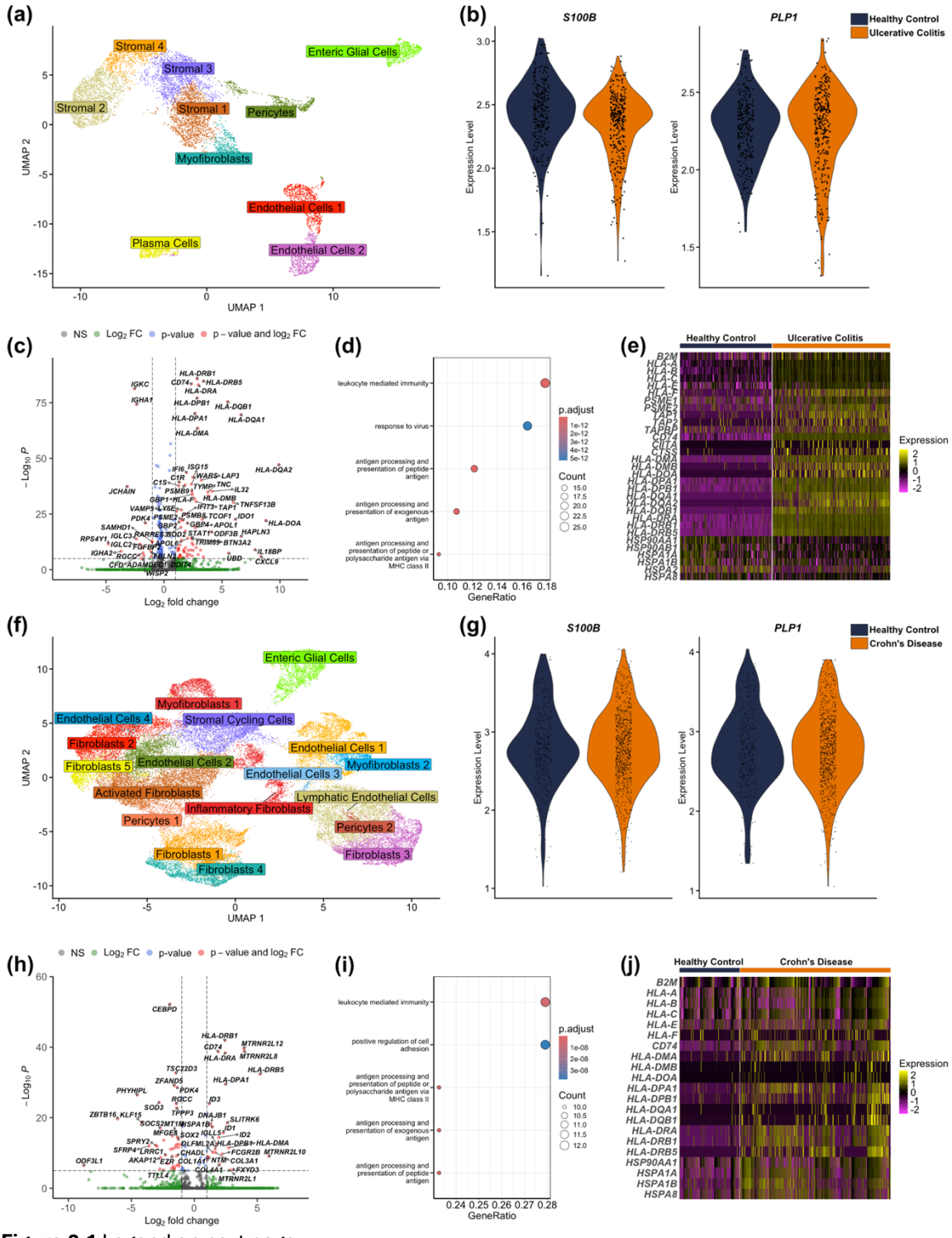

Figure 2.1 Legend on next page.

Figure 2.1 EGCs upregulate antigen presentation machinery during Inflammatory Bowel Disease

(a) UMAP depicting cell clusters observed by reanalyzing scRNAseq dataset from Ulcerative Colitis patients and Healthy Controls. Dataset originally published by *Kinchen et. al.* (b) Expression of EGC core markers *S100B and PLP1* after subsetting EGC cell cluster. Y-axis depicts scaled data showing Pearson's residuals. (c) Volcano plot highlighting EGC cluster genes that are significantly differentially expressed in Ulcerative Colitis compared to Healthy Controls. Log_2 Fold Change is indicated on the x-axis and p-value on the y-axis. Significantly differentially expressed genes are colored red with the criteria $log_2FC > |2|$ and p value <= $10e^{-6}$. (d) GO terms that are significantly overrepresented in EGCs during Ulcerative Colitis (e) Heatmap depicting EGC genes in the KEGG Antigen Processing and Presentation gene set that are significantly upregulated during Ulcerative Colitis. (f) UMAP depicting cell clusters observed by reanalyzing scRNAseq dataset from Crohn's Disease patients and Healthy Controls. Dataset originally published by *Kong et. al.* (g) Expression of EGC core markers *S100B and PLP1* after subsetting EGC cell cluster. Y-axis depicts scaled data showing Pearson's residuals. (h) Volcano plot highlighting EGC cluster genes that are significantly differentially expressed in Crohn's Disease compared to Healthy Controls. Log_2 Fold Change is indicated on the x-axis and p-value on the y-axis. Significantly differentially expressed genes are colored red with the criteria $log_2FC > |2|$ and p value <= $10e^{-6}$. (i) GO terms that are significantly overrepresented in EGCs during Crohn's Disease (j) Heatmap depicting EGC genes in the KEGG Antigen Processing and Presentation gene set that are significantly upregulated during Crohn's Disease.

2.4.2 Investigating antigen presentation using primary murine enteric glial cells

To further investigate EGCs as antigen presenting cells, we utilized primary cultures derived from PLP-EGFP reporter mice. We prepared primary cultures as described by Progatzky et al. (Figure 2.4a) [5], and treated with IFNγ alone, or IFNγ plus either the SIINFEKL peptide or Ovalbumin (Figure 2.3a). This allows us to probe for cell surface expression of MHC I and MHC II and functional antigen presentation, as the SIINFEKL peptide will permeate the cell membrane and be processed onto MHC I via the endogenous pathway, whereas Ovalbumin will be endocytosed and processed onto MHC II via the exogenous pathway.

2.4.3 Interferon gamma induces MHC I and MHC II expression by EGCs

Upon treating primary EGC cultures, we performed flow cytometry to check for MHC I/II expression in GFP^+ EGCs. As there are other cell types present in the culture, we also used cell surface markers to detect immune cells (CD45) as well as endothelial cells and fibroblasts (CD31, CD13). EGCs were characterized as CD45 negative, CD13/31 negative, GFP positive (Figure 2.4b). We observed baseline expression of MHC I in 45.6 ± 17.7% of EGCs, which was significantly increased to near 100% in all stimulation conditions (IFNγ: mean = 96.85 ± 3.05%, p = .0428; IFNγ + SIINFEKL: mean = 95.2 ± 4.6%, p = .0474; IFNγ + Ovalbumin: mean = 95.45 ± 4.45%, p = .0467) (Figure 2.3b). EGC MHC I expression level as determined by mean fluorescence intensity (MFI) was modestly increased upon stimulation though not statistically significant (Unstimulated: mean = 13460 ± 5846 A.U.; IFNγ: mean =

493524 ± 292476 A.U., p = .4795 A.U.; IFNγ + SIINFEKL: mean = 423331 ± 229670 A.U., p = .5796; IFNγ + Ovalbumin: mean = 531178 ± 343822 A.U., p = .4313) (Figure 2.4d). We observed little to no MHC II expression by EGCs at baseline (mean = 2.210 ± .95%) and a significant increase with all stimulation conditions (IFNγ: mean = 34.2 ± 1.7%, p = .0076; IFNγ + SIINFEKL: mean = 33.45 ± 6.05%, p = .0083; IFNγ + Ovalbumin: mean = 31.15 ± 3.45%, p = .011) (Figure 2.3c). EGC MHC II MFI was also significantly increased with all stimulation conditions (Unstimulated: mean = 26033 ± 7153 A.U.; IFNγ: mean = 92608 ± 9813 A.U., p = .0077; IFNγ + SIINFEKL: mean = 88497 ± 761 A.U., p = .0097; IFNγ + Ovalbumin: mean = 85133 ± 8923 A.U., p = .0119) (Figure 2.4e). To validate our flow cytometry results, we performed immunofluorescence staining for SIINFEKL-bound MHC I and MHC II in primary EGC cultures stimulated with IFNγ + SIINFEKL and confirmed EGC MHC I and MHC II expression (Figure 2.3d). These data indicate that IFNγ alone is sufficient to induce MHC I and MHC II expression in EGCs *in vitro*.

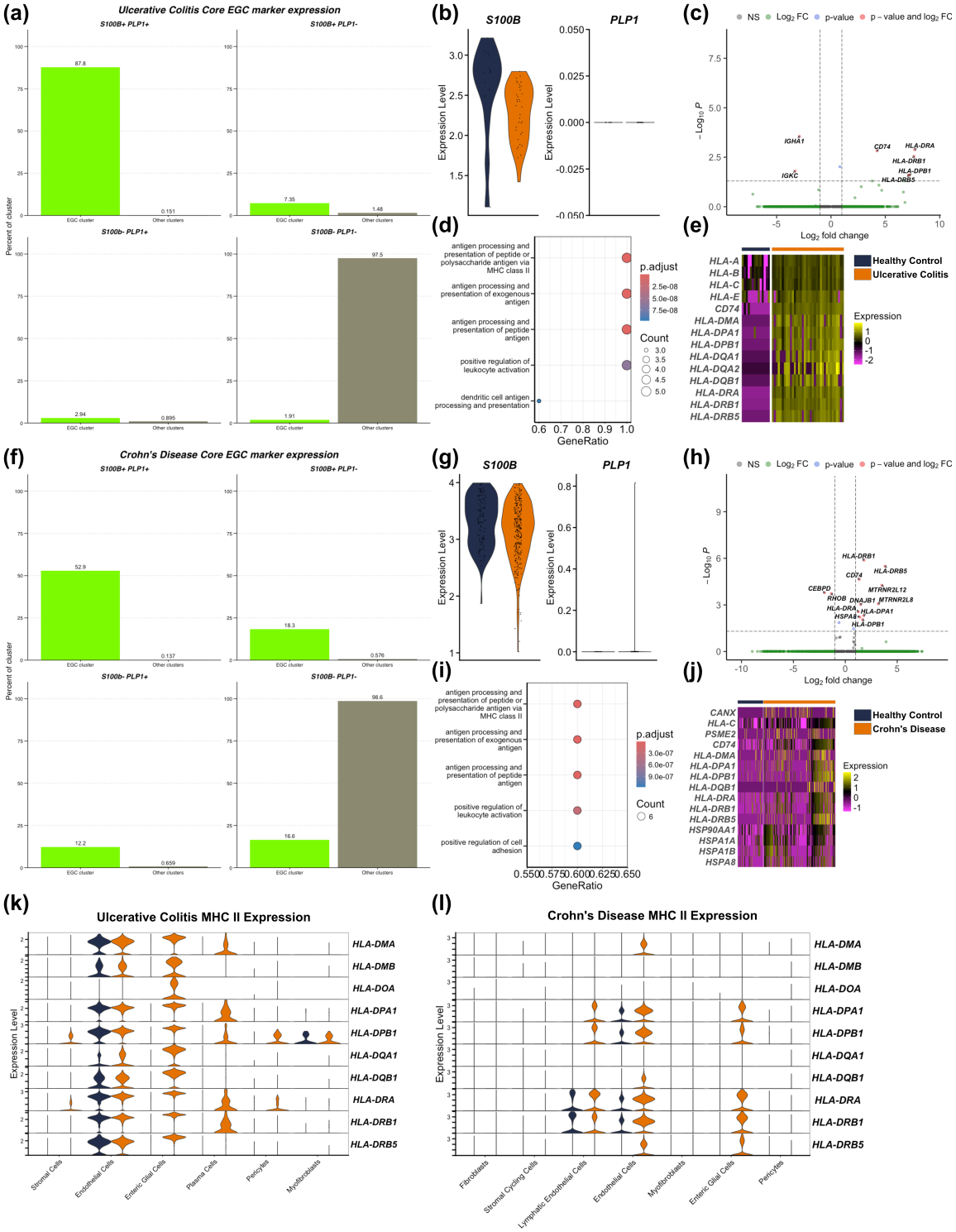

Figure 2.2 Legend on next page.

Figure 2.2 IBD scRNAseq supplementary data

(a) Bar plots depicting S100B/PLP1 expression by the EGC cluster and all other clusters combined in the Ulcerative Colitis dataset. (b) Violin plots depicting S100B/PLP1 expression in subsetted $S100B^+/PLP1^-$ EGCs. Y-axis depicts scaled data showing Pearson's residuals. (c) Volcano plot highlighting $S100B^+/PLP1^-$ EGC cluster genes that are significantly differentially expressed in Ulcerative Colitis compared to Healthy Controls. Log_2 Fold Change is indicated on the x-axis and p-value on the y-axis. Significantly differentially expressed genes are colored red with the criteria $log_2FC > |2|$ and p value <= .05. (d) GO terms that are significantly overrepresented in $S100B^+/PLP1^-$ EGCs during Ulcerative Colitis (e) Heatmap depicting $S100B^+/PLP1^-$ EGC genes in the KEGG Antigen Processing and Presentation gene set that are significantly upregulated during Ulcerative Colitis. (f) Bar plots depicting S100B/PLP1 expression by the EGC cluster and all other clusters combined in the Crohn's Disease dataset. (b) Violin plots depicting S100B/PLP1 expression in subsetted $S100B^+/PLP1^-$ EGCs. Y-axis depicts scaled data showing Pearson's residuals. (c) Volcano plot highlighting $S100B^+/PLP1^-$ EGC cluster genes that are significantly differentially expressed in Crohn's Disease compared to Healthy Controls. Log_2 Fold Change is indicated on the x-axis and p-value on the y-axis. Significantly differentially expressed genes are colored red with the criteria $log_2FC > |2|$ and p value <= .05. (d) GO terms that are significantly overrepresented in $S100B^+/PLP1^-$ EGCs during Crohn's Disease (e) Heatmap depicting $S100B^+/PLP1^-$ EGC genes in the KEGG Antigen Processing and Presentation gene set that are significantly upregulated during Ulcerative Colitis.

2.4.4 Primary murine EGCs are capable of antigen presentation on MHC I, but not MHC II

To interrogate if EGCs are capable of functional antigen presentation *in vitro*, we utilized a coculture system. We prepared primary EGC cultures from female C57BL/6 mice and stimulated with IFNγ alone, IFNγ + SIINFEKL, or IFNγ + Ovalbumin, then cocultured with OT-I or OT-II T cells labeled with a proliferation dye (Figure 2.5a). After 72 hours of coculture, we performed flow cytometry to probe for OT-I/II proliferation as a proxy for functional antigen presentation (Figure 2.4c). More specifically, OT-I cells are $CD8^+$ T cells that possess a transgenic TCR specific for SIINFEKL loaded on MHC I, whereas OT-IIs are $CD4^+$ T cells with a transgenic TCR specific for $Ovalbumin_{323-339}$ loaded on MHC II. We observed robust OT-I proliferation upon incubating EGCs with SIINFEKL (Figure 2.5b) (Table 2.1), suggesting EGCs are capable of MHC I-mediated antigen presentation through the cytosolic pathway. We also observed robust OT-I proliferation upon incubating EGCs with Ovalbumin (Figure 2.5b, Table 2.1), suggesting EGCs are capable of antigen cross-presentation. Importantly, we observed little to no OT-I proliferation in both negative control conditions where no antigen was present (Figure 2.5b, Table 2.1). Meanwhile, we did not observe increased OT-II proliferation upon incubating EGCs with Ovalbumin relative to no antigen controls (Figure 2.5c, Table 2.1), suggesting that EGCs are not capable of functional antigen presentation on MHC II *in vitro*. To confirm our results, we repeated these experiments with FACS-purified EGCs. We expanded primary EGC cultures from PLP-EGFP mice then isolated GFP positive cells by FACS. Purified EGCs were $S100B^+$ as assessed by immunofluorescence staining (Figure 2.4a). Purified EGCs from either female or male mice were stimulated with IFNγ alone, IFNγ + SIINFEKL, or IFNγ + Ovalbumin, then cocultured with sex-matched OT-I or OT-II T cells labeled with a proliferation

dye (Figure 2.5d). We again observed robust OT-I proliferation upon incubating GFP^+ EGCs with SIINFEKL regardless of sex (Figure 2.5e,f, Table 2.2). We also observed robust OT-I proliferation upon incubating GFP^+ EGCs with Ovalbumin regardless of sex, though female-derived cultures appeared to drive more OT-I proliferation than male-derived cultures (Figure 2.5e,f, Table 2.2). We still did not observe increased OT-II proliferation upon incubating GFP^+ EGCs with Ovalbumin relative to no antigen controls in either sex (Figure 2.5g,h, Table 2.2). As a positive control, we performed OT-II cocultures using primary murine Bone Marrow-derived Dendritic Cells (BMDCs). As BMDCs are professional antigen presenting cells, we expected they would stimulate OT-II T cells, and indeed we observed robust proliferation of both OT-IIs upon incubating BMDCs with Ovalbumin (Figure 2.4f). These results suggest that EGCs are capable of functional *in vitro* antigen presentation on MHC I, but not MHC II.

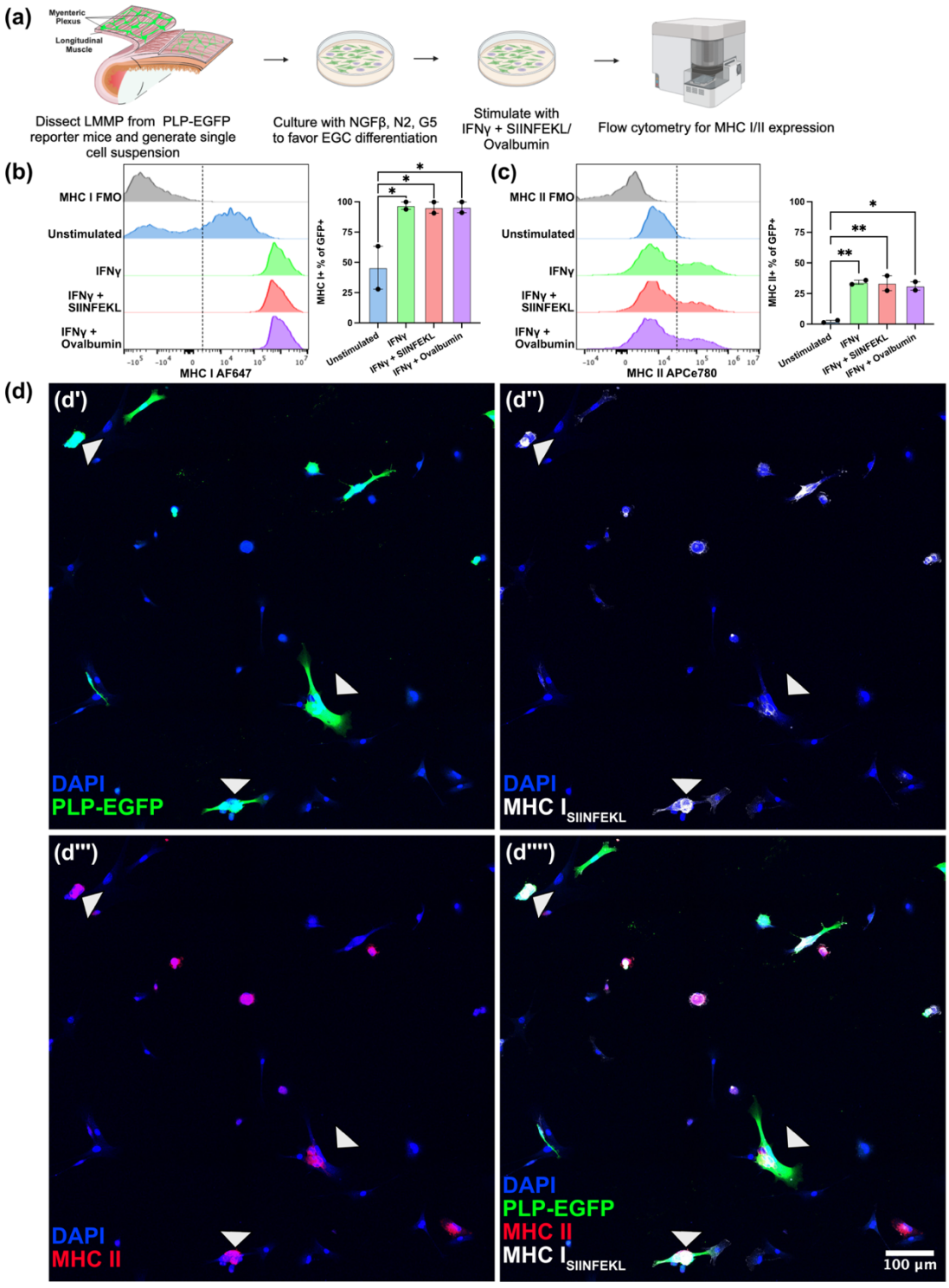

Figure 2.3 Legend on next page.

Figure 2.3 Interferon gamma induces MHC I and MHC II expression by EGCs *in vitro*

(a) Schematic showing EGC culture preparation and treatment. (b) Left: Histogram traces of MHC I expression by EGCs under each condition. Dashed line indicates gate set on FMO. Histograms are normalized to the mode and displayed as a percentage of the peak value. Right: Quantification of MHC I expression by EGCs under each condition. Results are expressed as mean ± SEM, N=2, n = 2 primary cultures/group (biological replicates). Ordinary one-way ANOVA and Dunnett's multiple comparisons test was used, *p < .05. (c) Left: Histogram traces of MHC II expression by EGCs under each condition. Dashed line indicates gate set on FMO. Histograms are normalized to the mode and displayed as a percentage of the peak value. Right: Quantification of EGC MHC II MFI under each condition. Results are expressed as mean ± SEM, N=2, n = 2 primary cultures/group (biological replicates). Ordinary one-way ANOVA and Dunnett's multiple comparisons test was used, *p < .05, ** p < .01. (d) Representative 20x magnification of IFNγ + SIINFEKL-treated GFP^+ EGCs (green) immunostained for SIINFEKL-bound MHC I (white), MHC II (red), and DAPI (blue). Arrowheads indicate MHC $I_{SIINFEKL}$, MHC II double positive EGCs. (d') Isolated DAPI and GFP staining. (d'') Isolated DAPI and MHC $I_{SIINFEKL}$ staining. (d''') Isolated DAPI and MHC II staining. (d'''') merged image of IFNγ + SIINFEKL-treated GFP^+ EGCs (green) stained for SIINFEKL-bound MHC I (white), MHC II (red), and DAPI (blue).

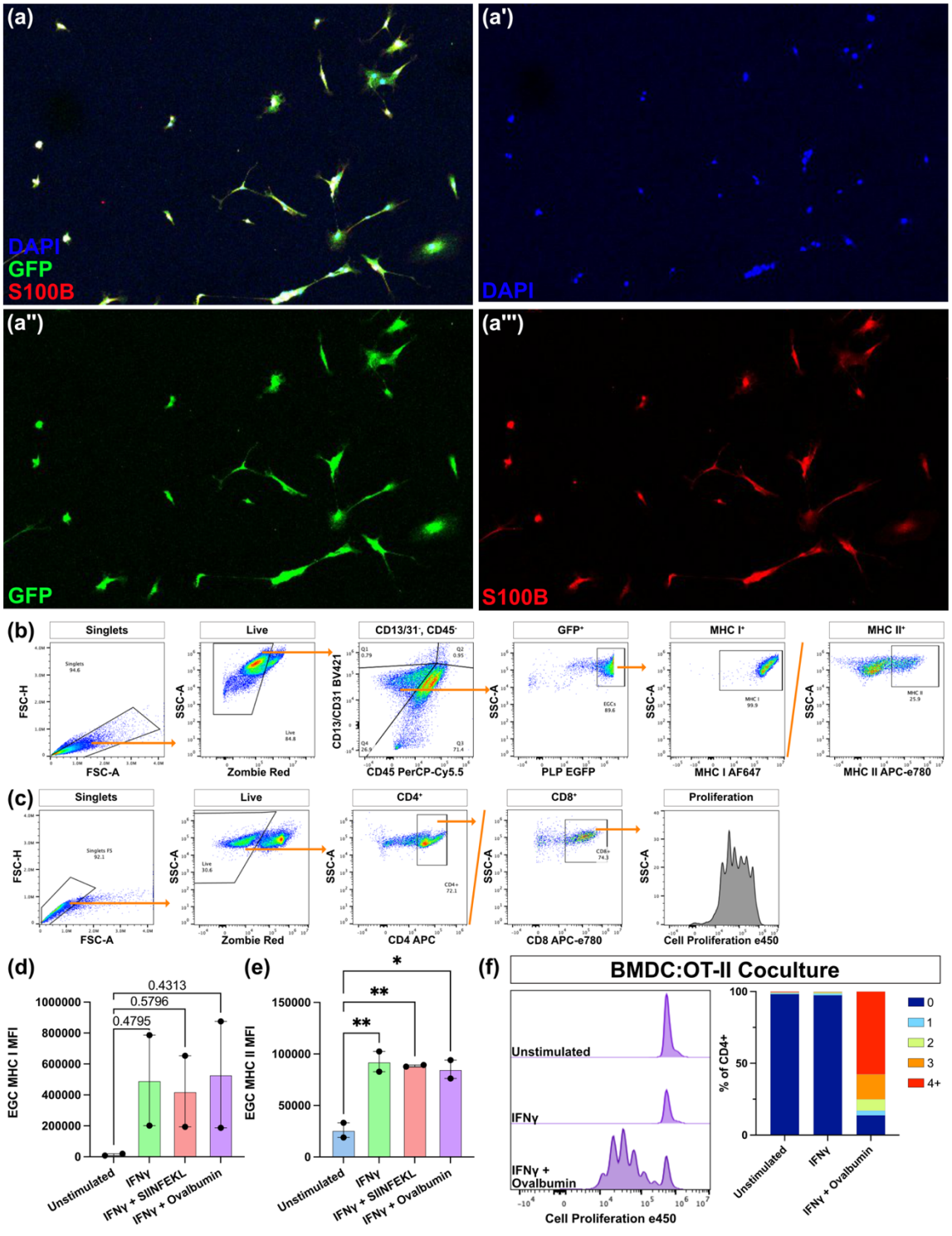

Figure 2.4 Legend on next page.

Figure 2.4 Primary EGC culture validation and BMDC:OT-II coculture

(a) Validation of primary EGC cultures – merged images for primary FACS-enriched EGC cultures stained with anti-GFP and anti-S100β. All GFP^+ cells co-express the EGC core marker S100β. (a') Isolated DAPI stain. (a'') Isolated GFP immunolabeling. (a''') Isolated S100B immunolabeling (b) Representative gating strategy for flow cytometry to detect EGC cell surface MHC I/II expression. (c) Representative gating strategy for flow cytometry to detect proliferation of OT-I/OT-II cells. (d) Quantification of EGC MHC I MFI under each condition, related to Figure 2b. Results are expressed as mean ± SEM, N=2, n = 2 primary cultures/group (biological replicates). Ordinary one-way ANOVA and Dunnett's multiple comparisons test was used. (e) Quantification of EGC MHC II MFI under each condition, related to Figure 2c. Results are expressed as mean ± SEM, N=2, n = 2 primary cultures/group (biological replicates). Ordinary one-way ANOVA and Dunnett's multiple comparisons test was used, *p < .05, **p<.01. (f) BMDC:OT-II coculture results. Left: Representative histogram traces showing OT-II proliferation events after coculture with EGCs under each condition. Histograms are normalized to the mode and displayed as a percentage of the peak value. Right: Quantification of fraction of proliferating OT-II T cells under each condition. n=1.

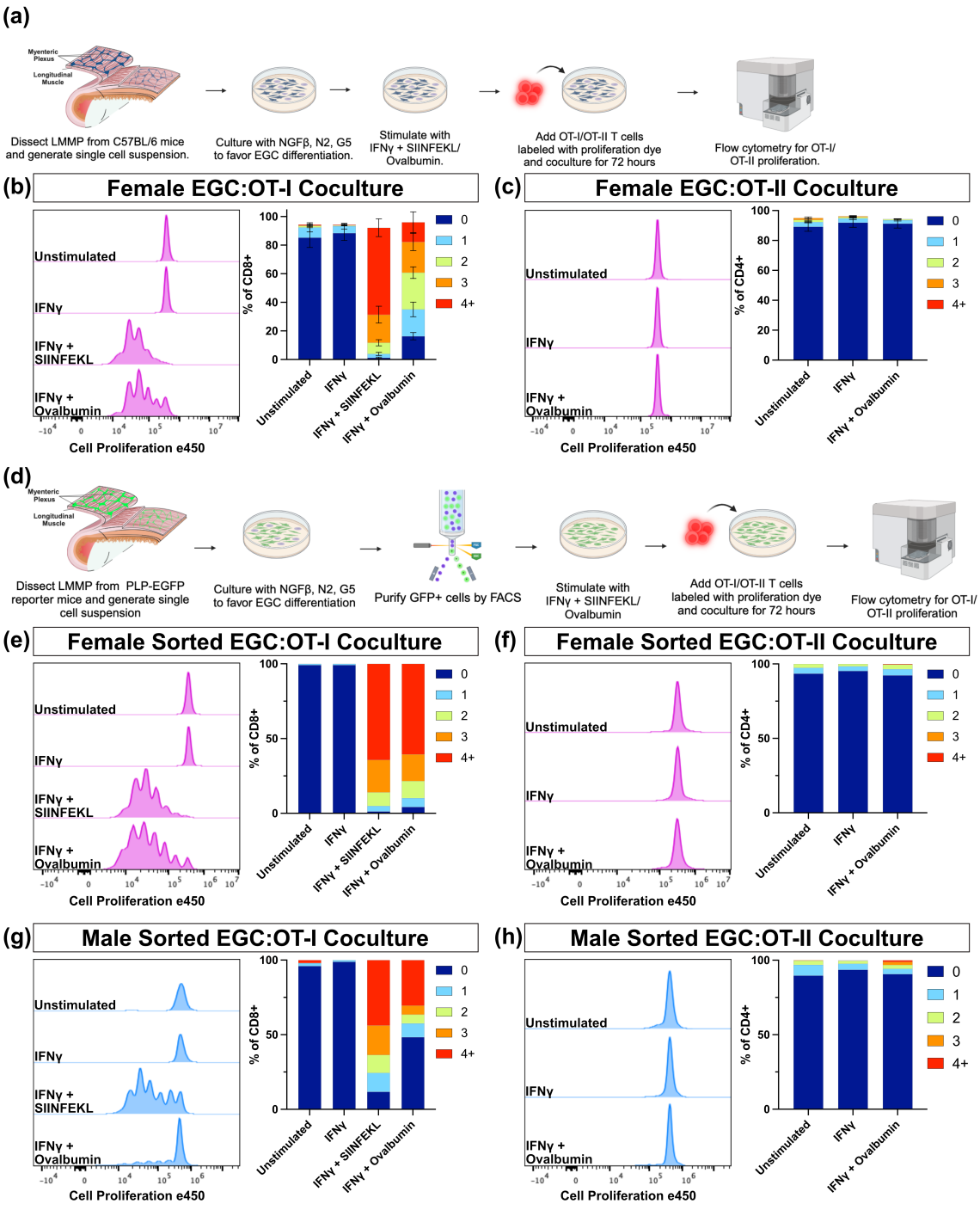

Figure 2.5 Legend on next page.

Figure 2.5 Primary murine EGCs are capable of antigen presentation on MHC I, but not MHC II

(a) Schematic showing EGC culture preparation, treatment and coculture. (b) Female EGC:OT-I coculture results. Left: Representative histogram traces showing OT-I proliferation events after coculture with EGCs under each condition. Histograms are normalized to the mode and displayed as a percentage of the peak value. Right: Quantification of fraction of proliferating OT-I T cells under each condition. N=3, n = 3 (biological replicates). (c) Female EGC:OT-II coculture results. Left: Representative histogram traces showing OT-II proliferation events after coculture with EGCs under each condition. Histograms are normalized to the mode and displayed as a percentage of the peak value. Right: Quantification of fraction of proliferating OT-II T cells under each condition. n=3 (biological replicates). (d) Schematic showing EGC culture preparation, FACS sorting, treatment, and coculture. (e) Female sorted GFP^+ EGC:OT-I coculture results. Left: Representative histogram traces showing OT-I proliferation events after coculture with EGCs under each condition. Histograms are normalized to the mode and displayed as a percentage of the peak value. Right: Quantification of fraction of proliferating OT-I T cells under each condition. n = 1. (f) Female sorted GFP^+ EGC:OT-II coculture results. Left: Representative histogram traces showing OT-II proliferation events after coculture with EGCs under each condition. Histograms are normalized to the mode and displayed as a percentage of the peak value. Right: Quantification of fraction of proliferating OT-II T cells under each condition. n=1. (g) Male sorted GFP^+ EGC:OT-I coculture results. Left: Representative histogram traces showing OT-I proliferation events after coculture with EGCs under each condition. Histograms are normalized to the mode and displayed as a percentage of the peak value. Right: Quantification of fraction of proliferating OT-I T cells under each condition. n =1. (h) Male sorted GFP^+ EGC:OT-II coculture results. Left: Representative histogram traces showing OT-II proliferation events after coculture with EGCs under each condition. Histograms are normalized to the mode and displayed as a percentage of the peak value. Right: Quantification of fraction of proliferating OT-II T cells under each condition. n=1.

	Female B6 EGC:OT-I				Female B6 EGC:OT-II		
Proliferation Events	Unstimulated	IFNγ	IFNγ + SIINFEKL	IFNγ + Ovalbumin	Unstimulated	IFNγ	IFNγ + Ovalbumin
0	99.1%	98.8%	2.08%	12.5%	95.2%	97%	97%
	79.6%	83.8%	0.87%	15.3%	84.9%	86.1%	86.6%
	77.2%	82.7%	0.78%	21.1%	87.6%	92.9%	90.4%
1	0.72%	0.88%	4.87%	10.6%	2.64%	1.93%	1.67%
	9.55%	7.07%	1.44%	17.6%	4.25%	1.98%	3.54%
	11.2%	6.64%	1.79%	28.1%	2.48%	4.42%	1.74%
2	0.097%	0.077%	12.1%	17.8%	0.16%	0.13%	0.14%
	1.43%	0.37%	5.82%	27.8%	2.32%	1.98%	1.18%
	1.7%	1%	5.44%	31.5%	1.86%	0.44%	0.43%
3	0%	0%	31.3%	30.6%	0%	0.032%	0.015%
	0.32%	0.37%	15.2%	23.8%	1.16%	1.32%	0%
	0.52%	0.27%	12.4%	9.98%	2.48%	0.44%	0.43%
4+	0%	0%	48.5%	27.8%	0%	0%	0%
	0.8%	0.58%	67.6%	10.2%	0%	0%	0%
	1.17%	0.86%	66.4%	3.52%	0%	0%	0%

Table 2.1 C57BL/6 EGC coculture OT:I/OT:II proliferation quantification - related to Figure 2.5

	Female Sorted EGC:OT-I				Male Sorted EGC:OT-I				Female Sorted EGC:OT-II			Male Sorted EGC:OT-II		
	Unstim	IFNγ	IFNγ + SIINFEKL	IFNγ + Ovalbumin	Unstim	IFNγ	IFNγ + SIINFEKL	IFNγ + Ovalbumin	Unstim	IFNγ	IFNγ + Ovalbumin	Unstim	IFNγ	IFNγ + Ovalbumin
0	99.22 %	99.23 %	1.31%	4.32%	96.08 %	98.89 %	11.78 %	48.41 %	93.56 %	95.26 %	92.34%	89.67 %	93.59 %	90.71 %
1	0.78 %	0.77%	3.67%	5.90%	1.96 %	1.11%	12.71 %	9.24%	3.92 %	3.23%	4.21%	7.32 %	4.14%	3.57%
2	0.00 %	0.00%	9.06%	11.38 %	0%	0%	12.01 %	5.85%	2.52 %	1.51%	3.07%	2.75 %	1.87%	2.62%
3	0.00 %	0.00%	21.63 %	17.89 %	0%	0%	19.7%	6.03%	0.00 %	0.00%	0.00%	0.26 %	0.27%	1.99%
4+	0.00 %	0.00%	64.33 %	60.51 %	1.96 %	0%	43.8%	30.43 %	0.00 %	0.00%	0.38%	0.00 %	0.13%	1.10%

Table 2.2 PLP-EGFP sorted EGC coculture OT:I/OT:II proliferation quantification - related to Figure 2.5

2.4.5 Enteric Glial Cells Express MHC I, but not MHC II during DSS colitis

To interrogate EGC antigen presentation *in vivo*, we utilized the Dextran Sodium Sulfate (DSS) colitis model. We chose this model of intestinal inflammation since EGCs upregulate antigen presentation machinery in human IBD. We subjected male PLP-EGFP reporter mice to two one-week treatments with 2.5% DSS in drinking water with a two-week recovery period in between treatments. We chose male mice as they present with more robust disease compared to females [204]. At the end of the second treatment, mice were euthanized to perform flow cytometry on isolated large intestine (Figure 2.6a). We gated out $CD45^+$ immune cells and autofluorescent cells prior to gating of GFP^+ EGCs. We probed for MHC I/II expression on EGCs, as well as $CD45^+$ immune cells as an internal positive control (Figure 2.6b). We observed a modest yet insignificant increase in the percentage of EGCs that expressed MHC I (Naïve mean = 29.73 ± 0.69%; DSS mean = 39.68 ± 6.48%, p = .1176) (Supplementary 3c,d, top) as well as EGC MHC I MFI (Naïve mean = 11404 ± 212.4 A.U.; DSS mean = 12918 ± 709.6 A.U., p = .0869) (Figure 2.6c,d;bottom). Meanwhile, nearly all $CD45^+$ cells expressed MHC I at baseline as anticipated – this was not changed in DSS (Naïve mean = 88.48 ± 3.599%; DSS mean = 92.63 ± 2.764%, p = .3957) (Figure 2.6c,e;top), nor was the MFI of CD45 MHC I (Naïve mean = 50059 ± 4864 A.U.; DSS mean = 47388 ± 3195 A.U., p = .6624) (Figure 2.6c,e;bottom). We observed fewer than 5% of EGCs were $MHC\ II^+$ in either condition (Naïve mean = 4.35 ± .2691%; DSS mean = 4.858 ± 1.409%, p = .7356) (Figure 2.6f,g;top) with no significant difference in EGC MHC II MFI (Naïve mean = 9863 ± 776.9 A.U., DSS mean = 8713 ± 328.8 A.U., p = .2218) (Figure 2.6f,g;bottom). There was also no significant change in the percent of $CD45^+$ cells that were $MHC\ II^+$ (Naïve mean = 62.33 ± 4.57%; DSS mean = 63.7 ± 5.456**%,** p = .8532) (Figure 2.6f,h;top) nor CD45 MHC II MFI (Naïve mean = 109536 ± 21462, DSS mean = 100430 ± 12642, p =.7272) (Figure 2.6f,h;bottom). Notably, the MFI of CD45 MHC II expression was about tenfold higher than EGC MHC II expression. These results indicate that EGCs do not express cell surface MHC II at a detectable level during DSS colitis.

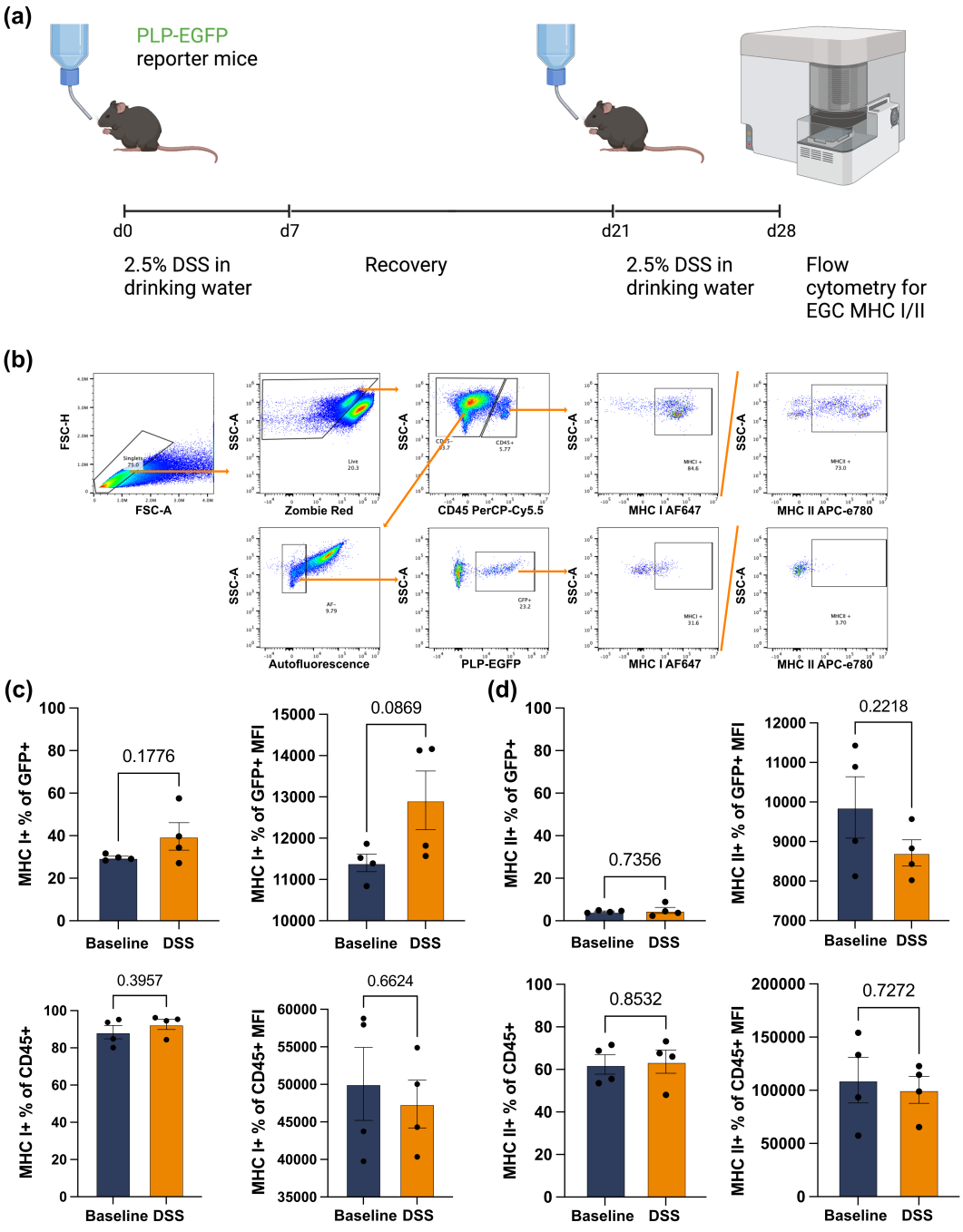

Figure 2.6 Legend on next page.

Figure 2.6 EGCs modestly upregulate MHC I and do not appear to express MHC II during DSS colitis

(a) Schematic of DSS administration timeline. (b) Representative gating strategy for flow cytometry probing for MHC I/II expression by EGCs and CD45$^+$ immune cells. (c) Histogram traces of MHC I expression by CD45$^+$ immune cells and GFP$^+$ EGCs in naïve and DSS-treated mice measured by flow cytometry. Dotted line indicates positive gate set on FMOs. Histograms are normalized to the mode and displayed as a percentage of the peak value. (d) Quantification of MHC I expression by CD45$^+$ immune cells. Top: Percentage of CD45$^+$ cells that are MHC I$^+$. Bottom: CD45$^+$ MHC I Mean Fluorescence Intensity. Unpaired student's t-test was used, N=1, n =4 mice/group. (e) Quantification of MHC I expression by GFP$^+$ enteric glial cells. Top: Percentage of GFP$^+$ cells that are MHC I$^+$. Bottom: GFP$^+$ MHC I Mean Fluorescence Intensity. Unpaired student's t-test was used, N=1, n =4 mice/group. (f) Histogram traces of MHC II expression by CD45$^+$ immune cells and GFP$^+$ EGCs in naïve and DSS-treated mice measured by flow cytometry. Dotted line indicates positive gate set on FMOs. Histograms are normalized to the mode and displayed as a percentage of the peak value. (g) Quantification of MHC II expression by CD45$^+$ immune cells. Top: Percentage of CD45$^+$ cells that are MHC II$^+$. Bottom: CD45$^+$ MHC II Mean Fluorescence Intensity. Unpaired student's t-test was used, n =4 mice/group.

2.4.6 Acute *Toxoplasma gondii* infection as a model of T-cell mediated intestinal inflammation

As adaptive immunity is not required for the development of DSS-induced colitis [205], we utilized acute *Toxoplasma gondii* infection as a model for robust intestinal inflammation marked by a Th1 CD4$^+$ T cell response [206]. We infected female PLP-EGFP reporter mice with 20 cysts per mouse of *Toxoplasma gondii* strain Me49 [207] via oral gavage. We chose female mice as they display a more robust immune response during *T. gondii* infection compared to males [208]. Eight days later, we sacrificed the mice to perform flow cytometry, qPCR, and immunofluorescence on isolated intestines as well as spleen and mesenteric lymph nodes (Figure 2.7a, Figure 2.6a). We observed significantly elevated serum IFNγ levels

in *T. gondii*-gavaged mice (Naïve mean = 0; *T. gondii* mean = 7864 ± 1430 pg/mL, $p < .0001$) (Figure 2.7b), confirming the infection was successful. We also detected *T. gondii*-specific *Act1* gene expression by qPCR in ~2mm colon samples isolated from *T. gondii*-infected mice – though this was not statistically significant relative to control samples, it suggests that there is active parasite throughout the large intestine (Naïve mean = 1 ± .3151 A.U.; *T. gondii* mean = 63.93 ± 41.06 A.U., $p = .1862$) (Figure 2.7c).

To further probe for elevated intestinal immunity, we performed qPCR for several inflammatory cytokines in the colon and distal ileum (Figure 2.7d). In the colon, we observed significant upregulation of *Ifng* (Naïve mean = 1 ± .9084 A.U.; *T. gondii* mean = 24.25 ± 2.962 A.U., $p < .0001$), *Tnf* (Naïve mean = 1 ± .3473 A.U.; *T. gondii* mean = 2.378 ± .3206 A.U., $p = .0137$), and *Il33* (Naïve mean = 1 ± .2755 A.U.; *T. gondii* mean = 4.574 ± 1.056 A.U., $p = .0113$). We observed a trend towards increased *Il1b* expression (Naïve mean = 1 ± .5389 A.U.; *T. gondii* mean = 3.116 ± .8710 A.U., $p = .0733$), with no changes in *Il6* (Naïve mean = 1 ± .2987 A.U.; *T. gondii*

mean = 2.119 ± .6241 A.U., p = .1544) and *Il17a* (Naïve mean = 1 ± .2299 A.U.; *T. gondii* mean = .7761 ± .1704 A.U., p = .4702). In the distal ileum, we observed significant upregulation of *Ifng* (Naïve mean = 1 ± .6968 A.U.; *T. gondii* mean = 23.26 ± 4.866 A.U., p = .0015), with trends towards increased expression of *Il1b* (Naïve mean = 1 ± .3948 A.U.; *T. gondii* mean = 2.734 ± .7519 A.U., p = .0786) and *Il17a* (Naïve mean = 1 ± .2982 A.U.; *T. gondii* mean = 2.109 ± .4457 A.U., p = .0891). Meanwhile, we observed no changes in *Tnf* (Naïve mean = 1 ± .2087 A.U.; *T. gondii* mean = 3.626 ± 1.345 A.U., p = .1368), *Il33* (Naïve mean = 1 ± .2752 A.U.; *T. gondii* mean = .5049 ± .1371 A.U., p = .1197), and *Il6* (Naïve mean = 1 ± .1859 A.U.; *T. gondii* mean = 3.338 ± 1.261 A.U., p = .1186).

For immunophenotyping by flow cytometry, we performed a similar gating strategy as previously, with the addition of CD11b to look for myeloid cells and CD4/CD8/CD69 for T cell activation (Figure 2.9a). We observed significantly increased $CD4^+$ and $CD8^+$ T cell activation in the spleen (Activated $CD4^+$ T cells: Naïve mean = 21.25 ± 1.664%; *T. gondii* mean = 57.03 ± 2.385%, p < .0001; Activated $CD8^+$ T cells: Naïve mean = 20.42 ± 3.447%; *T. gondii* mean = 55.84 ± 2.22%, p < .0001), mesenteric lymph nodes (Activated $CD4^+$ T cells: Naïve mean = 33.58 ± 2.662%; *T. gondii* mean = 65.17 ± 5.198%, p = .0003; Activated $CD8^+$ T cells: Naïve mean = 23.88 ± 1.845%; *T. gondii* mean = 68.59 ± 2.937%, p < .0001), and colon (Activated $CD4^+$ T cells: Naïve mean = 41.12 ± 3.87%; *T. gondii* mean = 62.96 ± 4.392%, p = .0057; Activated $CD8^+$ T cells: Naïve mean = 35.56 ± 7.38%; *T. gondii* mean = 84.63 ± 3.98%, p < .0001) (Figure 2.7e). Together, these results demonstrate robust intestinal inflammation and T cell activation occurs in the colon of *T. gondii* infected mice at day 8, validating our choice of model to interrogate EGC antigen presentation.

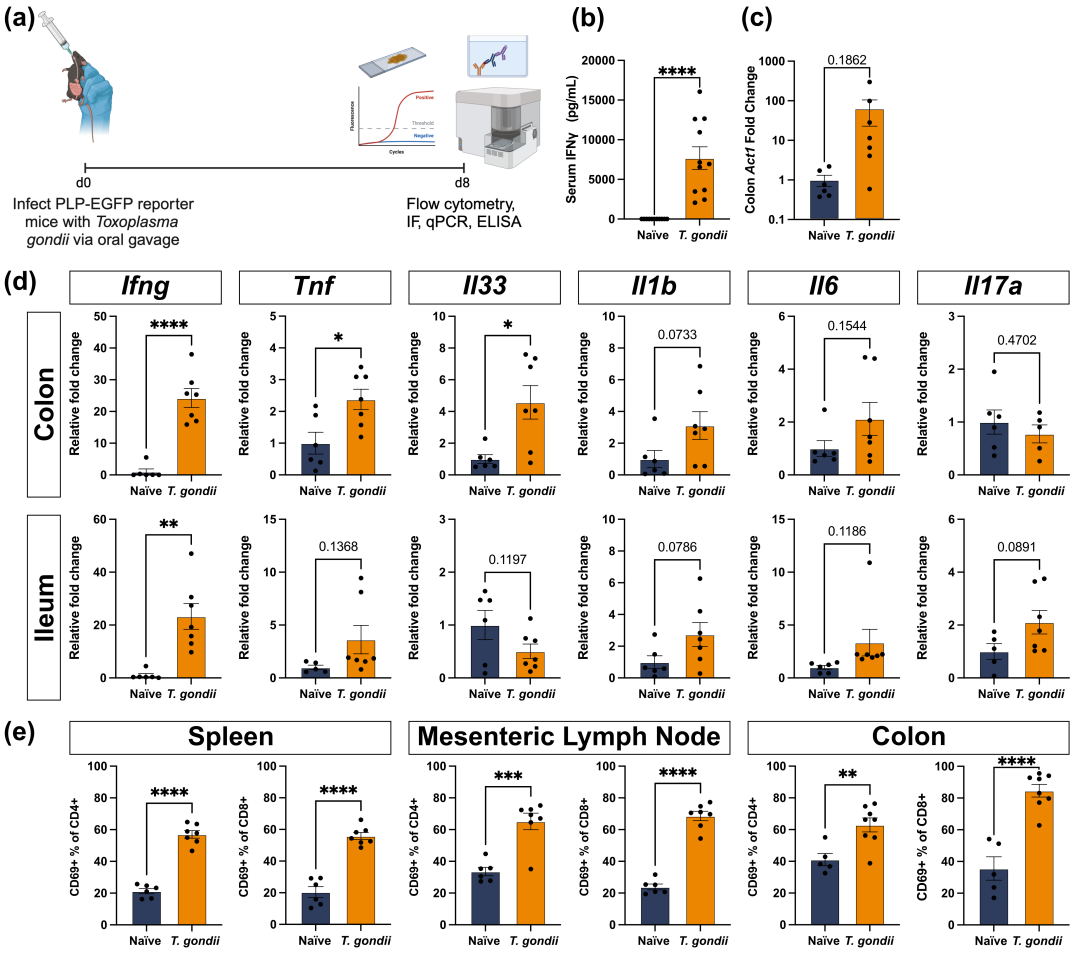

Figure 2.7 Acute Toxoplasma gondii infection as a model of T-cell mediated intestinal inflammation

(a) Schematic showing *T. gondii* infection timeline and downstream tissue processing. (b) Serum IFNγ levels measured by ELISA. Unpaired student's t-test was used, ****p < .0001, N=2, n=11 mice/group. (b) *T. gondii* specific *Act1* gene expression measured by qPCR. Unpaired student's t-test was used, n =5-7 mice/group. (c) qPCR analysis for inflammatory cytokines in the colon (top) or distal ileum (bottom). Unpaired student's t-test was used, *p < .05, **p < .01, ****p < .0001, N=2, n = 6-7 mice/group. (e) CD4 and CD8 T cell expression of the activation marker CD69 in the spleen (left), mesenteric lymph node (middle) and colon (right) measured by flow cytometry. Unpaired student's t-test was used, **p < .01, ***p < .001, **** p < .0001, N=2, n= 5-7 mice/group.

2.4.7 EGCs express MHC I, but not MHC II during acute *Toxoplasma gondii* infection

As anticipated, nearly 100% of CD11b$^+$ myeloid cells were MHC I$^+$ regardless of condition (Naïve mean = 99.50 ± .1401%; *T. gondii* mean = 99.61 ± .1390%, p = .5894) (Figure 2.8a,b;top), though CD11b$^+$ MHC I MFI was significantly increased during *T. gondii* infection (Naïve mean = 79068 ± 15260 A.U.; *T. gondii* mean = 164822 ± 17780 A.U., p = .0016) (Figure 2.8a,b;bottom). We observed a significant

increase in the percent of MHC I$^+$ EGCs (Naïve mean = 62.75 ± 8.242%; *T. gondii* mean = 95.86 ± 1.315%, p = .0005) (Figure 2.8a,c;top) and EGC MHC I MFI (Naïve mean = 28905 ± 3552 A.U.; *T. gondii* mean = 82078 ± 9251 A.U., p < .0001) (Figure 2.8a,c;bottom). We also observed a significant increase in the percent of autofluorescent cells that expressed MHC I (Naïve mean = 58.26 ± 10.51%; *T. gondii* mean = 93.63 ± 2.338%, p = .0026) (Figure 2.9b;left, middle). Autofluorescent cells also showed a significant increase in MHC MFI during *T. gondii* infection (Naïve mean = 11102 ± 2162 A.U.; *T. gondii* mean = 32544 ± 6168 A.U., p = .0065) (Figure 2.9b;left, right). We observed a significant increase in MHC II expression by CD11b$^+$ myeloid cells (Naïve mean = 57.30 ± 2.498%; *T. gondii* mean = 68.66 ± 3.985%, p = .0278) (Figure 2.8d,e;top), though there was no significant difference in CD11b$^+$ MHC II MFI (Naïve mean = 253991 ± 36455 A.U.; *T. gondii* mean = 209226 ± 27685 A.U., p = .3343) (Figure 2.8d,e;bottom). We observed a fraction of EGCs that were MHC II$^+$ in Naïve mice and this was significantly increased during *T. gondii* infection (Naïve mean = 12.46 ± 2.789%; *T. gondii* mean = (Naïve mean = 57.30 ± 2.498%; *T. gondii* mean = 68.66 ± 3.985%, p = .0278) (Figure 2.8d,e;top), 36.18 ± 6.281%, p = .0031) (Figure 2.8d,f;top), as well as EGC MHC II MFI (Naïve mean = 14895 ± 629.2 A.U.; *T. gondii* mean = 37726 ± 4637 A.U., p = .0001) (Figure 2.8d,f;bottom). EGC MHC II MFI in infected mice was 5-fold lower than the one observed in CD11b$^+$ cells. We observed very little baseline expression of MHC II by autofluorescent cells in naïve mice, but it was significantly induced during *T. gondii* infection (Naïve mean = 3.015 ± .9089%; *T. gondii* mean = 83.67 ± 4.009%, p < .0001) (Figure 2.9c;left, middle). Autofluorescent cells also showed significantly increased MHC II MFI during infection (Naïve mean = 39669 ± 3539 A.U.; *T. gondii* mean = 75128 ± 9642 A.U., p = .0032) (Figure 2.9c;left, right).

To further interrogate MHC II expression by EGCs during *T. gondii* infection, we performed immunofluorescent staining of naïve and infected colons, staining for GFP, the myeloid cell marker Iba1, and MHC II (Figure 2.8f,g). Line profile traces in the myenteric plexus and mucosa both showed that in either condition the peaks of MHC II signal intensity appear to closely overlap with that of Iba1 signal intensity, whereas MHC II and GFP signal do not appear to strongly overlap (Figure 2.8f;bottom,g;bottom), which is also observed in 3D renderings (Figure 2.10). Furthermore, we observed increased MHC II coverage in the myenteric plexus (Naïve mean = 1.798 ± .1287%; *T. gondii* mean = 5.04 ± .6049%, p = .0019) (Figure 2.8h;left), though MHC II signal intensity was unchanged (Naïve mean = 90.52 ± 1.012 A.U.; *T. gondii* mean = 91.43 ± 3.164 A.U., p = .7952) (Figure 2.8h;middle). In the mucosa, with observed no significant difference in MHC II coverage (Naïve mean = .9768 ± .3081%; *T. gondii* mean = 1.177 ± .2150%, p = .6128) (Figure 2.8i;left) or signal intensity (Naïve mean = 147.1 ± 3.123 A.U.; *T. gondii* mean = 146.5 ± 1.528 A.U., p = .8672) (Figure 2.8i;middle). To quantitatively assess MHC II/Iba1 and MHC II/GFP colocalization, we determined the Mander's colocalization coefficient of MHC II overlapping with either GFP or Iba1 in colon samples regardless of condition. We observed a significantly higher colocalization coefficient between

MHCII/Iba1 compared to MHC II/GFP in the myenteric and submucosal plexuses (MHC II/GFP mean = .2249 ± .02581 A.U.; MHC II/Iba1 mean = .5955 ± .05025 A.U., $p < .0001$) (Figure 2.8h;right) as well as in the mucosa (MHC II/GFP mean = .08913 ± .01576; MHC II/Iba1 mean = .6845 ± .04842, $p < .0001$) (Figure 2.8i;right) of the large intestine. These results support our conclusion that EGCs do not express MHC II during intestinal inflammation.

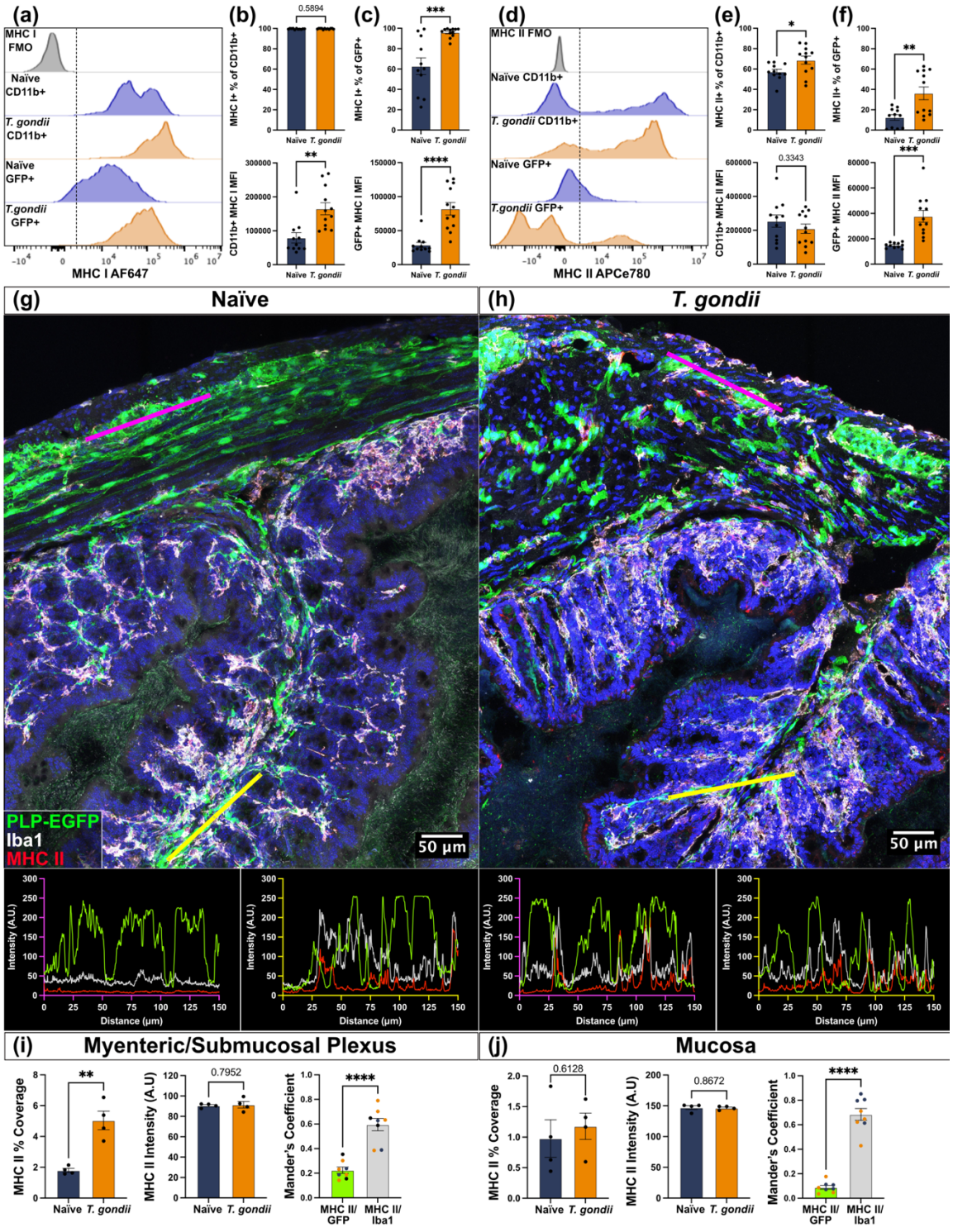

Figure 2.8 Legend on next page.

Figure 2.8 EGCs express MHC I, but not MHC II during acute *Toxoplasma gondii* infection

(a) Histogram traces of MHC I expression by $CD11b^+$ myeloid cells and GFP^+ EGCs in naïve and *T. gondii* infected mice measured by flow cytometry. Dotted line indicates positive gate set on FMOs. Histograms are normalized to the mode and displayed as a percentage of the peak value. (b) Quantification of MHC I expression by $CD11b^+$ myeloid cells. Top: Percentage of $CD11b^+$ cells that are MHC I^+. Bottom: $CD11b^+$ MHC I Mean Fluorescence Intensity. Unpaired student's t-test was used, $^{**}p < .01$, N=3, n = 11-12 mice/group. (c) Quantification of MHC I expression by GFP^+ Enteric Glial cells. Top: Percentage of GFP^+ cells that are MHC I^+. Bottom: GFP^+ MHC I Mean Fluorescence Intensity. Unpaired student's t-test was used, $^{***}p < .001$, $^{****}p < .0001$, N=3, n = 11-12 mice/group. (d) Histogram traces of MHC II expression by $CD11b^+$ myeloid cells and GFP^+ EGCs in naïve and *T. gondii* infected mice measured by flow cytometry. Dotted line indicates positive gate set on FMOs. Histograms are normalized to the mode and displayed as a percentage of the peak value. (e) Quantification of MHC II expression by $CD11b^+$ myeloid cells. Top: Percentage of $CD11b^+$ cells that are MHC II^+. Bottom: $CD11b^+$ MHC II Mean Fluorescence Intensity. Unpaired student's t-test was used, $^{*}p < .05$, N=3, n = 11-12 mice/group. (f) Quantification of MHC II expression by GFP^+ Enteric Glial cells. Top: Percentage of GFP^+ cells that are MHC II^+. Bottom: GFP^+ MHC II Mean Fluorescence Intensity. Unpaired student's t-test was used, $^{**}p < .01$, $^{***}p < .001$, N=3, n = 11-12 mice/group. (g,h) Immunofluorescence analysis for GFP, Iba1, and MHC II in the colon of *T. gondii* and uninfected mice. (g) Top: 63x magnification of representative uninfected colon. Bottom left: Profile plot demonstrating fluorescence intensity across the magenta line in the myenteric plexus in f. Bottom right: Profile plot demonstrating fluorescence intensity across the yellow line in the mucosa in f. (h) Top: 63x magnification of representative *T. gondii* infected colon. Bottom left: Profile plot demonstrating fluorescence intensity across the magenta line in the myenteric plexus in g. Bottom right: Profile plot demonstrating fluorescence intensity across the yellow line in the mucosa in g. (i) Left: MHC II percent coverage in the myenteric and submucosal plexuses. Middle: MHC II mean grey value (intensity) in the myenteric plexus. Right: Mander's colocalization coefficient between MHC II/GFP and MHC II/Iba1 in the myenteric and submucosal plexuses. Unpaired student's t-test was used, $^{**}p < .01$, $^{****}p < .0001$, N=2, n=4 mice/group for MHC II coverage/intensity, n=8 mice/group for colocalization. (j) Left: MHC II percent coverage in the mucosa. Middle: MHC II mean grey value (intensity) in the mucosa. Right: Mander's colocalization coefficient between MHC II/GFP and MHC II/Iba1 in the mucosa. Unpaired student's t-test was used, $^{****}p < .0001$, N=2, n=4 mice/group for MHC II coverage/intensity, N=2, n=8 mice/group for colocalization.

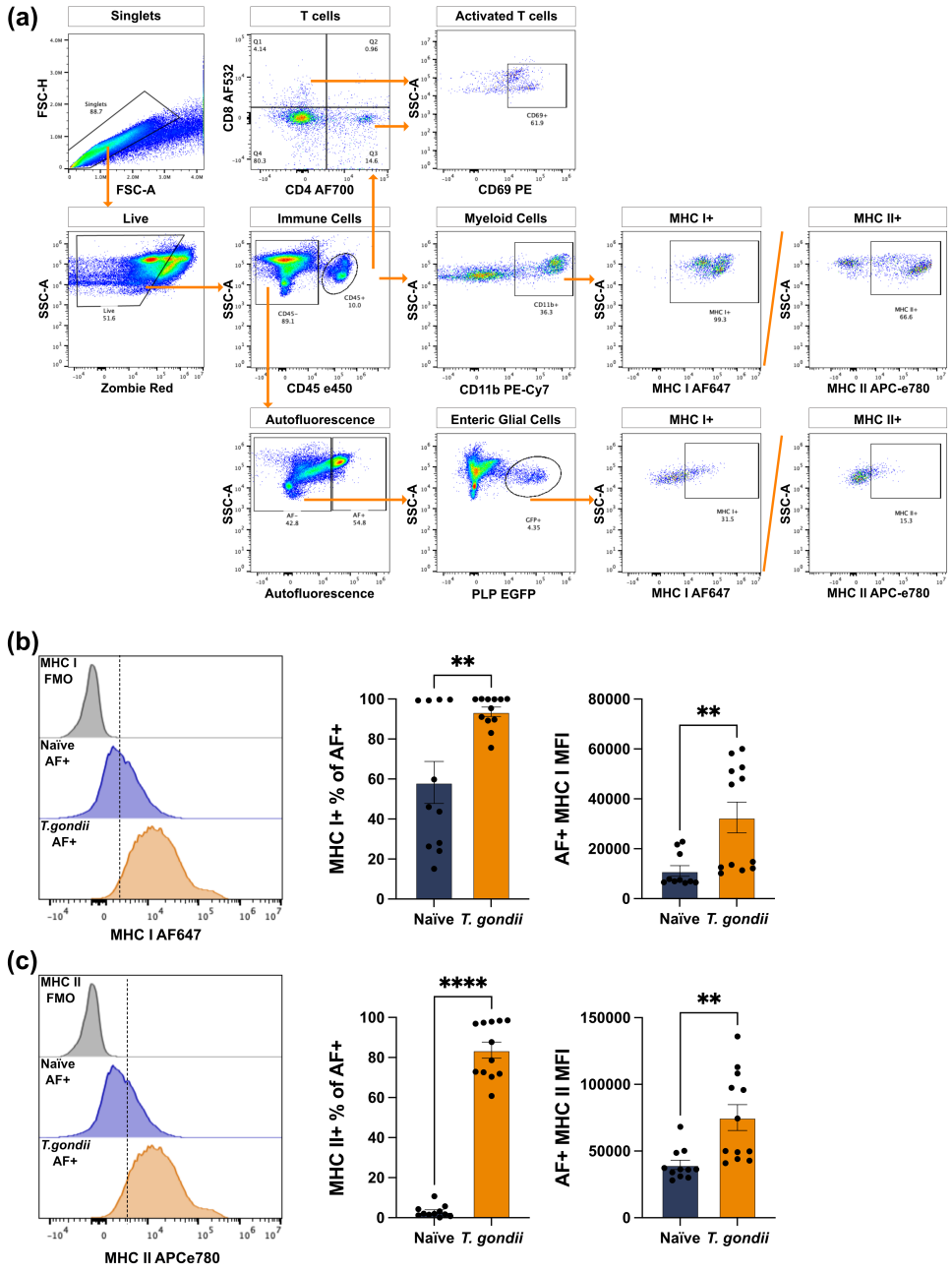

Figure 2.9 Legend on next page.

Figure 2.9 *T. gondii* flow cytometry gating strategy and epithelial cell MHC II expression

(a) Representative gating strategy for flow cytometry probing for T cell activation and MHC I/II expression by EGCs, Iba1$^+$ myeloid cells, and autofluorescent cells. (b) Left: Histogram traces of MHC I expression by autofluorescent cells in naïve and *T. gondii*-infected mice measured by flow cytometry. Dotted line indicates positive gate set on FMOs. Histograms are normalized to the mode and displayed as a percentage of the peak value. Middle: Quantification of MHC I expression by autofluorescent cells. Right: Autofluorescent cell MHC I Mean Fluorescence Intensity. Unpaired student's t-test was used, p**< .01, p**** < .0001, N=3, n = 11-12 mice/group. (c) Left: Histogram traces of MHC II expression by autofluorescent cells in naïve and *T. gondii*-infected mice measured by flow cytometry. Dotted line indicates positive gate set on FMOs. Histograms are normalized to the mode and displayed as a percentage of the peak value. Middle: Quantification of MHC II expression by autofluorescent cells. Right: Autofluorescent cell MHC II Mean Fluorescence Intensity. Unpaired student's t-test was used, p** < .01, N=3, n = 11-12 mice/group.

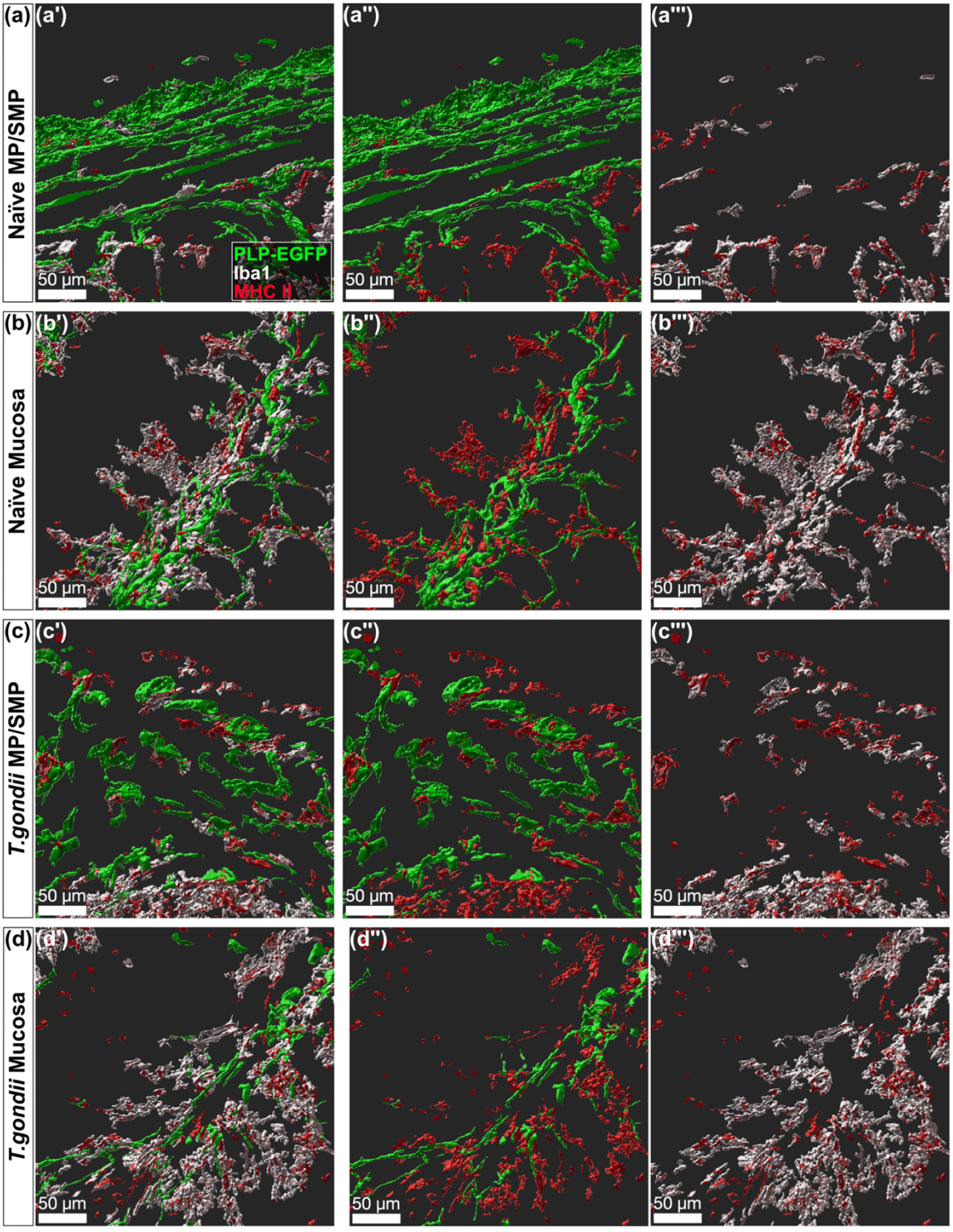

Figure 2.10 Legend on next page.

Figure 2.10 MHC II immunostaining 3D rendering

(a) 3D rendering of PLP1, IBA1, and MHC II immunostaining in Naïve Myenteric and Submucosal Plexuses, related to Figure 2.8g. (a') PLP1, IBA1, MHC II merged image. (a'') Isolated PLP1 and MHC II. (a''') Isolated IBA1 and MHC II. (b) 3D rendering of PLP1, IBA1, and MHC II immunostaining in Naïve Mucosa, related to Figure 2.8g. (b') PLP1, IBA1, MHC II merged image. (b'') Isolated PLP1 and MHC II. (b''') Isolated IBA1 and MHC II. (c) 3D rendering of PLP1, IBA1, and MHC II immunostaining in Naïve Myenteric and Submucosal Plexuses, related to Figure 2.8g. (c') PLP1, IBA1, MHC II merged image. (c'') Isolated PLP1 and MHC II. (c''') Isolated IBA1 and MHC II. (d) 3D rendering of PLP1, IBA1, and MHC II immunostaining in Naïve Mucosa, related to Figure 2.8g. (d') PLP1, IBA1, MHC II merged image. (d'') Isolated PLP1 and MHC II. (d''') Isolated IBA1 and MHC II.

2.5 Discussion

In this study, we examined the ability of murine Enteric Glial Cells to act as antigen presenting cells on both MHC I and MHC II. To this end, we utilized *in vitro* antigen presentation assays to assess the capacity of EGCs to engage in functional antigen presentation, as well as using spectral flow cytometry and confocal microscopy to assess EGC MHC I/II expression during intestinal inflammation. Together our results suggest that Enteric Glial Cells are capable of functional antigen presentation *in vitro* on MHC I, but not on MHC II. Meanwhile, EGCs appear to modestly induce low-level cell surface MHC II expression in an acute *T. gondii* infection model which presents with robust type I immunity and T cell activation in the large intestine (Figure 2.11).

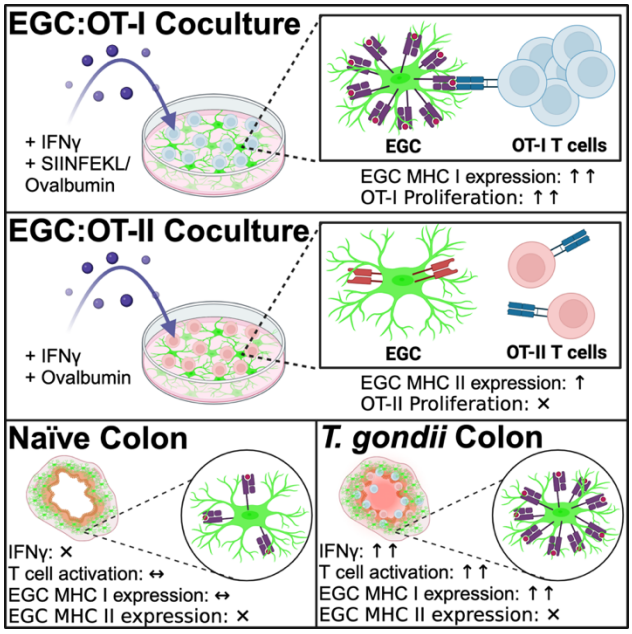

Figure 2.11 Summary of experimental results

Previous studies have suggested a putative role of EGCs acting as nonconventional antigen presenting cells via MHC II [179,180,199]. The study described by Geboes et al. reports MHC II expression by enteric glial cells in ileum biopsy samples derived from patients with Crohn's Disease – however the study is limited to analysis of singleplex immunohistochemistry staining which did not include any EGC-specific markers. Instead, EGCs (referred to as 'Enteroglial cells') were identified based on morphological characteristics. This level of resolution does not well distinguish between EGCs and closely associated muscularis macrophages – in fact the authors report 'strong' enteroglial MHC II staining positivity in lesions where macrophages are involved but reduced staining positivity in lesions where macrophages are uninvolved. The study described by Barcelos Morais da Silveira et

al. reports MHC II expression by enteric glial cells in colon samples derived from patients with Chagas disease – a condition caused by *Trypanosoma cruzi* infection that can lead to abnormal dilation of the colon (megacolon). The authors report MHC II expression by ~15% of EGCs in myenteric and submucosal ganglia – however it is not clearly reported how coexpression was determined and furthermore the authors do not account for closely associated muscularis macrophages. Still, our analysis of publicly available scRNAseq data from IBD patients suggests EGC transcript level expression of MHC II alleles and other genes involved in class II antigen presentation. It remains unclear whether this is observed at the protein level and more importantly whether human EGCs are capable of functional antigen presentation on MHC II. Several possible explanations could account for the discrepancies observed between our observations of EGC MHC II transcript expression yet no functional MHC II-mediated antigen presentation. MHC II posttranslational modifications could be a potential factor as MHC II ubiquitination is integral in regulating MHC II cell surface expression in professional APCs [209]. Another potential factor could be lack of expression of costimulatory molecules by EGCs – for instance endothelial cells are reported to not express the costimulatory molecules CD80 and CD86 and thus cannot activate naïve $CD4^+$ T cells, though they are reported to express other costimulatory molecules to activate effector memory $CD4^+$ T cells [210]. Future studies should interrogate costimulatory/coinhibitory molecule expression in EGCs. Furthermore, another possible explanation to reconcile the dichotomy related to MHC II expression could be linked to a difference between murine and human EGCs as several facets of immunity are unique to either species [211]. Such dichotomies in MHC II expression have been reported in other cell types, as most human endothelial cells constitutively express MHC II whereas mouse endothelial cells only express MHC II upon inflammation [210]. Future studies should aim to interrogate functional antigen presentation in developing experimental models of human enteric glia [212].

In mice, Chow, et al. reports MHC II expression in murine EGCs by immunofluorescent staining following delivery of LPS and IFNγ. Again, the authors here do not perform co-staining of closely associated muscularis macrophages to rule out MHC II signal coming from neighboring cells. Furthermore, the authors do not detect changes in expression of the class II transactivator (*Ciita*) in LPS/IFNγ treated EGCs, which is an essential regulator of MHC II expression [213]. The authors also knockout MHC II in Sox10 expressing cells and report a decrease in $CD4^+$ T cell activation in the mesenteric lymph node. As Sox10 is expressed by several cell types it is unclear if this reduction is attributed to EGCs.

Our study is the first to assess functional antigen presentation in primary murine EGC cultures. We note that all primary culture models have limitations in that the heterogeneity observed *in vivo* may not be sustained in culture but chose this approach as an initial characterization prior to further investigations *in vivo*. The method we used for deriving primary EGC cultures has been firmly established and

well-characterized [5,135]. It has been described that cultured primary murine EGCs possess neurogenic potential and generate mixed neuron-glia cultures by 20 days *in vitro* (DIV), and it is postulated that inflammatory cytokines such as IFNγ might inhibit this process [135]. To this end, we conducted all *in vitro* experiments after 7-10 DIV. We are confident that our primary cultured cells are indeed EGCs as they express core markers S100B and PLP1 and are responsive to IFNγ. Interestingly, ~30% of primary cultured EGCs express cell-surface MHC II upon IFNγ stimulation. However, our *in vitro* antigen presentation assay demonstrated that despite cell-surface expression of MHC II, primary murine EGCs are unable to functionally present soluble antigen on MHC II to OT-II T cells. It has been postulated that EGCs are not capable of engulfment following IFNγ stimulation and instead process antigen onto MHC II via autophagy [180]. This is not supported by our data, as we observed robust antigen-cross presentation to OT-I T cells upon incubation with soluble ovalbumin, suggesting engulfment by EGCs – though the particular endocytic pathway was not investigated. These differences could be explained by the differences in culture prep – the engulfment studies performed by Chow et al. [180] were done on whole mount myenteric plexus preparations whereas our *in vitro* studies were done on dissociated cell cultures. Nonetheless, the discovery that EGCs are capable of antigen-cross presentation is enticing, as similar roles have been described by oligodendrocyte progenitor cells in the Central Nervous System which may influence autoreactive $CD8^+$ T cell activity in Experimental Autoimmune Encephalomyelitis [214]. Future studies should investigate whether there is a role for EGC antigen-cross presentation during intestinal inflammation *in vivo*.

Another strength of our study is the use of spectral flow cytometry to reliably detect EGCs and probe for cell surface expression of MHC I/II. Analyzing EGCs by conventional flow cytometry is limited by a lack of compatible antibodies that result in incomplete labeling of all EGC populations [215]. As PLP is ubiquitously expressed by EGCs [123], we are confident that our preparation will capture all subsets of EGCs. The use of spectral flow cytometry allows us to effectively gate out autofluorescent cells and negate any false positive GFP signal. We observed a modest and significant induction of cell surface MHC II expression by EGCs measured by flow cytometry during acute *T. gondii* infection. However, EGC MHC II expression levels as measured by mean fluorescence intensity were > 5-fold lower than myeloid cell MHC II expression. By immunofluorescence staining, our results suggest that while EGCs are in close proximity to MHC II^+ macrophages, they infrequently express detectable amount of MHC II. We did observe a significant increase in the percentage of MHC I^+ EGCs and EGC MHC I MFI during acute *T. gondii* infection, though EGC MHC I expression level as measured by mean fluorescence intensity was ~ 2-fold lower than observed in myeloid cells. This is intriguing as MHC I expression levels have been shown to correlate with the ability to present *T. gondii*-derived antigen in *in vitro* systems [216]. A role for MHC I-mediated antigen presentation by non-hematopoietic cells including fibroblasts and astrocytes has been implicated as robust *T. gondii*-antigen specific $CD8^+$ T cell activation is still

observed when cell-surface MHC I is disrupted selectively in hematopoietic cells [216]. A role for antigen-cross presentation in *T. gondii* infection is less clearly defined, as studies have shown little to no contribution of antigen cross presentation to *T. gondii* specific T-cell activation *in vitro* [216,217]. However, live imaging by two-photon microscopy has shown *T. gondii*-antigen dependent interactions between uninfected Dendritic Cells and *T. gondii*-reactive $CD8^+$ T cells, implicating putative antigen cross presentation occurring during *T. gondii* infection *in vivo* [218]. It is unclear if EGCs are directly infected during *T. gondii*, though studies in rats have shown structural changes to the ENS including reductions in numbers of enteric neurons and glia [219–221]. Thus, it is compelling to speculate a putative role in EGC MHC I-mediated antigen presentation contributing to $CD8^+$ T cell responses and intestinal inflammation during acute *T. gondii* infection and other T cell mediated intestinal pathologies. We also note that EGCs appear to display an altered morphology during acute *T. gondii* infection, suggesting potential reactive gliosis [126,222]. Future studies should interrogate signaling pathways that are implicated in antigen presentation and reactive gliosis.

In summary, our data demonstrate that murine EGCs are capable of MHC I mediated antigen presentation, as well as antigen cross-presentation, and that EGCs upregulate MHC I expression during acute *T. gondii* infection. We further demonstrate that EGCs are not capable of MHC II mediated antigen presentation *in vitro*. EGCs do not appear to express cell surface MHC II in DSS colitis, though we did observe a fraction of EGCs that expressed low levels of cell surface MHC II expression during acute *T. gondii* infection. Future studies should further interrogate the contribution of EGC MHC I antigen presentation to cytotoxic $CD8^+$ responses during *T. gondii* infection, as well as the functional relevance of EGC MHC II expression.

2.6 Methods

2.6.1 Animals

PLP-EGFP (033357), OT-I (003831), OT-II (004194), and C57BL/6 (000664) mice were purchased from Jackson Laboratories. All mice were kept on a 12-hour light/dark schedule. All procedures were approved by the University of Virginia IACUC (protocol #1918, #3968).

2.6.2 Single cell RNA sequencing data analysis

Single cell RNA sequencing data analysis was performed in R (Version 4.4.0) [223]. Clustering was performed with integration using the Seurat package (Version 5.1.0) [224], with parameters adjusted to closely match the output from the original datasets. This included transforming the data using the SCTransform command in the Seurat package. EGCs were subsetted by cluster as well as coexpression of *S100B* and *PLP1* >1 in order to further validate cell identity. EGCs were then clustered with

integration prior to downstream analyses. Differential expression testing was done using the FindMarkers command in the Seurat package. The differential expression results were used to generate volcano plots with the package EnhancedVolcano (Version 1.22.0) [225]. Gene ontology plots were generated with the package clusterProfiler (Version 4.12.0).

2.6.3 Enteric glial cell culture preparation

Primary enteric glial cell cultures were prepared from C57BL/6 or PLP-EGFP mice following a protocol adapted from [5]. Following CO_2 euthanasia, small and large intestines were removed, flayed open and washed thoroughly in ice cold HBSS (Gibco; 14025-092). Intestines were pinned mucosa-down in a sylgard-coated plate and immersed in ice cold HBSS. The longitudinal muscle/myenteric plexus (LMMP) was isolated by gently teasing apart using sterile cotton swabs under a dissection scope in a laminar flow hood. Isolated LMMP was shaken at 215 rpm for 10 minutes at 37°C in 5 mL sterile DMEM F12 (Gibco; 11330-032). The LMMP was then homogenized using a sterilized razor blade and suspended in 5 mL digestion buffer containing DMEM F12, .13 Wünsch units/mL Liberase TM (Roche, 05401127001), and 500 U/mL DNase I (Worthington; LS002139). Samples were shaken at 215 rpm for 45 minutes at 37°C, triturating 10 times with a 5 mL serological pipette every 15 minutes. After digestion was complete, the sample was passed through a 40 μm cell strainer (Celltreat; 229481), diluted with 10 mL DMEM F12, and centrifuged at 1200 RPM for 5 minutes. Pellets from 3 mice were pooled and resuspended in 20 mL proliferation media containing DMEM F12 with 10% FBS (R&D Systems; S12450H). The pooled sample was plated in T175 cell culture flasks (Greiner; 661175) coated with 20 μg/mL fibronectin (Millipore Sigma; F1141) Cultures were incubated at 37°C for 24 hours, then media was replaced with EGC culture medium containing DMEM F12, 2% N-2 Supplement (Gibco; 17502048), 2% G-5 Supplement (Gibco; 17503012), and 50 ng/mL recombinant murine NGF-β (PeproTech; 450-34) and refreshed every 3-4 days. Cells were expanded until the cultures reached ~80% confluency (7-10 days) before being used for experiments.

2.6.4 FACS sorting

GFP-positive cells were sorted from primary EGC cultures using a Sony MA900 Cell Sorter and was performed by the University of Virginia Flow Cytometry Core Facility.

2.6.5 Flow cytometry

Flow Cytometry was performed using a Cytek Aurora 3 Laser (16V-14B-8R) Spectral Flow Cytometer. The following antibodies were used: CD11b (M1/70, eBioscience), CD4(RM4-5, BD Biosciences), CD45 (30-F11, eBioscience), CD69 (H1.2F3, eBioscience), CD8α (53-6.7, eBioscience), MHC I (28-8-6, Biolegend), MHC II (M5/114.5.2, eBioscience). Viability was assessed using a Zombie Red Fixable Viability Kit (Biolegend; 423109).

2.6.6 Bone marrow derived dendritic cell preparation

Bone Marrow Derived Dendritic Cells were prepared from C57BL/6 mice as previously described [226]. Briefly, femurs were dissected and flushed with 10 mL sterile RPMI 1640 (Gibco; 11875-903) with 1% FBS, collecting into a 50 mL conical tube, followed by centrifugation for 5 minutes at 1200 RPM. The pellets were then resuspended in 1 mL ACK Lysing Buffer (Quality Biological, 118-156-101) and incubated at room temperature for 5 minutes. The sample was then diluted with 10 mL RPMI 1640 with 1% FBS and centrifuged for 5 minutes at 1200 RPM. The pellet was then resuspended in BMDC media containing RPMI 1640 with 10% FBS, 20 ng/mL recombinant murine GM-CSF (PeproTech; 315-03), and 10 ng/mL recombinant murine IL-4 (PeproTech; 214-14) and plated at 2.2 x 10^6 cells per mL in a 100 mm cell culture dish (ThermoFisher Scientific; 150350). Media was refreshed the following day and once more on day 4. BMDCs were ready to use for experiments on day 7.

2.6.7 *In vitro* antigen presentation assays

In vitro antigen presentation assays were performed as described in [214]. FACS-isolated GFP^+ EGCs were plated in a 96 well plate (ThermoFisher Scientific; 167008) coated with 20 μg/mL fibronectin at 10,000 cells per well. Cells were allowed to expand for 24-48 hours prior to stimulation. For experiments with BMDCs, cells were passaged to 96 well plates at 10,000 cells per well. Cells were treated with 10 ng/ml recombinant murine IFNγ (PeproTech; 315-05) in EGC media for 12 hours, followed by treatment with either 50 μg/mL SIINFEKL peptide (Genscript; RP10611) or 500 μg/mL Ovalbumin (ThermoFisher Scientific; 77210) in EGC media with 10 ng/mL IFNγ for 8 hours. During the 8-hour incubation, OT-I $CD8^+$ T cells and OT-II $CD4^+$ T cells were isolated from spleen of OT-I and OT-II mice by negative selection according to the manufacturer's instructions (Stem Cell Technologies; 19852, 19852). Sorted T cells were labeled with Cell Proliferation Dye e450 (eBioscience, 65-0842-85) per manufacturer instructions. Following the 8-hour incubation EGCs/BMDCs were washed with PBS, and 160,000 OT-I or OT-II T cells were added in a 1:1 mixture of EGC media and RPMI complete. After 72 hours of coculture, T cell proliferation was examined using flow cytometry.

2.6.8 Dextran sodium sulfate induced colitis

Dextran Sodium Sulfate was prepared at 2.5% w/v in sterile water and administered to male PLP-EGFP mice *ad libitum* for two one-week cycles with a two-week recovery period in between. Mice were weighed daily.

2.6.9 *Toxoplasma gondii* parasite strains and infection

The avirulent, type II ME49 strain of *T. gondii* was used for all infections as previously described [207]. The parasite was maintained in chronically infected (2 to 6 months) Swiss Webster mice and passaged through CBA/J mice. For infections,

tissue cysts were prepared from homogenized brains of chronically infected (4 to 8 weeks) CBA/J mice. Female PLP-EGFP mice were then administered 20 tissue cysts of ME49 in 200 µL PBS via oral gavage.

2.6.10 Tissue harvest and digestion

Mice were perfused with saline with 5 units/mL heparin (Medefil; MIH-3333) and tissues of interest were harvested and processed as described below:

Small Intestine: Whole small intestine was dissected and placed into ice cold HBSS. A ~2 cm segment of the distal ileum was collected into formalin for immunofluorescence and another ~1 cm segment of the distal ileum was collected and snap frozen for RNA isolation/qPCR.

Large Intestine: Whole large intestine was dissected and placed into ice cold HBSS. A ~2 cm segment of the proximal colon was collected into formalin for immunofluorescence and another ~1 cm segment of the proximal colon was collected and snap frozen for RNA isolation/qPCR. The remaining large intestine was prepared for flow cytometry. The tissue was flayed open and fecal contents were washed away with ice cold HBSS. Tissue was cut into ~2 cm pieces and collected into 20 mL Colon Predigestion media containing HBSS, 10 mM HEPES (Gibco; 15630-080), 5 mM EDTA (Invitrogen; 15575-038), and 10% FBS. Samples were shaken at 215 rpm for 15 minutes at 37°C to remove mucus and debris. Gut pieces were filtered over a mosquito net then placed in fresh Colon Predigestion media and shaken again at 215 rpm for 15 minutes at 37°C. Samples were again filtered over a mosquito then transferred to a weigh boat and homogenized using a sterilized razor blade. The homogenized tissue was transferred to a 50 mL conical tube and suspended in 20 mL gut digest buffer containing RPMI 1640 with .13 Wünsch units Liberase TM and 100 Units/mL DNase I. Samples were shaken at 215 rpm for 30-45 minutes at 37°C. Once digested, the samples were passed through a 70 µm cell strainer and diluted with 20 mL Colon Predigestion media. Samples were centrifuged at 652 RCF for 5 minutes at 4°C, then washed two more times in FACS buffer containing PBS with 5 mM EDTA and 5% FBS prior to cell counting and staining for flow cytometry.

Mesenteric Lymph nodes: Lymph nodes were collected in 5 mL RPMI 1640, then passed through a 70 µm cell strainer using the plunger of a sterile 1 mL syringe and washed with an additional 10 mL RPMI 1640. The samples were centrifuged at 1200 RPM for 5 minutes, then washed twice in FACS buffer prior to cell counting and staining for flow cytometry.

Spleen: Spleens were collected in 5 mL RPMI 1640, then passed through a 70 µm cell strainer using the plunger of a sterile 1 mL syringe and washed with an additional 10 mL RPMI 1640. The samples were centrifuged at 1200 RPM for 5 minutes, then resuspended in 1 mL ACK Lysing buffer and incubated for 5 minutes

at room temperature. Samples were diluted with 10 mL RPMI 1640, centrifuged at 1200 RPM for 5 minutes, then washed twice in FACS buffer prior to cell counting and staining for flow cytometry.

Serum: Blood was collected by cardiac puncture and transferred to serum collection tubes (Becton Dickenson; 365967), centrifuged for 5 minutes at 11,000 RPM, then frozen at -80°C until further analysis.

2.6.11 RNA extraction and qPCR

RNA was extracted from snap frozen tissue sections using a Bioline Isolate II RNA mini kit (Meridian Bioscience; BIO-52073) as per manufacturer's instructions. RNA was quantified using a Biotek Epoch Microplate Spectrophotometer and normalized for each tissue. Equal amounts of RNA were reverse-transcribed to cDNA using an AzuraFlex cDNA Synthesis Kit (Azura genomics; AZ-1997) using 2 μM random hexaprimers and .5 μM oligodT primers per sample. qPCR reactions were prepared using a Bioline Sensifast NO-ROX kit (Meridian Bioscience; BIO-86020) for Taqman probes. The following Taqman probes were used: *Gapdh* (Mm99999915_g1), *Ifng* (Mm01168134_m1), *Tnf* (Mm00443258_m1), *Il33* (Mm00505403), *Il1b* (Mm00434228_m1), *Il6* (Mm00446190_m1), and *Il17a* (Mm00439618_m1). For *T. gondii Act1* quantification, a Bioline Sensifast SYBR NO-ROX kit (Meridian Bioscience; BIO-98020) was used with the following primer pair – Forward: 5'CGTGAGAGAATGACCCAGATTAT3'; Reverse: 5'ACCGGAGGAGTACAGAGAAA3' (Integrated DNA Technologies). PCR amplification was done over 40 cycles using a BioRad CFX Opus 384 Real-Time PCR System. Results were analyzed using the ΔΔCt method using *Gapdh* as the reference gene and fold change was normalized to the mean of the control group.

2.6.12 Serum IFNγ ELISA

A sandwich ELISA was used to determine serum IFNγ levels. High binding 96 well plates (Greiner Bio-One; 655081) were coated 50 μL/well with 2 μg/mL anti-mouse IFNγ (BioLegend; 517902) in Carbonate binding buffer overnight at 4°C. The next day, plates were washed 5 times with ELISA wash solution containing TBS with .05% Tween 20 (Fisher Scientific; BP337-500), then incubated with 200μL/well ELISA blocking buffer containing PBS with 1% BSA (Fisher bioreagents; 9048-46-8) at room temperature for 2 hours. Next, the blocking buffer was removed, and serum samples were plated in duplicate three-fold serial dilutions from 1:3 to 1:27, along with recombinant murine IFNγ (PeproTech; 315-05) in duplicate two-fold serial dilutions from 5 ng/mL to 1:1024 for the standard curve. Samples were incubated overnight at 4°C, then washed 5 times with ELISA wash solution. 1 μg/mL biotinylated anti-mouse IFNγ (BioLegend; 505704) was added and incubated for 1 hour at room temperature. Samples were washed 5 times and incubated with 1:1000 Avidin-AP (Sigma; A7295) for 30 minutes at room temperature. Samples were washed 5 times and incubated with ELISA detection solution containing PBS

with 1% BSA, .05% Tween 20, 2 mg/ml PNPP (Thermo Scientific;34045), 1:500 1M $MgCl_2$ at 37°C until color change was developed within the range of the standard curve. Absorbance at 405 nm was measured with a Biotek Epoch Microplate Spectrophotometer.

2.6.13 Immunofluorescence and data analysis

For immunofluorescence of PLP-EGFP cultures, cultures were plated on 6 well plates with 22mm x 22mm glass coverslips coated with 20 μg/mL fibronectin. Samples were fixed in 10% formalin solution at room temperature for 20 minutes, followed by permeabilization by incubation with TBS + 0.5% Triton X-100 (Fisher bioreagents; BP151-100) at room temperature for 15 minutes. Staining was performed in wells – primary antibodies were incubated overnight at 4°C and secondary antibodies were incubated at room temperature for 2 hours. Antibodies used are listed in Table 2.3. Coverslips were mounted onto microscope slides (Globe scientific; 1324) using Prolong Gold AntiFade Reagent (Life Technologies; P36980).

Following intestinal tissue harvest, samples were fixed in 10% formalin solution overnight at 4°C, then they were transferred to 30% sucrose in PBS until the sample reaches equilibration and sinks to the bottom of the solution. At this point, samples were mounted in cryomolds with OCT (Tissue-Tek;4583) and flash frozen. 20 μm cryosections (cross sections) were collected onto charged slides (Fisher Scientific; 12-550-17) and stored at 4°C until staining. Sections were stained with primary antibodies overnight at 4°C and secondary antibodies at room temperature for 2 hours. Antibodies used are listed in Table 2.3. Glass coverslips were mounted using Prolong Gold and imaged at 10x and 63x magnification using a Leica Stellaris confocal microscope. Laser intensity and gain were set using secondary only controls and were kept constant for all image acquisitions. Image analysis was performed in ImageJ (Version 2.14.0/1.54f). Regions of interest were drawn tracing the longitudinal muscle/myenteric + submucosal plexuses and mucosa respectively. Percent area was calculated by thresholding to the same value for each image. For fluorescence intensity measurements, an additional region of interest was determined based on the thresholded image, and mean grey value was measured in this region on the unaltered images. Mander's colocalization coefficients were calculated using the JaCoP plugin. 3D renderings were done in Imaris (Version 10.2).

Target	Species	Manufacturer	Catalogue #
GFP	Chicken	Thermo Scientific	A21311
Iba1	Rabbit	Wako Chemicals	019-19741
MHC II	Rat	Thermo Scientific	14-5321-85
S100B	Rabbit	Proteintech	15146-1-AP
Siinfekl-bound MHC I (APC conjugated)	Hamster	Biolegend	141606
Chicken IgY (AF488 conjugated)	Donkey	Jackson ImmunoResearch	703-545-155
Rabbit IgG (Cy3 conjugated)	Donkey	Jackson ImmunoResearch	711-165-152
Rat IgG (AF647 conjugated)	Donkey	Jackson ImmunoResearch	711-605-152
Hoechst Nuclear Stain	N/A	Thermo Scientific	H3570

Table 2.3 Antibodies used for immunofluorescence

2.6.14 Statistical analysis

Unless otherwise stated, all statistical analyses were run on GraphPad Prism 9 Version 10.2.3. Statistical tests and p values for each comparison are listed in the figure legends. Sample sizes are reported in the figure legends, where n denotes the total number of experimental units used in each analysis, and N denotes the total number of experimental replicates included in each analysis. A significance level of $\alpha = 0.05$ was used throughout unless indicated otherwise.

Declaration of competing Interest

Authors declare that they have no competing interests. A.G. is a consultant for Novoron Bioscience.

Data availability

The data that support the findings of this study are available from the corresponding authors upon reasonable request. R code for scRNAseq analysis is included at: https://github.com/ryan715b/IBD-EGC-scRNAseq-analysis

Acknowledgements

The authors are supported by grants from the NINDS R56 NS120352, UVA Trans University Microbiome Initiative pilot grant, the Miller family, and the Owens Family Foundation. R.M.B is supported by the UVA CMB Training Grant (T32GM008136-35) and UVA Wagner Fellowship. I.W.B. is supported by the UVA Immunology Training Grant (T32AI007496). T.H.H is supported by NIH grants R01NS112516 and R21NS128551. Cell sorting for this manuscript was performed in the University of Virginia Flow Cytometry Core Facility (RRid:SCR_017829) and is partially supported by the NCI Grant (P30-CA044579). Cell sorting was performed on the Sony MA900 cell sorter funded through the NIH S10 instrumentation program (1S10OD028518-

1). Graphical abstract and experimental design schematics were created with BioRender.com.

Chapter 3: Investigating Enteric Glial Cells in the context of demyelinating diseases

3.1 Abstract

Gastrointestinal dysfunction is commonly reported in patients with Multiple Sclerosis (MS). Notably, many individuals experience gastrointestinal symptoms long before their first clinically isolated syndrome, suggesting that gut dysfunction may precede autoimmune-mediated damage to the central nervous system. While the enteric nervous system lacks conventional myelin sheaths, enteric glial cells express transcripts for several myelin proteins that serve as autoimmune targets in MS. We hypothesize that myelin proteins derived from enteric glial cells may trigger the initial immune tolerance breakdown, initiating the autoimmune response in MS. To investigate this, we used the Experimental Autoimmune Encephalomyelitis (EAE) mouse model, immunizing mice with myelin antigens shared by enteric glial cells. We then examined antigen presentation machinery and T cell activation in the intestines. Although we did not find evidence of T cell-mediated immune activation in the intestines of immunized EAE models, our findings highlight the potential for autoimmune targeting of enteric nervous system-derived antigens and introduce a novel model of selective enteric glial cell ablation to further explore their role in EAE pathogenesis. These results support further investigation into enteric glial cells as possible autoimmune targets in MS.

3.2 List of abbreviations

CFA, Complete Freund's Adjuvant; CID, Chemical Inducer of Dimerization; CNP, 2'-3'-Cyclic Nucleotide 3'-Phosphodiesterase; CNS, Central Nervous System; EAE, Experimental Autoimmune Encephalomyelitis; EGC, Enteric Glial Cell; ENS, Enteric Nervous System; FACS, Fluorescence Activated Cell Sorting; GFP, Green Fluorescent Protein; GI, Gastrointestinal; IBD, Inflammatory Bowel Disease; iCP9, inducible Caspase 9; LMMP, Longitudinal Muscle and Myenteric Plexus; MAG, Myelin Associated Glycoprotein; MBP, Myelin Basic Protein; MFI, Mean Fluorescence Intensity; MHC, Major Histocompatibility Complex; mLN, mesenteric Lymph Node; MOBP, Myelin-associated Oligodendrocyte Basic Protein; MOG, Myelin Oligodendrocyte Glycoprotein; MPZ, Myelin Protein Zero; MS, Multiple Sclerosis; PLP, Proteolipid Protein; SI, Small Intestine; SNP, Single Nucleotide Polymorphism

3.3 Introduction

Though the ENS has traditionally been considered to lack myelinated nerves[23], EGCs express an assortment of myelin-related genes – including PLP1, MBP, MPZ, and CNP[123]. These represent major constituents of central and peripheral myelin, though other key myelin proteins including MOG, MOBP, and MAG are not detected

in EGCs. As such, the importance of myelin gene and protein expression by EGCs and how this might contribute to homeostatic gut function is unclear. PLP1 expression has been shown in other subsets of non-myelinating cells which include perisynaptic Schwann cells and inner ear supporting cells[227,228]. Functions beyond myelination have been considered for PLP1, MBP, and CNP in oligodendrocytes. For example, PLP1 appears to influence ion transport, transmembrane signaling, and survival; MBP might act as a scaffolding protein in intracellular signaling processes, and CNP may affect cell shape and process outgrowth[229]. PLP1 expression at the protein level is observed ubiquitously across all EGC types, and predominately encompasses the DM20 isoform[124]. Intricate neuron-glia interactions are observed across subsets, and types II and IV appear closely associated with tracts of interganglionic and intramuscular nerve fibers. Although an absence of myelin in the ENS has been described, observationally it seems that EGCs are poised to support conductance in enteric neurons.

The presence of myelin proteins in the gut make EGCs a compelling cell-type in the etiology of Multiple Sclerosis (MS). MS is a chronic neurodegenerative disorder characterized by the immune system recognizing and attacking CNS myelin. Gastrointestinal (GI) symptoms are frequently observed in MS, as one study reported that two-thirds of MS patients surveyed presented with at least one persistent GI symptom[191]. While some observed GI symptoms such as constipation and fecal incontinence may be derived from musculoskeletal deficits following CNS injury, some GI symptoms that are not associated with musculoskeletal deficits such as dysphagia and dyspepsia are also overrepresented in MS patients (~30% of MS patients surveyed compared to ~8% of the general population)[191]. There is also evidence that gut dysfunction precedes CNS-mediated symptoms in a subset of MS patients, some of which presented with bowel symptoms over three years prior to MS diagnosis[230]. Intriguingly, there is an apparent association between MS and Inflammatory Bowel Diseases such as Crohn's Disease and Ulcerative Colitis, as a meta-analysis suggests that patients with these IBDs have a 50% increased risk of MS comorbidity, though this association is bidirectional[231]. There are also shared genetic risk components between MS and UC as there are several shared SNPs associated with both diseases, many of which are present on the MHC gene locus[232]. As these conditions also present with similar immunological patterns, a common origin may be at play here.

The gut environment plays a critical role in the development of MS pathology which is reflected in the gut microbiome. Dysbiosis is keenly observed in MS patients with increased abundance of *Akkermansia* and *Methanobrevibacter*[233,234]. The effects of the gut microbiota on MS disease progression have been interrogated using the animal model Experimental Autoimmune Encephalomyelitis (EAE), where germ free mice were colonized with microbiota from either MS patients or healthy controls via fecal microbiota transplant. Mice colonized with MS patient derived microbiota presented with more severe disease marked by a reduction in regulatory T cell (Treg)

responses in the gut-associated mesenteric lymphnodes[233]. The importance of the intestinal immune compartment in adoptive transfer EAE models has also been well described. In a study by Duc et al., the authors used adoptive transfer of MOG transgenic Th17 cells to establish disease – while monitoring Th17 proliferation and migration dynamics in the gut and spinal cord[235]. MOG-specific Th17s were observed to migrate to then proliferate in the large intestine – this migration and retention requires Th17 expression of the integrin $\alpha4\beta7$. While in the colon, MOG-specific Th17s acquire expression of the CNS- specific integrin $\alpha4\beta1$, egressing through gut lymphatics which drain into the mesenteric lymph node (mLN). Here, key questions that remain to be addressed are: what induces the expression of $\alpha4\beta1$ in the gut? – and how might this be reflected in human MS where a variety of myelin antigens are present.

In MS patients, autoantibodies against several myelin proteins expressed by EGCs are observed, which include PLP, MBP, and MAG[236]. A link between CNS autoimmunity and ENS pathology is demonstrated by the MP_4 EAE model[167]. In this study by Wunsch et al., EAE is administered by delivery of an MBP-PLP fusion protein called MP_4. This more accurately represents MS pathology by means of a robust B cell/autoantibody response that remains chronic. In this model, ENS pathology preceded the onset of clinical scores, measured by immune cell infiltrate into the myenteric plexus, axonal damage of enteric neurons, and muscle atrophy in the small intestine. Additionally, antigen spreading was observed in the ENS as the authors demonstrated that serum IgG from MP_4 immunized mice bound four proteins in ENS cell lysates (3 from enteric neuron lysates, 1 from both enteric neuron/glia lysates), whereas IgG from control immunized mice did not. Importantly, antibodies to these proteins were also observed in the sera of human MS patients. Gastric dysmotility is also observed in the more common $PLP_{139-151}$ and MOG_{35-55} models, along with autoantibodies against enteric neurons and glia[237]. Given this information, it is intriguing to consider EGCs both as a potential source of myelin autoantigen and driver of inflammation via antigen presentation in the gut, possibly jumpstarting MS pathology in the CNS (Figure 3.1).

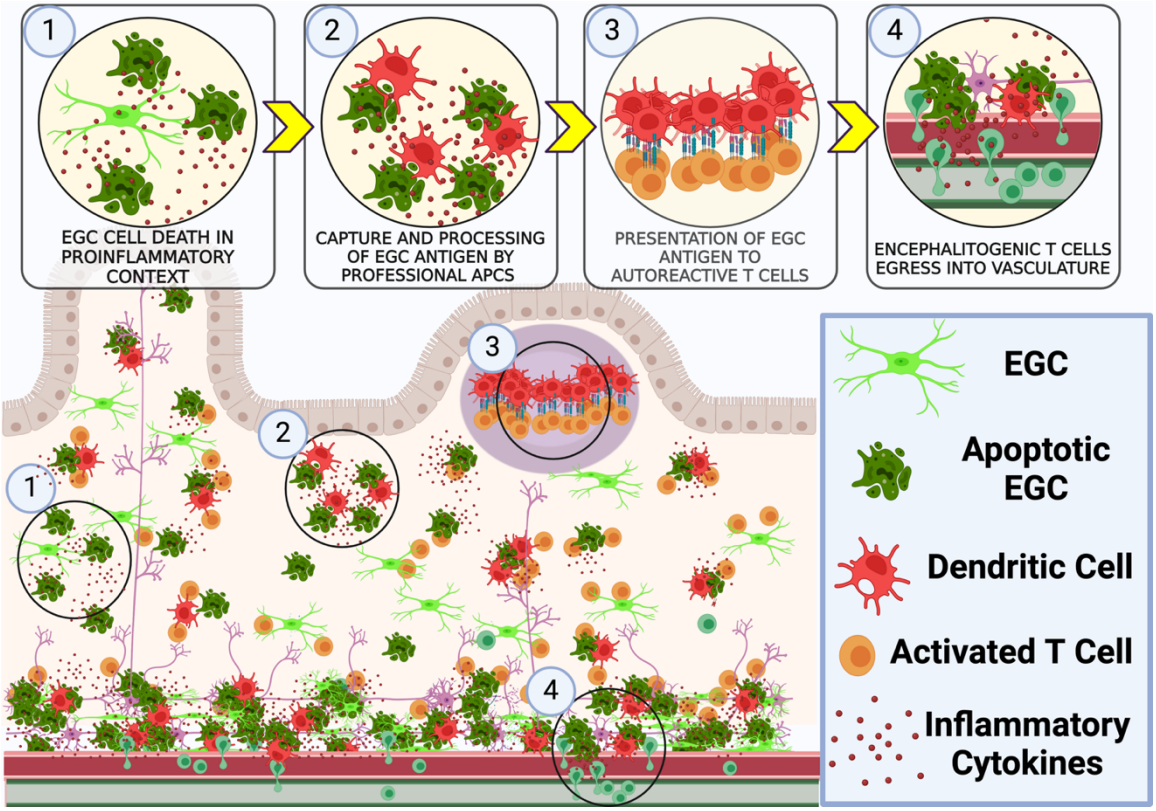

Figure 3.1 Proposed model of EGC-derived myelin antigens in MS

Given the expression of myelin proteins by EGCs, our hypothesis is that EGC-derived myelin antigen may initiate autoimmune responses in MS. In this proposed model, EGCs undergo cell death in a proinflammatory context (i.e. infection) (1), then EGC cell debris is captured and processed by professional antigen presenting cells (2) and presented to autoreactive T cells in gut-associated lymphoid structures (3). Encephalitogenic T cells would then egress into the vasculature and target CNS myelin (4).

3.4 Results

3.4.1 Characterization of intestinal adaptive immune responses in acute Experimental Autoimmune Encephalomyelitis

In order to explore potential autoimmune targeting of EGCs, we explored two models of Experimental Autoimmune Encephalomyelitis driven by different myelin antigens. We assessed intestinal antigen presenting cells and T cells by flow cytometry in the early/preclinical phases of disease. We utilized a similar approach as Wunsch et al., where as soon as one mouse in an EAE cohort began to develop loss of motor function, we sacrificed the entire cohort to perform flow cytometry on intestinal tissue. We examined MHC II expression by professional antigen presenting cells (Figure 3.2a) as well as the distribution of T cell populations (Figure 3.2b) in the small intestine and colon.

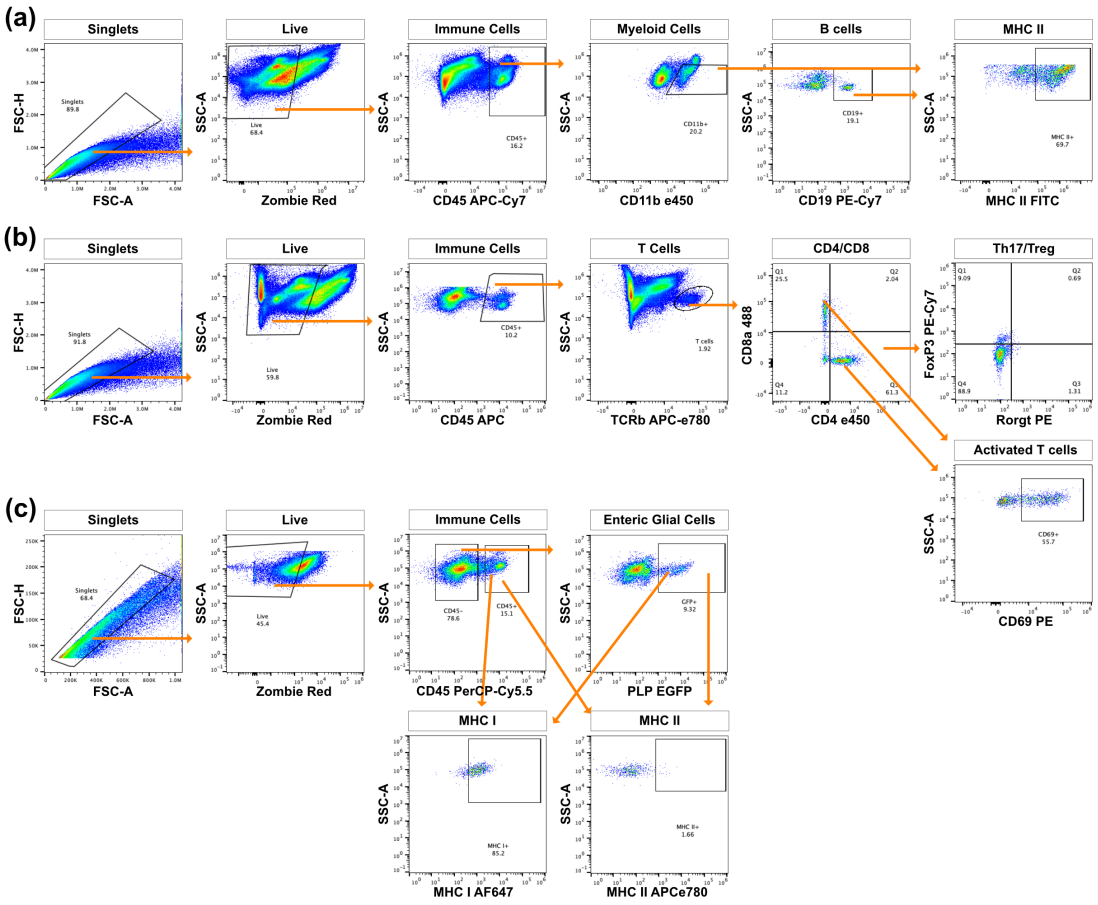

Figure 3.2 Flow cytometry gating strategies

(a) Professional APC panel gating strategy for Myelin and $PLP_{178-191}$ acute EAE. (b) T cell panel gating strategy for Myelin and $PLP_{178-191}$ acute EAE. (c) EGC antigen presentation panel gating strategy for $PLP_{178-191}$ chronic EAE.

Myelin EAE in C57BL/6

This EAE model is driven by immunizing C57BL/6 mice with purified mouse myelin emulsified in Complete Freund's Adjuvant (CFA). We chose this model as it should prime a T cell-mediated autoimmune response that targets several myelin peptides, hypothesizing that the diversity of myelin autoantigens will increase the likelihood of EGCs being targeted. We observed no significant changes in MHC II expression levels by $CD11b^+$ myeloid cells or $CD19^+$ B cells in either the small or large intestine (Figure 3.3a-h). We also observed no significant changes in the distribution of $CD4^+/CD8^+$ T cells, nor in the distribution of Th17/Treg $CD4^+$ T cell subsets (Figure 3.4a-j). Notably, we observed that the majority of the $CD4^+$ T cells we observed were Tregs. Together, these data suggest there was not significant adaptive immunity in the gut in the early phases of this myelin driven EAE.

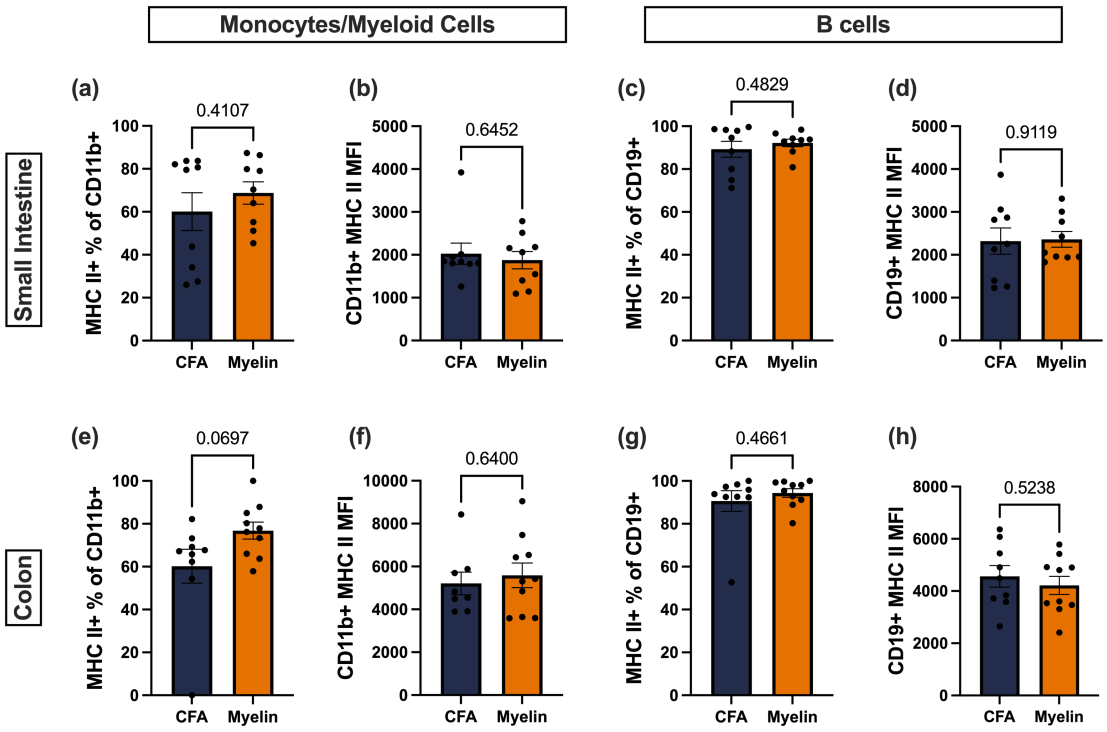

Figure 3.3 MHC II expression by professional APCs during acute Myelin EAE

(a) Percentage of CD11b$^+$ cells that are MHC II$^+$ in the small intestine. CFA mean = 60.12 ± 8.792%; Myelin mean = 68.76 ± 5.210%, p = .4107 (b) CD11b$^+$ MHC II Mean Fluorescence Intensity in the small intestine. CFA mean = 2026 ± 247.5; Myelin mean = 1876 ± 201.4, p = .6452 (c) Percentage of CD19$^+$ cells that are MHC II$^+$ in the small intestine. CFA mean = 89.27 ± 3.723%; Myelin mean = 92.21 ± 1.714%, p = .4829 (d) CD19$^+$ MHC II Mean Fluorescence Intensity in the small intestine. CFA mean = 23321 ± 305.1; Myelin mean = 2360 ± 181.5, p = .9119 (e) Percentage of CD11b$^+$ cells that are MHC II$^+$ in the colon. CFA mean = 60.21 ± 7.935%; Myelin mean = 76.83 ± 3.943%, p = .0697 (f) CD11b$^+$ MHC II Mean Fluorescence Intensity in the colon. CFA mean = 5209 ± 527.4; Myelin mean = 5589 ± 572.8, p = .6400 (g) Percentage of CD19$^+$ cells that are MHC II$^+$ in the colon. CFA mean = 90.63 ± 4.831%; Myelin mean = 94.38 ± 1.979%, p = .4661 (h) CD19$^+$ MHC II Mean Fluorescence Intensity in the colon. CFA mean = 4564 ± 413.4; Myelin mean = 4216 ± 344.9, p = .5238. Unpaired student's t-test was used, N=2, n = 9-10 mice/group.

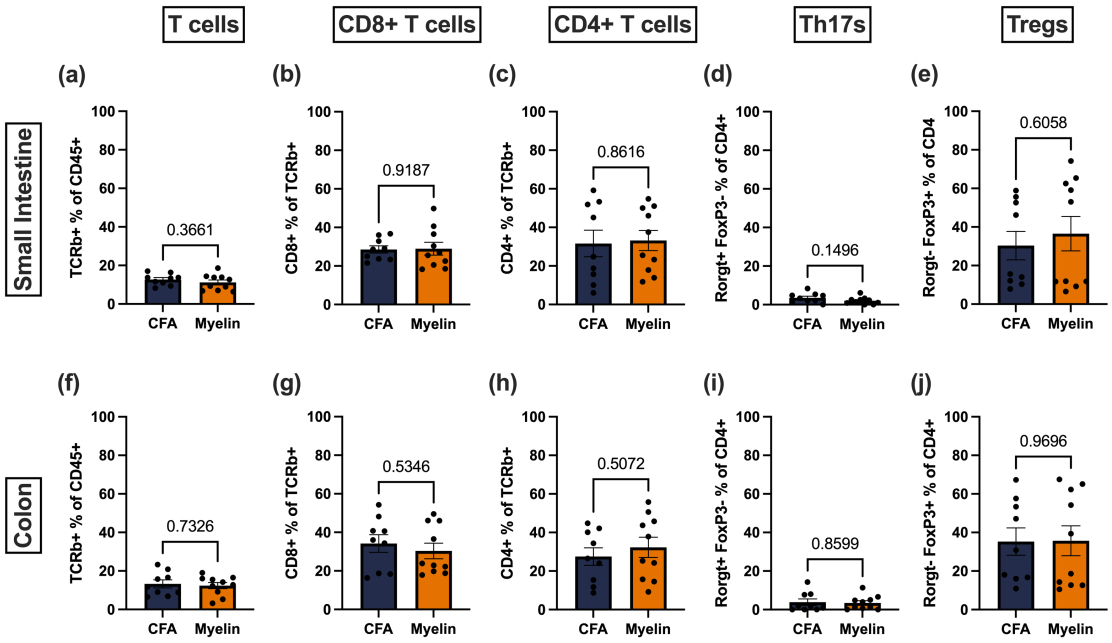

Figure 3.4 T cell populations during acute Myelin EAE

(a) Percentage of $CD45^+$ cells that are $TCRb^+$ in the small intestine. CFA mean = 12.72 ± .9821%; Myelin mean = 11.18 ± 1.290%, p = .3361 (b) Percentage of $TCRb^+$ cells that are $CD8^+$ in the small intestine. CFA mean = 28.54 ± 1.876%; Myelin mean = 28.95 ± 3.302%, p = .9187 (c) Percentage of $TCRb^+$ cells that are $CD4^+$ in the small intestine. CFA mean = 31.66 ± 6.878%; Myelin mean = 33.17 ± 5.239%, p = .8616 (d) Percentage of $CD4^+$ cells that are $Rorgt^+$,$FoxP3^-$ (Th17) in the small intestine. CFA mean = 3.536 ± .8564%; Myelin mean = 2.010 ± .5724%, p = .1496 (e) Percentage of $CD4^+$ cells that are $Rorgt^-$,$FoxP3^+$ (Treg) in the small intestine. CFA mean = 30.36 ± 7.379%; Myelin mean = 36.54 ± 8.936%, p = .6058 (f) Percentage of $CD45^+$ cells that are $TCRb^+$ in the colon. CFA mean = 13.29 ± 2.050%; Myelin mean = 12.39 ± 1.604%, p = .7326 (g) Percentage of $TCRb^+$ cells that are $CD8^+$ in the colon. CFA mean = 34.20 ± 4.556%; Myelin mean = 30.36 ± 4.029%, p = .5346 (h) Percentage of $TCRb^+$ cells that are $CD4^+$ in the colon. CFA mean = 27.52 ± 4.563%; Myelin mean = 32.27 ± 5.240%, p = .5072 (i) Percentage of $CD4^+$ cells that are $Rorgt^+$,$FoxP3^-$ (Th17) in the colon. CFA mean = 3.851 ± 1.676%; Myelin mean = 3.493± 1.152%, p = .8599 (j) Percentage of $CD4^+$ cells that are $Rorgt^-$,$FoxP3^+$ (Treg) in the colon. CFA mean = 35.31 ± 7.092 %; Myelin mean = 35.72± 7.737%, p = .9696. Unpaired student's t-test was used, N=2, n = 9-10 mice/group.

$PLP_{178-191}$ EAE in C57BL/6

This EAE model is driven by immunizing C57BL/6 mice with the myelin peptide $PLP_{178-191}$. We chose this peptide because it is present in both the full length PLP protein as well as the DM20 isoform predominately expressed by EGCs[124]. Again, we did not observe significant changes in MHC II expression levels by $CD11b^+$ myeloid cells or $CD19^+$ B cells in the small intestine (Figure 3.5a-d). In the colon, we surprisingly observed a significant decrease in the expression level of MHC II in $CD11b^+$ myeloid cells as measured by Mean Fluorescence Intensity (MFI), though no significant changes were observed in B cells (Figure 3.5e-h). We then probed for the T cell activation marker CD69 in the colon by flow cytometry and observed no significant changes in T cell activation in $CD4^+$ or $CD8^+$ T cells (Figure 3.6a-j).

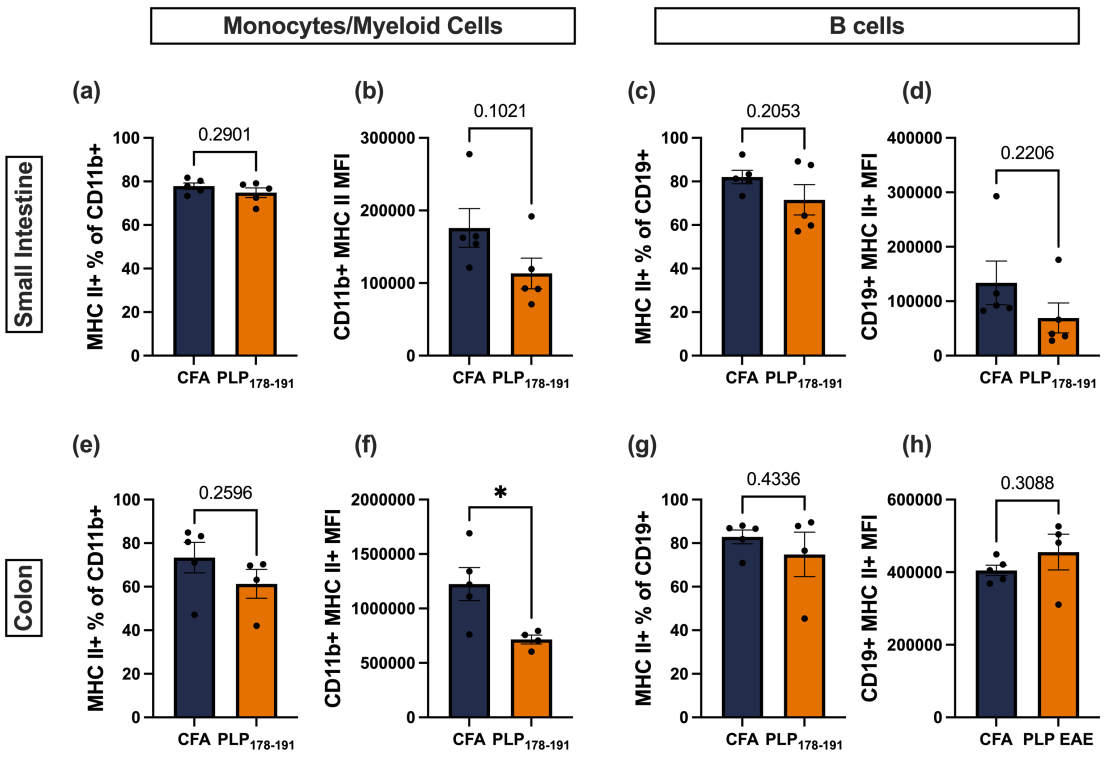

Figure 3.5 MHC II expression by professional APCs during acute $PLP_{178-191}$ EAE

(a) Percentage of $CD11b^+$ cells that are MHC II^+ in the small intestine. CFA mean = 60.12 ± 8.792%; $PLP_{178-191}$ mean = 77.84 ± 1.491%, p = .2901 (b) $CD11b^+$ MHC II Mean Fluorescence Intensity in the small intestine. CFA mean = 176000 ± 26584; $PLP_{178-191}$ mean = 113328 ± 21123, p = .1021 (c) Percentage of $CD19^+$ cells that are MHC II^+ in the small intestine. CFA mean = 82.06 ± 3.082%; $PLP_{178-191}$ mean = 71.58 ± 6.947%, p = .2053 (d) $CD19^+$ MHC II Mean Fluorescence Intensity in the small intestine. CFA mean = 133826 ± 40079; $PLP_{178-191}$ mean = 69217 ± 27534, p = .2206 (e) Percentage of $CD11b^+$ cells that are MHC II^+ in the colon. CFA mean = 73.36 ± 6.985%; $PLP_{178-191}$ mean = 61.30 ± 6.631%, p = .2596 (f) $CD11b^+$ MHC II Mean Fluorescence Intensity in the colon. CFA mean = 1224200 ± 151326; $PLP_{178-191}$ mean = 715250 ± 41343, p = .0432 (g) Percentage of $CD19^+$ cells that are MHC II^+ in the colon. CFA mean = 82.86 ± 3.168%; $PLP_{178-191}$ mean = 74.83 ± 10.23%, p = .4336 (h) $CD19^+$ MHC II Mean Fluorescence Intensity in the colon. CFA mean = 404971 ± 14267; $PLP_{178-191}$ mean = 455475 ± 49059, p = .3088. Unpaired student's t-test was used, N=1, n = 4-5 mice/group.

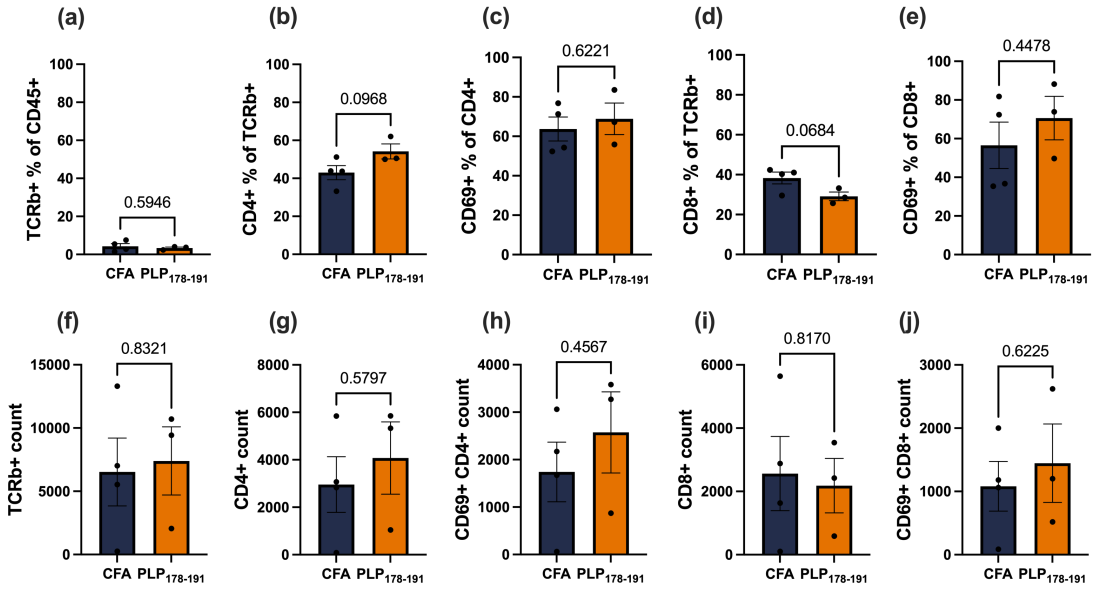

Figure 3.6 T cell populations during acute $PLP_{178-191}$ EAE

(a) Percentage of $CD45^+$ cells that are $TCRb^+$ in the colon. CFA mean = 4.310 ± 1.365%; $PLP_{178-191}$ mean = 3.369 ± .5173%, p = .5946 (b) Percentage of $TCRb^+$ cells that are $CD4^+$ in the colon. CFA mean = 43.00 ± 3.703%; $PLP_{178-191}$ mean = 54.17± 3.919%, p = .0968 (c) Percentage of $CD4^+$ cells that are $CD69^+$ in the colon. CFA mean = 63.70 ± 6.092%; $PLP_{178-191}$ mean = 68.87 ± 8.011%, p = .6221 (d) Percentage of $TCRb^+$ cells that are $CD8^+$ in the colon. CFA mean = 38.30 ± 2.966%; $PLP_{178-191}$ mean = 29.13 ± 2.188 %, p = .0684 (e) Percentage of $CD8^+$ cells that are $CD69^+$in the colon. CFA mean = 56.58 ± 12.01%; $PLP_{178-191}$ mean = 70.60 ± 11.24%, p = .4478 (f) Number of $TCRb^+$ cells in the colon. CFA mean = 6527 ± 2683; $PLP_{178-191}$ mean = 7397 ± 2693, p = .8321 (g) Number of $CD4^+$, $TCRb^+$ cells in the colon. CFA mean = 2957 ± 1176; $PLP_{178-191}$ mean = 4073 ± 1524, p = .5797 (h) Number of $TCRb^+$,$CD4^+$,$CD69^+$ cells in the colon. CFA mean = 1740 ± 629.1; $PLP_{178-191}$ mean = 2573 ± 856.4, p = .4567 (i) Number of $CD8^+$, $TCRb^+$ cells in the colon. CFA mean = 2564 ± 1172; $PLP_{178-191}$ mean = 2182 ± 860.7, p = .8170 (j) Number of $TCRb^+$,$CD8^+$,$CD69^+$ cells in the colon. CFA mean = 1081 ± 392.2; $PLP_{178-191}$ mean = 1446 ± 619.1, p = .6225. Unpaired student's t-test was used, N=1, n = 3-4 mice/group.

3.4.2 Characterization of intestinal adaptive immune responses in chronic Experimental Autoimmune Encephalomyelitis

We proceeded to examine antigen presentation by immune cells and EGCs in the intestine during the chronic phase of $PLP_{178-191}$ EAE. To achieve this, we immunized PLP-EGFP reporter mice with $PLP_{178-191}$ and performed flow cytometry at three- and five-weeks post immunization compared to unimmunized controls. For the small intestine, we dissected the longitudinal muscle/myenteric plexus (LMMP) and examined separately from the mucosa to compare mucosal and inter/intraganglionic EGCs separately. Meanwhile, we examined the entire colon due to limited tissue amounts. We performed flow cytometry on these three tissues probing for MHC I/II expression on CD45+ immune cells and GFP+ EGCs (Figure 3.2c).

MHC I/II expression by immune cells during chronic $PLP_{178-191}$ EAE

In the SI LMMP, we observed a significant increase in the percentage of CD45+ immune cells that were MHC I+ at both EAE timepoints (Figure 3.7a), along with a significant increase in CD45 MHC I expression level at the 5-week timepoint (Figure 3.7b). We observed a decrease in the percentage of CD45+ immune cells that were MHC II+ at both timepoints (Figure 3.7c). There was no significant change in CD45+ MHC II expression levels at either timepoint, though a trending increase was observed at 5-weeks (Figure 3.7d). In the SI Mucosa, there was no change in the percentage of CD45+ cells that were MHC I+ (Figure 3.7e), though CD45+ MHC I expression levels were significantly decreased by the 5-week timepoint (Figure 3.7f). The percentage of CD45+ cells that were MHC II+ were also significantly reduced by the 5-week timepoint (Figure 3.7g), as well as CD45+ MHC II expression levels (Figure 3.7h). In the colon, there were no significant changes in the percentage of CD45+ cells that were MHC I+ (Figure 3.7i), nor in CD45+ MHC I expression levels (Figure 3.7j). There was again a decrease in the percentage of CD45+ cells that were MHC II+ at both timepoints (Figure 3.7k), with a trend towards decreased CD45+ MHC II expression levels (Figure 3.7l).

MHC I/II expression by EGCs during chronic $PLP_{178-191}$ EAE

In the SI LMMP, we observed a significant decrease in the percentage of GFP+ EGCs that were MHC I+ at the 5-week timepoint (Figure 3.8a), along with a significant increase in EGC MHC I expression level at the 5-week timepoint (Figure 3.8b). We observed few MHC II+ EGCs with no significant differences at either timepoint (Figure 3.8c). Despite the low frequency of MHC II+ EGCs, we did observe a significant increase in EGC MHC II expression levels at the 5-week timepoint (Figure 3.8d). In the SI Mucosa, we observed a significant decrease in the percentage of EGCs that were MHC I+ at the 5-week timepoint (Figure 3.8e), along a trend towards decreased EGC MHC I expression levels (Figure 3.8f). There were few MHC II+ EGCs with no significant difference between timepoints (Figure 3.8g), as well as no significant difference in EGC MHC II expression levels (Figure 3.8h). In the colon, there was again a significant decrease in the percentage of EGCs that were MHC I+ by the 5-week timepoint (Figure 3.8i), along with significantly decreased EGC MHC I expression levels (Figure 3.8j). There was no significant difference in the percentage of EGCs that were MHC II+ (Figure 3.8k), nor in EGC MHC II expression levels (Figure 3.8l).

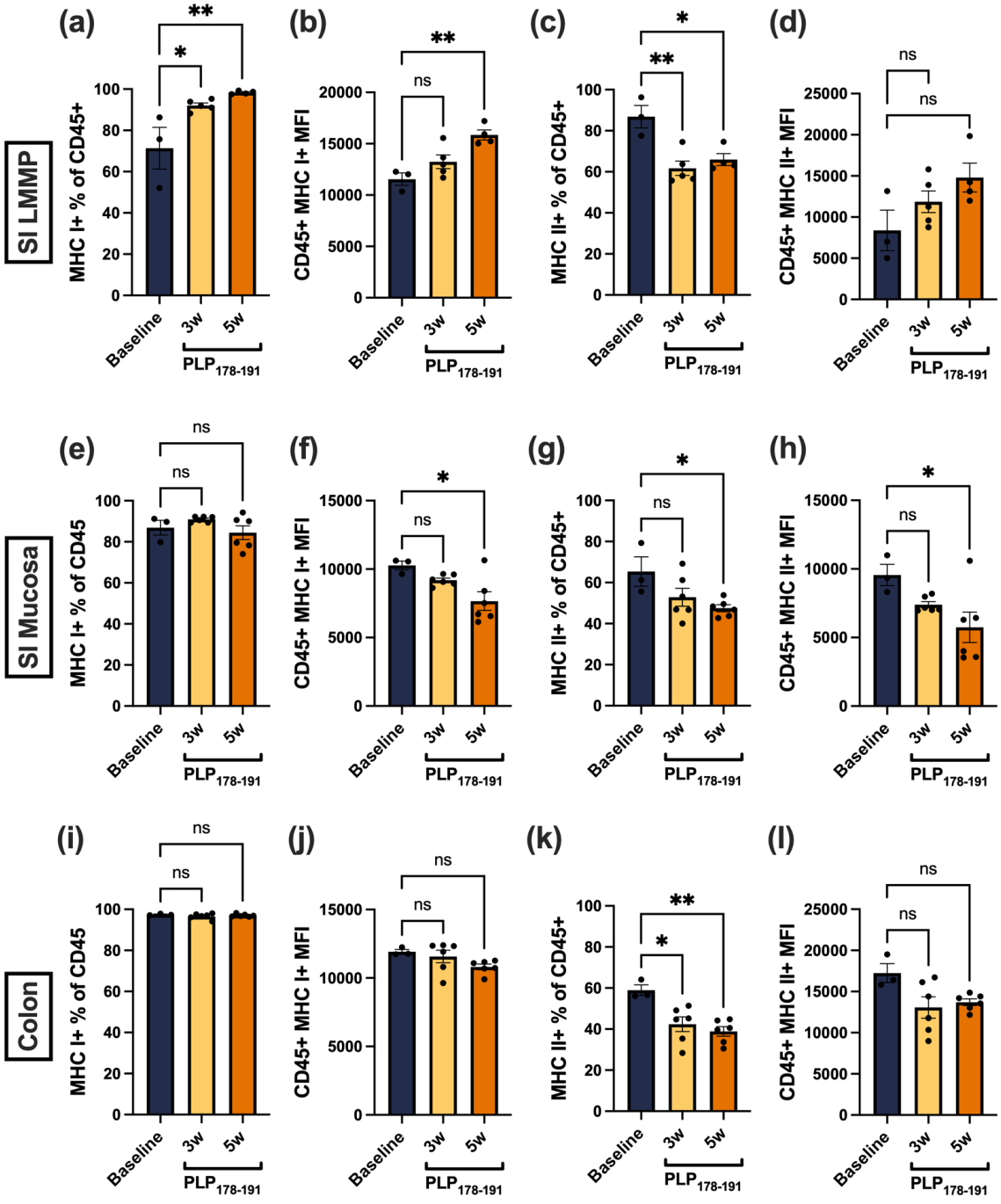

Figure 3.7 Legend on next page

Figure 3.7 MHC I/II expression by immune cells during chronic $PLP_{178-191}$ EAE

(a) Percentage of $CD45^+$ cells that are MHC I^+ in the SI LMMP. Baseline mean = 71.33 ± 10.14%, 3w mean = 92.06 ± 1.223%, 5w mean = 98.35 ± .4031%. Baseline vs 3w p-adj = .0212, Baseline vs 5w p-adj = .0062. (b) $CD45^+$ MHC I MFI in the SI LMMP. Baseline mean = 11544 ± 607.2, 3w mean = 13240 ± 666.4, 5w mean = 15851 ± 492.6. Baseline vs 3w p-adj = .2050, Baseline vs 5w p-adj = .0037. (c) Percentage of $CD45^+$ cells that are MHC II^+ in the SI LMMP. Baseline mean = 86.83 ± 5.428%, 3w mean = 61.68 ± 3.497%, 5w mean = 65.95 ± 2.936%. Baseline vs 3w p-adj = .0038, Baseline vs 5w p-adj = .0147. (d) $CD45^+$ MHC II MFI in the SI LMMP. Baseline mean = 8389 ± 2457, 3w mean = 11864 ± 1320, 5w mean = 14801 ± 1745. Baseline vs 3w p-adj = .3925, Baseline vs 5w p-adj = .0881. (e) Percentage of $CD45^+$ cells that are MHC I^+ in the SI Mucosa. Baseline mean = 86.90 ± 3.576%, 3w mean = 90.95 ± .5548%, 5w mean = 84.45 ± 3.352%. Baseline vs 3w p-adj = .6119, Baseline vs 5w p-adj = .8314. (f) $CD45^+$ MHC I MFI in the SI Mucosa. Baseline mean = 10274 ± 313.2, 3w mean = 9188 ± 160.7, 5w mean = 7662 ± 681.3. Baseline vs 3w p-adj = .3909, Baseline vs 5w p-adj = .0170. (g) Percentage of $CD45^+$ cells that are MHC II^+ in the SI Mucosa. Baseline mean = 65.37 ± 7.152%, 3w mean = 52.87 ± 4.380%, 5w mean = 47.50 ± 1.671%. Baseline vs 3w p-adj = .1621, Baseline vs 5w p-adj = .0385. (h) $CD45^+$ MHC II MFI in the SI Mucosa. Baseline mean = 9555 ± 778.8, 3w mean = 7393 ± 223.6, 5w mean = 5743 ± 1108. Baseline vs 3w p-adj = .2695, Baseline vs 5w p-adj = .0342. (i) Percentage of $CD45^+$ cells that are MHC I^+ in the Colon. Baseline mean = 97.43 ± .2404%, 3w mean = 96.57 ± .5608%, 5w mean = 97.02 ± .2774%. Baseline vs 3w p-adj = .4638, Baseline vs 5w p-adj = .8295. (j) $CD45^+$ MHC I MFI in the Colon. Baseline mean = 11914 ± 167.0, 3w mean = 11573 ± 459.9, 5w mean = 10810 ± 203.6. Baseline vs 3w p-adj = .8228, Baseline vs 5w p-adj = .1695. (k) Percentage of $CD45^+$ cells that are MHC II^+ in the Colon. Baseline mean = 58.93 ± 2.587%, 3w mean = 42.37 ± 3.578%, 5w mean = 38.88 ± 2.335%. Baseline vs 3w p-adj = .0149, Baseline vs 5w p-adj = .0042. (l) $CD45^+$ MHC II MFI in the Colon. Baseline mean = 17246 ± 1143, 3w mean = 13064 ± 1294, 5w mean = 13703 ± 402.3. Baseline vs 3w p-adj = .0581, Baseline vs 5w p-adj = .1138. One-way ANOVA with multiple comparisons was used, *p < .05, **p < .01, ***p < .001. N = 1, n = 3-6 mice/group.

.

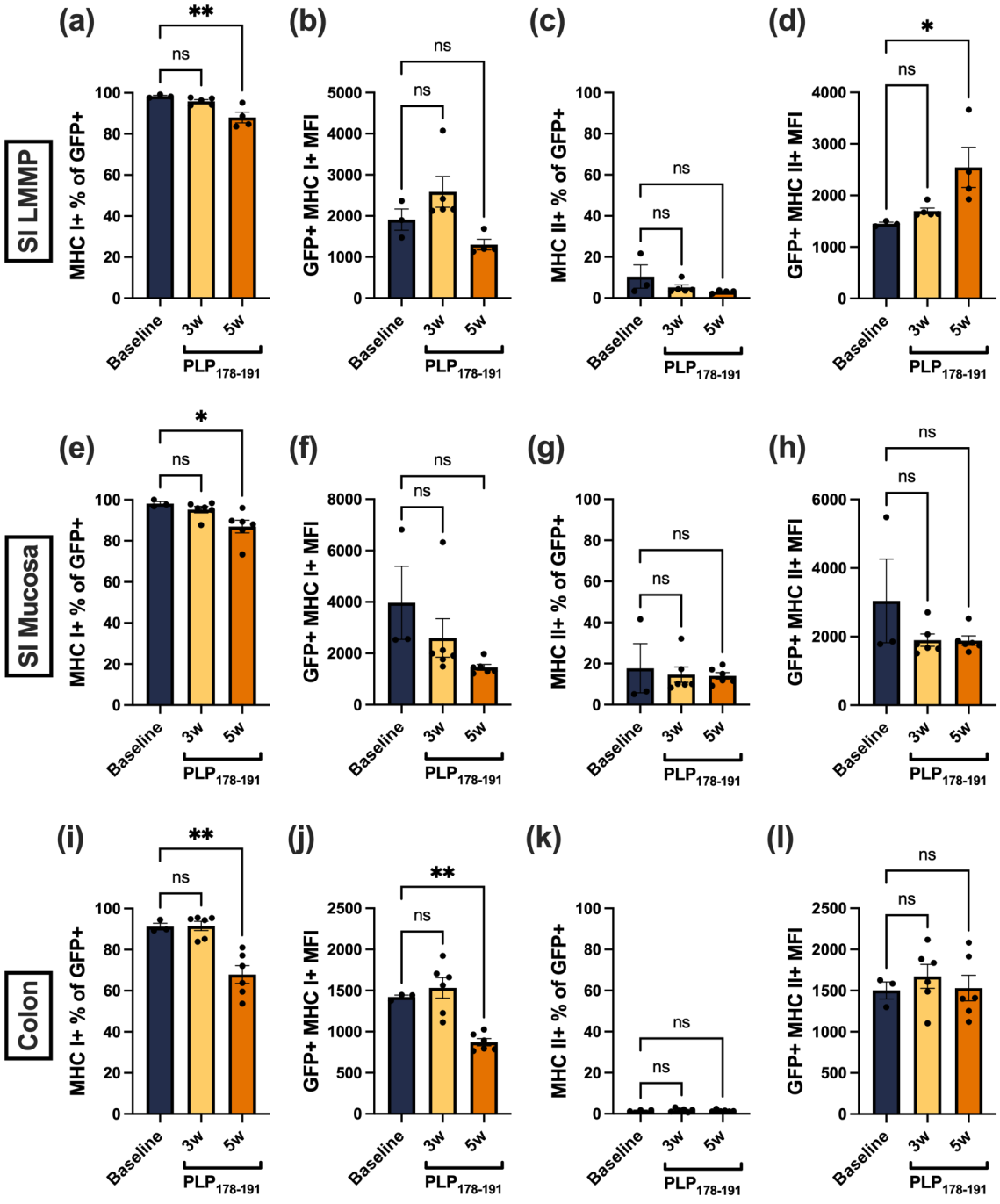

Figure 3.8 Legend on next page

Figure 3.8 MHC I/II expression by EGCs during chronic $PLP_{178-191}$ EAE

(a) Percentage of GFP^+ cells that are MHC I^+ in the SI LMMP. Baseline mean = 98.33 ± .4667%, 3w mean = 95.88 ± .7965%, 5w mean = 88.03 ± 2.621%. Baseline vs 3w p-adj = .5799, Baseline vs 5w p-adj = .0066. (b) GFP^+ MHC I MFI in the SI LMMP. Baseline mean = 1911 ± 257.3, 3w mean = 2586 ± 375.6, 5w mean = 1302 ± 128.9. Baseline vs 3w p-adj = .3359, Baseline vs 5w p-adj = .4327. (c) Percentage of GFP^+ cells that are MHC II^+ in the SI LMMP. Baseline mean = 10.45 ± 5.687%, 3w mean = 5.182 ± 1.313%, 5w mean = 3.128 ± 3562%. Baseline vs 3w p-adj = .3685, Baseline vs 5w p-adj = .1951. (d) GFP^+ MHC II MFI in the SI LMMP. Baseline mean = 1450 ± 29.81, 3w mean = 1700 ± 55.97, 5w mean = 2545 ± 389.1. Baseline vs 3w p-adj = .7432, Baseline vs 5w p-adj = .0294. (e) Percentage of GFP^+ cells that are MHC I^+ in the SI Mucosa. Baseline mean = 98.13 ± .9615%, 3w mean = 95.18 ± 1.581%, 5w mean = 86.95 ± 3.073%. Baseline vs 3w p-adj = .7349, Baseline vs 5w p-adj = .0348. (f) GFP^+ MHC I MFI in the SI Mucosa. Baseline mean = 3968 ± 1423, 3w mean = 2599 ± 749.9, 5w mean = 1458 ± 111.7. Baseline vs 3w p-adj = .4553, Baseline vs 5w p-adj = .0996. (g) Percentage of GFP^+ cells that are MHC II^+ in the SI Mucosa. Baseline mean = 17.73 ± 11.94%, 3w mean = 14.61 ± 3.730%, 5w mean = 14.02 ± 1.581%. Baseline vs 3w p-adj = .9091, Baseline vs 5w p-adj = .8746. (h) GFP^+ MHC II MFI in the SI Mucosa. Baseline mean = 3041 ± 1220, 3w mean = 1896 ± 179.1, 5w mean = 1884 ± 136.2. Baseline vs 3w p-adj = .2325, Baseline vs 5w p-adj = .2261. (i) Percentage of GFP^+ cells that are MHC I^+ in the Colon. Baseline mean = 91.23 ± 1.642%, 3w mean = 91.55 ± 2.226%, 5w mean = 67.85 ± 4.328%. Baseline vs 3w p-adj = .4638, Baseline vs 5w p-adj = .8295. (j) GFP^+ MHC I MFI in the Colon. Baseline mean = 1421 ± 23.03, 3w mean = 1532 ± 125.0, 5w mean = 872 ± 43.82. Baseline vs 3w p-adj = .7403, Baseline vs 5w p-adj = .0080. (k) Percentage of GFP^+ cells that are MHC II^+ in the Colon. Baseline mean = 1.620 ± .1904%, 3w mean = 1.745 ± .3613%, 5w mean = 1.462 ± .2040%. Baseline vs 3w p-adj = .9624, Baseline vs 5w p-adj = .9405. (l) GFP^+ MHC II MFI in the Colon. Baseline mean = 1503 ± 103.2, 3w mean = 1673 ± 145.1, 5w mean = 1531 ± 155.8. Baseline vs 3w p-adj = .7703, Baseline vs 5w p-adj = .9928. One-way ANOVA with multiple comparisons was used, *p < .05, **p < .01, ***p < .001. N = 1, n = 3-6 mice/group.

Detection of autoantibodies against ENS-derived antigens

We performed an ELISA to determine if we could detect serum antibodies that are reactive against ENS-derived autoantigens. To do this, we collected serum from Naïve and 5w EAE mice and performed a direct ELISA with plated coated with tissue lysate from dissected LMMP and thus enriched in ENS antigens, while using $PLP_{178-191}$ coated plates as a positive control. We observed a trend towards increased autoantibody reactivity against LMMP lysate (Figure 3.9a) and a significant enrichment of autoantibody reactivity against $PLP_{178-191}$ (Figure 3.9b).

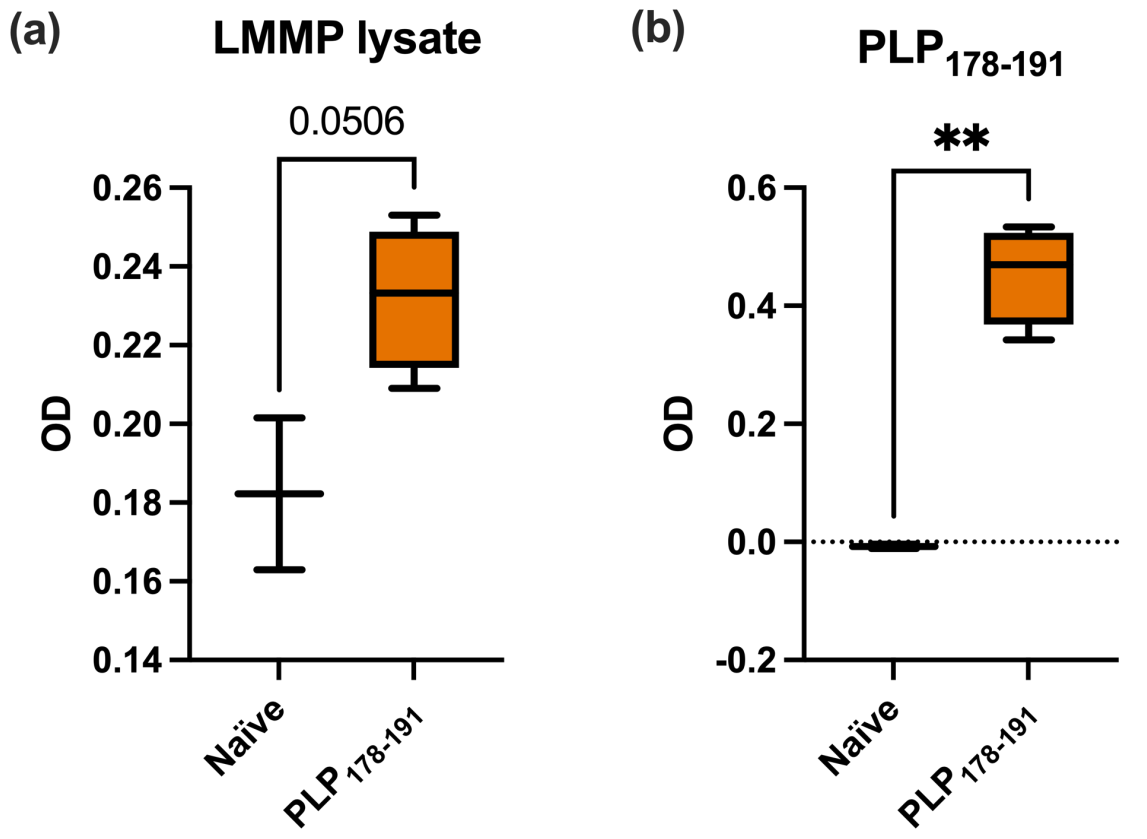

Figure 3.9 Serum IgG reactivity against LMMP-derived antigens in chronic $PLP_{178-191}$ EAE

(a) Optical density (OD) absorbance values of serum IgG binding to LMMP tissue lysate. Naïve mean = .1823 ± .01925, $PLP_{178-191}$ mean = .2321 ± .009102, p = .0506. (b) OD absorbance values of serum IgG binding to $PLP_{178-191}$. Naïve mean = -.007500 ± .003500, $PLP_{178-191}$ mean = .4540 ± .04120, p = .0017. Unpaired student's t-test was used, N=1, n = 2-3 mice/group, **p < .01.

3.4.3 A model for selective ablation of enteric glial cells

Despite observing putative autoreactivity against ENS-derived antigens in $PLP_{178-191}$ EAE, we did not observe any evidence of enteric glial or neuronal cell death (data not shown). To circumvent this, we plan on utilizing a model of selective EGC ablation to artificially drive EGC cell death in an inflammatory setting and observe how this impacts autoimmunity in EAE models. The limitation with conventionally used methods of EGC ablation such as the PLP-DTA system[147] is that oligodendrocyte-lineage cells in the CNS are also targeted. To avoid this, we utilized GFAP-iCP9 mice. These mice express an inducible Caspase 9 driven by the mouse GFAP promoter. Local delivery of chemical inducer of dimerization (CID) results in caspase 9 activation and apoptotic cell death. This system has been previously utilized to selectively ablate astrocytes in the CNS, which required local delivery of CID as it does not readily cross the Blood-Brain-Barrier[238]. Given this, we hypothesized intraperitoneal (i.p.) delivery of CID would effectively ablate EGCs

while sparing CNS astrocytes. We tested this in a pilot study where we delivered 50 mg/kg CID to female GFAP-iCP9 mice i.p. and sacrificed 24 hours later to stain for EGCs and astrocytes. We observed a robust depletion of EGCs throughout the gastrointestinal tract (Figure 3.10a-d), with no apparent effect on CNS astrocytes (Figure 3.10e).

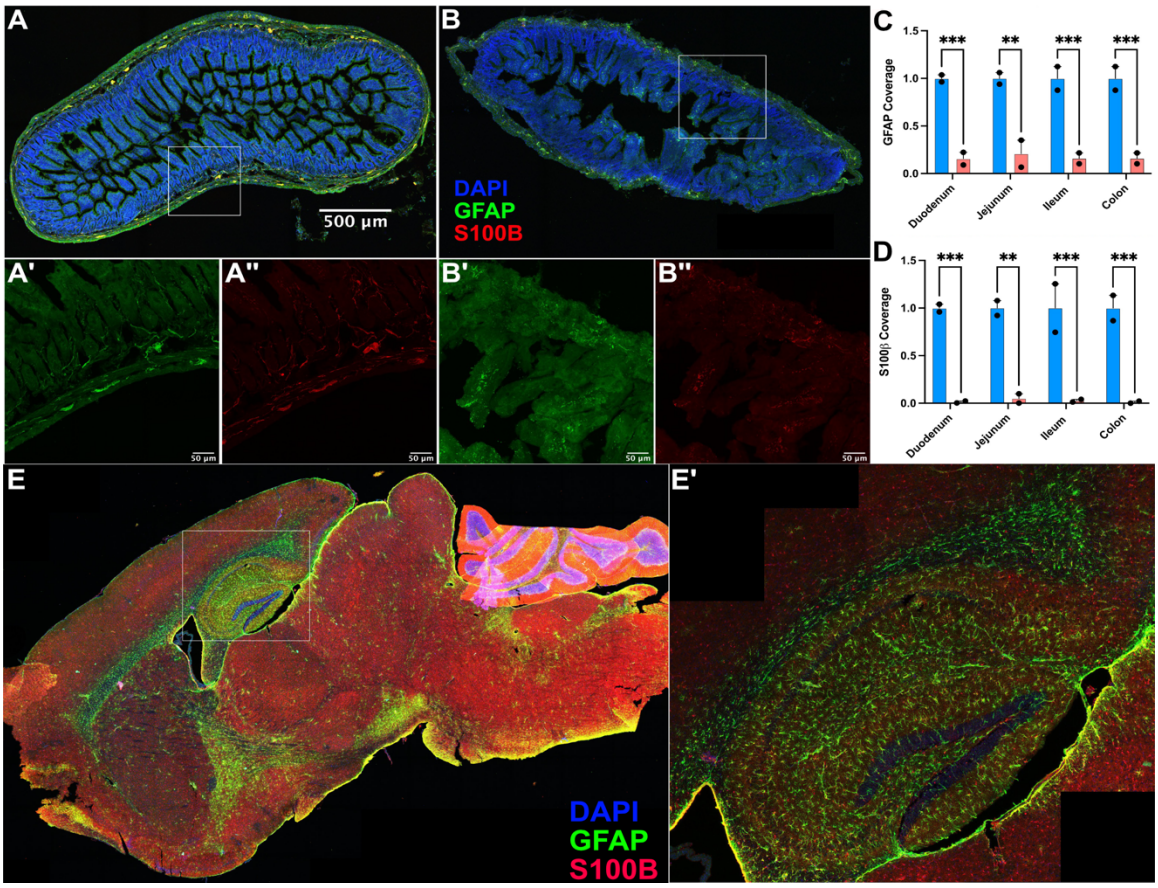

Figure 3.10 A model for selective ablation of enteric glial cells

(a) Representative 10x image of a GFAP-iCP9- ileum 24 hours post CID delivery. (a') Isolated GFAP channel at 63x magnification of the boxed region in a. (a'') Isolated S100B channel at 63x magnification of the boxed region in a. (b) Representative 10x image of a GFAP-iCP9+ ileum 24 hours post CID delivery. (b') Isolated GFAP channel at 63x magnification of the boxed region in b. (b'') Isolated S100B channel at 63x magnification of the boxed region in b. (c) Quantification of GFAP coverage throughout the gastrointestinal tract. (d) Quantification of S100B coverage throughout the gastrointestinal tract. (e) Representative 10x image of a GFAP-iCP9+ brain 24 hours post CID delivery. (e') 63x magnification of the boxed region in e. Unpaired student's t-test was used, *p < .05, **p< .01, N=1, n=2 mice/group.

3.5 Discussion

Together, these results suggest a limited capacity for autoimmune targeting of enteric glial cells in active EAE driven by purified myelin or $PLP_{178-191}$. In the acute phase, we did not observe any signs of antigen presentation or T cell activation in the intestine. This was also the case during the chronic phase of $PLP_{178-191}$ EAE – in fact we observed a significant decrease in MHC II expression by immune throughout the intestine as well as a decrease in MHC I expression by EGCs. Paired with our observation of a high Treg/Th17 ratio during the acute phase, a more regulatory adaptive immune response may be occurring in the intestines during these EAE models and should be further explored. A major limitation of these studies is that the primary site of T cell priming occurs in the spleen and inguinal lymph nodes near the site of injection[239]. As such, T-cell mediated immunity in the gut is not implicated in disease pathogenesis. A more relevant EAE model to utilize would be adoptive transfer-mediated EAE, in which gut homing of myelin-autoreactive T cells is observed to be important in disease pathogenesis[235]. We have begun to optimize adoptive transfer driven models of EAE where splenocytes are harvested from MOG_{35-55} immunized mice, restimulated *in vitro* under Th17 skewing conditions and transferred into RAG2 deficient mice which lack endogenous T/B cells. Using this model, we have demonstrated an accumulation of pathogenic Th17/Th1 CD4+ T cells in the large intestine during the chronic phase of disease (data not shown). While we did not observe any significant changes in MHC I/II expression by professional APCs in this model (data not shown), it should be noted that our initial studies to optimize the model utilized MOG_{35-55} antigen primed T cells which is not expressed by EGCs. As such, we would not expect robust autoimmune targeting of EGCs in this context. Future studies should continue to optimize adoptive transfer EAE models driven my $PLP_{178-191}$ peptide and further explore autoimmune targeting of EGCs.

Our pilot data utilizing the GFAP-iCP9 model to selectively ablate EGCs can further be utilized to model autoimmune targeting of EGCs in the context of demyelinating diseases. Selective ablation of EGCs is significant because most current methods used to ablate EGCs also target glia in the CNS[147]. A study has previously described a model driving the HSV-Tk transgene using the GFAP promoter paired with ganciclovir is sufficient to ablate of EGCs and results in lethal fulminant jejuno-ileitis while CNS glia are spared[157]. However, it has since been shown that while a model of EGC ablation driven by expressing the Diphtheria toxin subunit A in PLP-expressing cells also impacts CNS glia, there are no signs of robust intestinal inflammation in the same time period as reported in the GFAP HSV-Tk model – further these authors show the GFAP-HSV-tk model results in off target effects that may explain the lethality observed in this model[147]. We believe our proposed model will be the first to selectively ablate peripheral GFAP-expressing cells including EGCs for a prolonged time (2-4 weeks) and will be easily titratable, allowing us to determine their impact on EAE disease progression. Future studies will provide an

in-depth characterization of the kinetics of EGC ablation and repopulation in the GFAP-iCP9 model. Once this is achieved, it would be informative to combine targeted EGC ablation with adoptive transfer driven EAE models to investigate if EGC-derived antigens contribute to disease onset.

3.6 Methods

3.6.1 Animals

C57BL/6 (000664) and PLP-EGFP (033357) mice were purchased from Jackson Laboratories. All mice were kept on a 12-hour light/dark schedule. All procedures were approved by the University of Virginia IACUC (protocol #1918, #3968). GFAP-iCP9 mice and CID injections were performed by a collaborator at George Washington University.

3.6.2 Mouse myelin purification

Mouse myelin was prepared as previously described[240]. Briefly, brains from C57BL/6 mice were homogenized in 0.32 M sucrose first by a polytron homogenized then by a Dounce homogenizer. Myelin was recovered by sucrose gradient ultracentrifugation and washed in H_2O. The pellet was resuspended in 0.32 M sucrose, layered over 0.85 M sucrose and centrifuged at 75,000g for 30 min. Myelin was recovered and resuspended in PBS. Protein quantification was performed by BCA assay.

3.6.3 Experimental autoimmune encephalomyelitis

EAE was induced in female C57BL/6 mice between 8 and 12 weeks of age. Purified myelin or $PLP_{178-191}$ peptide (Anaspec; AS-62741) was emulsified in complete Freund's adjuvant containing *Mycobacterium tuberculosis* (1 mg/mL, Sigma; F5881; M. tuberculosis (BD 231141) added to final concentration of 4 mg/mL) and was injected subcutaneously (100 µL volume) at the base of the tail at a concentration of 100 µg/mouse. Pertussis toxin (200 ng, List Biologicals; 180) was administered i.p. on the day of and 1 day after immunization. Mice were scored daily by 2 blinded evaluators using the following scale: 0-no clinical disease, 1-limp tail, 2-hindlimb incoordination, 3-hindlimb weakness, 4-hindlimb paralysis, 5-moribund.

3.6.4 Tissue harvest and digestion

Intestinal tissue was flayed open and fecal contents were washed away with ice cold HBSS. For experiments analyzing the SI LMMP separately, the small intestine was pinned mucosa-side down on a sylgard coated dish emerged in PBS and the LMMP was dissected away from the mucosa using sterile cotton swabs. Intestinal tissue was cut into ~2 cm pieces and collected into 20 mL predigestion media containing HBSS, 10 mM HEPES (Gibco; 15630-080), 5 mM EDTA (Invitrogen; 15575-038), and 10% FBS. Samples were shaken at 215 rpm for 15 minutes at 37°C to

remove mucus and debris. Gut pieces were filtered over a mosquito net then placed in fresh predigestion media and shaken again at 215 rpm for 15 minutes at 37°C. Samples were again filtered over a mosquito then transferred to a weigh boat and homogenized using a sterilized razor blade. The homogenized tissue was transferred to a 50 mL conical tube and suspended in 20 mL gut digest buffer containing RPMI 1640 with .13 Wünsch units Liberase TM and 100 Units/mL DNase I. Samples were shaken at 215 rpm for 30-45 minutes at 37°C. Once digested, the samples were passed through a 70 μm cell strainer and diluted with 20 mL Colon Predigestion media. Samples were centrifuged at 652 RCF for 5 minutes at 4°C, then washed two more times in FACS buffer containing PBS with 5 mM EDTA and 5% FBS prior to cell counting and staining for flow cytometry.

3.6.5 Flow cytometry

Flow Cytometry was performed using a Beckman Coulter Gallios flow cytometer. The following antibodies were used: CD4(RM4-5, BD Biosciences), CD45 (30-F11, eBioscience), CD69 (H1.2F3, eBioscience), CD8α (53-6.7, eBioscience), MHC I (28-8-6, Biolegend), MHC II (M5/114.5.2, eBioscience), FoxP3 (Invitrogen; 25-5773-82), Rorgt (Invitrogen, 12-6981-82). Viability was assessed using a Zombie Red Fixable Viability Kit (Biolegend; 423109). Data were analyzed with FlowJo software v10.10.0.

3.6.6 Serum IgG ELISA

A direct ELISA was used to determine serum IgG binding to ENS antigens. High binding 96 well plates (Greiner Bio-One; 655081) were coated 50 μL/well with either 100μg LMMP lysate or 50 μg $PLP_{178-191}$ in Carbonate binding buffer overnight at 4°C. The next day, plates were washed 5 times with ELISA wash solution containing TBS with .05% Tween 20 (Fisher Scientific; BP337-500), then incubated with 200μL/well ELISA blocking buffer containing PBS with 1% BSA (Fisher bioreagents; 9048-46-8) at room temperature for 2 hours. Next, the blocking buffer was removed, and serum samples were plated in duplicate three-fold serial dilutions from 1:100 to 1:8100. Samples were incubated overnight at 4°C, then washed 5 times with ELISA wash solution. 1 μg/mL biotinylated anti-mouse IgG (Thermo Scientific; 13-4013-85) was added and incubated for 1 hour at room temperature. Samples were washed 5 times and incubated with 1:1000 Avidin-AP (Sigma; A7295) for 30 minutes at room temperature. Samples were washed 5 times and incubated with ELISA detection solution containing PBS with 1% BSA, .05% Tween 20, 2 mg/ml PNPP (Thermo Scientific;34045), 1:500 1M $MgCl_2$ at 37°C until color change was developed. Absorbance at 405 nm was measured with a Biotek Epoch Microplate Spectrophotometer.

3.6.7 Immunofluorescence and confocal microscopy

Following intestinal and brain tissue harvest, samples were fixed in 10% formalin solution overnight at 4°C, then they were transferred to 30% sucrose in PBS until the sample reaches equilibration and sinks to the bottom of the solution. At this point,

samples were mounted in cryomolds with OCT (Tissue-Tek;4583) and flash frozen. 20 μm cryosections (cross sections) were collected onto charged slides (Fisher Scientific; 12-550-17) and stored at 4°C until staining. Sections were stained with primary antibodies overnight at 4°C and secondary antibodies at room temperature for 2 hours. Antibodies used are anti-GFAP (Abcam; ab4674) and anti-S100B (Proteintech; 15146-1-AP). Glass coverslips were mounted using Prolong Gold and imaged at 10x and 63x magnification using a Leica Stellaris confocal microscope. Laser intensity and gain were set using secondary only controls and were kept constant for all image acquisitions. Image analysis was performed in ImageJ (Version 2.14.0/1.54f). Percent area was calculated by thresholding to the same value for each image.

3.6.8 Statistical analysis

Unless otherwise stated, all statistical analyses were run on GraphPad Prism 9 Version 10.2.3. Statistical tests and p values for each comparison are listed in the figure legends. Sample sizes are reported in the figure legends, where n denotes the total number of experimental units used in each analysis, and N denotes the total number of experimental replicates included in each analysis. A significance level of $\alpha = 0.05$ was used throughout unless indicated otherwise.

Chapter 4: Summary and concluding remarks

4.1 Dissertation discussion

This dissertation has investigated the capacity of enteric glial cells to regulate T cell responses in mouse models of Inflammatory Bowel Disease, infection, and autoimmunity. We provided an in-depth characterization of the capacity of EGCs to act as antigen presenting cells (Chapter 2) and explored the possibility of EGC-derived myelin antigens impacting T cell mediated autoimmunity in demyelinating diseases (Chapter 3). These studies have provided new insights into the immune regulatory capacity of EGCs and have also lent to a plethora of outstanding questions. This discussion will summarize key findings and explore a few of these outstanding questions in detail.

Enteric glial cells as nonconventional antigen presenting cells

The ability of CNS glial cells to act as nonconventional antigen presenting cells has often been postulated, with several studies highlighting expression of MHC II in astrocytes and oligodendrocyte lineage cells, as summarized in a review by Sutter et al[241]. Despite reports of MHC II expression, functional studies observing antigen presentation by astrocytes and oligodendrocytes are limited. This has similarly been the case for enteric glial cells, as there were no direct functional studies investigating EGC antigen presentation prior to our work. Our work determined EGCs are capable of priming naïve $CD8^+$ T cells via MHC I-mediated antigen presentation through the conventional cytosolic pathway as well as through antigen cross-presentation. Meanwhile our results demonstrated that EGCs are not capable of priming naïve $CD4^+$ T cells via MHC II-mediated antigen presentation. A notable limitation in these studies is that we did not examine the capacity of EGCs to activate memory $CD4^+$ T cells. A study by Falcão et al. demonstrated that while Oligodendrocyte Progenitor Cells are not capable of priming naïve $CD4^+$ T cells *in vitro*, they are able to induce proliferation of memory $CD4^+$ T cells[242]. Future studies should explore the capacity of enteric glial cells to activate memory $CD4^+$ T cells. This could be achieved by utilizing *Toxoplasma gondii* infection driven by the Prugniaud strain of the parasite, which expresses a truncated Ovalbumin protein (hereon referred to as Pru OVA)[243]. Memory $CD4^+$ T cells could be isolated from Pru Ova infected mile and cocultured with primary EGCs after treatment with IFNγ and Ovalbumin. Still, the functional relevance of EGC MHC II expression *in vivo* remains a question, as our data showed that EGC MHC II expression levels were ~10-fold lower than professional antigen presenting cells. Addressing the functional relevance of EGC MHC II expression *in vivo* will require the development of novel systems to selectively target EGCs. This could be potentially achieved through intersectional genetic approaches – for example generation of GFAP-FLP, PLP-Cre mice should effectively target EGCs while sparing CNS oligodendrocytes and astrocytes as they do not express both of these markers.

Enteric glial cell phagocytosis and antigen cross-presentation

Our observation that primary EGC cultures are capable processing Ovalbumin and cross-presenting to $CD8^+$ T cells highlights previously undefined cellular functions. A study by Chow et al. reported that cultured EGCs are not capable of engulfment based on assays performed by incubating primary whole mount myenteric plexus cultures with fluorescent microspheres[180]. This is inconsistent with our findings, as the internalization and processing of Ovalbumin occurs via phagocytosis[244]. These inconsistencies could be explained by differences in culture preparations, where our studies utilized dissociated cell cultures instead of wholemount LMMP preps. It is unclear which EGC subtypes are represented in dissociated cell cultures though they do display with diverse morphological phenotypes. Live cell imaging with DQ Ova would be useful in determining if all EGCs in our culture system are capable of phagocytosis or if this is limited to a subset of cells – as DQ Ova is an ovalbumin conjugate that emits green fluorescence upon proteolytic degradation. Furthermore, analysis of single cell transcriptional data could help in determining if particular EGC subsets show differential expression of cell-surface receptors that are involved in engulfment and can open the door for the development of mouse models to study EGC phagocytosis *in vivo*.

The capacity of EGCs to act as antigen presenting cells *in vivo* should also be explored. Previous work in our lab has suggested that antigen cross presentation by Oligodendrocyte Progenitor Cells might be implicated in Experimental Autoimmune Encephalomyelitis[245]. I generated $PLP^{CreERT2}$,$B2m^{fl/fl}$ mice in an attempt to disrupt MHC I-mediated antigen presentation in EGCs. In this model, tamoxifen- inducible deletion of the MHC I-associated protein Beta-2 microglobulin (B2m) should result in impaired cell surface expression of MHC I. However, we did not observe any reduction in EGC MHC I cell surface expression upon tamoxifen administration either *in vivo* or *in vitro* (data not shown). Alternative approaches to address this could include deletion of MHC I using H-$2Kb^{fl/fl}$, H-$2kd^{fl/fl}$ mice which allow for Cre-recombinase inducible deletion of both MHC I alleles in C57BL/6 mice[246]. Given our observations of significant upregulation of MHC I by EGCs and increased $CD8^+$ T cell activation in the intestines during acute *T. gondii* infection, this would be an excellent model to further investigate the functional relevance of EGC antigen cross presentation.

Enteric glial cell responses to Toxoplasma gondii infection

We noted a distinct morphological change in intraganglionic EGCs during acute *T. gondii* infection, where EGCs appeared swollen and resembled a 'reactive gliosis' like phenotype observed in other models of inflammation[126,222]. A study by Dora et al. describe the existence of a physical blood-myenteric barrier that is characterized by extracellular matrix proteins agrin and collagen-4[222]. These authors further demonstrate deterioration of this barrier in DSS colitis which coincides with an increase in intraganglionic muscularis macrophages and glial swelling akin to

the morphological phenotype we observed in our studies. Ongoing studies seek to further characterize changes observed in myenteric ganglia by immunofluorescent labeling of enteric neurons (PGP 9.5, HuC/D) and glia (Sox10, GFAP), muscularis macrophages (Iba1), and basement membrane (Agrin). Additionally, we seek to determine transcriptional changes in EGCs during infection by bulk RNA sequencing of FACS-isolated GFP positive cells. These studies will provide new insights into EGC reactivity during intestinal inflammation caused by pathological infections and could help identify new targets that are relevant in disease contexts.

Enteric glia as a link between the gut and neurological disorders

Intestinal dysfunction is associated with a variety of neurological disorders, including Alzheimer's Disease[247–249], Parkinson's Disease[250], Autism Spectrum Disorder[192,251,252], and Multiple Sclerosis[230,234,253]. A putative role for EGCs contributing to autoimmune interactions against myelin in MS has been extensively discussed in the previous chapter and should continue to be explored in future studies. Beyond this, enteric glial cell regulation of intestinal barrier integrity, modulation of local and systemic immune responses, and interactions with the intestinal microbiome represent key facets of cellular functions that could influence neurological disorders. Amyloid-beta deposition is observed in the ENS in Alzheimer's Disease[186] and is being actively explored in rodent models[188,254,255]. In Parkinson's disease, alpha-synuclein aggregates are hypothesized to first appear in the ENS before spreading to the CNS[256,257], potentially implicating EGCs in early pathogenesis. Similarly, altered intestinal function and gut dysbiosis have been observed in autism spectrum disorder[251,252,258,259], highlighting putative roles for EGCs in neurodevelopmental disorders.

Understanding EGCs as mediators of gut-brain interactions can open avenues for novel therapies targeting the ENS to mitigate neurological disease progression, as well as potentially identifying novel biomarkers for earlier diagnoses of risk factors associated with neurological disorders. Future research should explore EGC-specific signaling mechanisms and therapeutic strategies to harness their neuroprotective potential.

4.2 Concluding remarks

This dissertation has furthered our knowledge of immune regulation by enteric glial cells. This work provided new insights into the functional capacity of enteric glial cells to act as antigen presenting cells and explored how enteric glial cell derived antigens might be implicated in the pathogenesis of Multiple Sclerosis. While not every question that was initially pondered in these studies has been answered, exciting new paths forward have been laid for future studies to continue to investigate this fascinating cell type.

Literature cited

1. Kunze, W. A. & Furness, J. B. The enteric nervous system and regulation of intestinal motility. *Annu Rev Physiol* **61**, 117–142 (1999).
2. Furness, J. B. The enteric nervous system and neurogastroenterology. *Nat Rev Gastroenterol Hepatol* **9**, 286–294 (2012).
3. Furness, J. B. Integrated Neural and Endocrine Control of Gastrointestinal Function. in *The Enteric Nervous System: 30 Years Later* (eds. Brierley, S. & Costa, M.) 159–173 (Springer International Publishing, Cham, 2016). doi:10.1007/978-3-319-27592-5_16.
4. Jarret, A. *et al.* Enteric Nervous System-Derived IL-18 Orchestrates Mucosal Barrier Immunity. *Cell* **180**, 50-63.e12 (2020).
5. Progatzky, F. *et al.* Regulation of intestinal immunity and tissue repair by enteric glia. *Nature* **599**, 125–130 (2021).
6. Furness, J. B., Callaghan, B. P., Rivera, L. R. & Cho, H.-J. The Enteric Nervous System and Gastrointestinal Innervation: Integrated Local and Central Control. in *Microbial Endocrinology: The Microbiota-Gut-Brain Axis in Health and Disease* (eds. Lyte, M. & Cryan, J. F.) 39–71 (Springer, New York, NY, 2014). doi:10.1007/978-1-4939-0897-4_3.
7. Furness, J. B. & Stebbing, M. J. The first brain: Species comparisons and evolutionary implications for the enteric and central nervous systems. *Neurogastroenterology & Motility* **30**, e13234 (2018).
8. Hoff, S. *et al.* Quantitative assessment of glial cells in the human and guinea pig enteric nervous system with an anti-Sox8/9/10 antibody. *Journal of Comparative Neurology* **509**, 356–371 (2008).
9. Gabella, G. & Trigg, P. Size of neurons and glial cells in the enteric ganglia of mice, guinea-pigs, rabbits and sheep. *J Neurocytol* **13**, 49–71 (1984).
10. Gabella, G. Ultrastructure of the nerve plexuses of the mammalian intestine: The enteric glial cells. *Neuroscience* **6**, 425–436 (1981).
11. McClain, J. L. *et al.* Ca2+ Responses in Enteric Glia Are Mediated by Connexin-43 Hemichannels and Modulate Colonic Transit in Mice. *Gastroenterology* **146**, 497-507.e1 (2014).
12. McClain, J. L., Fried, D. E. & Gulbransen, B. D. Agonist-Evoked Ca2+ Signaling in Enteric Glia Drives Neural Programs That Regulate Intestinal Motility in Mice. *Cell Mol Gastroenterol Hepatol* **1**, 631–645 (2015).
13. Savidge, T. C. *et al.* Enteric Glia Regulate Intestinal Barrier Function and Inflammation Via Release of *S*-Nitrosoglutathione. *Gastroenterology* **132**, 1344–1358 (2007).
14. Baghdadi, M. B. *et al.* Enteric glial cell heterogeneity regulates intestinal stem cell niches. *Cell Stem Cell* **29**, 86-100.e6 (2022).
15. Grubišić, V. *et al.* Enteric Glia Modulate Macrophage Phenotype and Visceral Sensitivity following Inflammation. *Cell Reports* **32**, 108100 (2020).
16. Schneider, K. M. *et al.* The enteric nervous system relays psychological stress to intestinal inflammation. *Cell* **186**, 2823-2838.e20 (2023).

17. Whytt, R. *The works of Robert Whytt, M.D. ... Published by his son. 1768*. (1768).
18. Abernethy, J. *The Abernethian Code of Health and Longevity, or, Every One's Health in His Own Keeping*. (J. Williams, No. 44, Paternoster Row, and sold by all Booksellers, 1829).
19. Bayliss, W. M. & Starling, E. H. The movements and innervation of the small intestine. *The Journal of Physiology* **24**, 99–143 (1899).
20. Bayliss, W. M. & Starling, E. H. The movements and the innervation of the large intestine. *The Journal of Physiology* **26**, 107–118 (1900).
21. Dogiel A. Uber den Bau der Ganglien in den Geflechten des Darmes und der Gallenblase des Menschen und der Saugethieren. *Arch. Anat. Physiol. (Leipzig)* **53**, 130–158 (1899).
22. Stöhr, P. Zusammenfassende Ergebnisse über die Endigungsweise des Vegetativen Nervensystems. I. *Acta Neurovegetativa* **10**, 21–61 (1954).
23. Gabella, G. Fine structure of the myenteric plexus in the guinea-pig ileum. *J Anat* **111**, 69–97 (1972).
24. Ramón y Cajal, S., Ramón y Cajal, S. & Azoulay, L. *Les Nouvelles Idées Sur La Structure Du Système Nerveux : Chez l'homme et Chez Les Vertébrés*. (C. Reinwald & Cie, Paris, 1894). doi:10.5962/bhl.title.48561.
25. Baumgarten, H. G., Holstein, A.-F. & Owman, Ch. Auerbach's plexus of mammals and man: Electron microscopic identification of three different types of neuronal processes in myenteric ganglia of the large intestine from rhesus monkeys, guinea-pigs and man. *Z. Zellforsch.* **106**, 376–397 (1970).
26. Gulbransen, B. D. Enteric Glia. *Colloquium Series on Neuroglia in Biology and Medicine: from Physiology to Disease* **1**, 1–70 (2014).
27. Heanue, T. A., Shepherd, I. T. & Burns, A. J. Enteric nervous system development in avian and zebrafish models. *Dev Biol* **417**, 129–138 (2016).
28. Anderson, R. B., Stewart, A. L. & Young, H. M. Phenotypes of neural-crest-derived cells in vagal and sacral pathways. *Cell Tissue Res* **323**, 11–25 (2006).
29. Fu, M., Lui, V. C. H., Sham, M. H., Cheung, A. N. Y. & Tam, P. K. H. HOXB5 expression is spatially and temporarily regulated in human embryonic gut during neural crest cell colonization and differentiation of enteric neuroblasts. *Dev Dyn* **228**, 1–10 (2003).
30. Yntema, C. L. & Hammond, W. S. The origin of intrinsic ganglia of trunk viscera from vagal neural crest in the chick embryo. *J Comp Neurol* **101**, 515–541 (1954).
31. Le Douarin, N. M. & Teillet, M. A. The migration of neural crest cells to the wall of the digestive tract in avian embryo. *J Embryol Exp Morphol* **30**, 31–48 (1973).
32. Burns, A. J. & Douarin, N. M. The sacral neural crest contributes neurons and glia to the post-umbilical gut: spatiotemporal analysis of the development of the enteric nervous system. *Development* **125**, 4335–4347 (1998).
33. Burns, A. J., Champeval, D. & Le Douarin, N. M. Sacral neural crest cells colonise aganglionic hindgut in vivo but fail to compensate for lack of enteric ganglia. *Dev Biol* **219**, 30–43 (2000).

34. Wang, X., Chan, A. K. K., Sham, M. H., Burns, A. J. & Chan, W. Y. Analysis of the sacral neural crest cell contribution to the hindgut enteric nervous system in the mouse embryo. *Gastroenterology* **141**, 992-1002.e1–6 (2011).
35. Zuhdi, N. *et al*. Slit molecules prevent entrance of trunk neural crest cells in developing gut. *Int J Dev Neurosci* **41**, 8–16 (2015).
36. Uesaka, T., Nagashimada, M. & Enomoto, H. Neuronal Differentiation in Schwann Cell Lineage Underlies Postnatal Neurogenesis in the Enteric Nervous System. *J. Neurosci.* **35**, 9879–9888 (2015).
37. Simkin, J. E., Zhang, D., Rollo, B. N. & Newgreen, D. F. Retinoic Acid Upregulates Ret and Induces Chain Migration and Population Expansion in Vagal Neural Crest Cells to Colonise the Embryonic Gut. *PLOS ONE* **8**, e64077 (2013).
38. Asai, N. *et al*. Targeted mutation of serine 697 in the Ret tyrosine kinase causes migration defect of enteric neural crest cells. *Development* **133**, 4507–4516 (2006).
39. Pattyn, A., Morin, X., Cremer, H., Goridis, C. & Brunet, J.-F. The homeobox gene Phox2b is essential for the development of autonomic neural crest derivatives. *Nature* **399**, 366–370 (1999).
40. Kim, J., Lo, L., Dormand, E. & Anderson, D. J. SOX10 maintains multipotency and inhibits neuronal differentiation of neural crest stem cells. *Neuron* **38**, 17–31 (2003).
41. Britsch, S. *et al*. The transcription factor Sox10 is a key regulator of peripheral glial development. *Genes Dev* **15**, 66–78 (2001).
42. Pham, T. D., Gershon, M. D. & Rothman, T. P. Time of origin of neurons in the murine enteric nervous system: Sequence in relation to phenotype. *Journal of Comparative Neurology* **314**, 789–798 (1991).
43. Lasrado, R. *et al*. Lineage-dependent spatial and functional organization of the mammalian enteric nervous system. *Science* **356**, 722–726 (2017).
44. Nagy, N. & Goldstein, A. M. Enteric nervous system development: A crest cell's journey from neural tube to colon. *Seminars in Cell & Developmental Biology* **66**, 94–106 (2017).
45. Rao, M. & Gershon, M. D. Enteric nervous system development: what could possibly go wrong? *Nat Rev Neurosci* **19**, 552–565 (2018).
46. Jean, A. Brain stem control of swallowing: neuronal network and cellular mechanisms. *Physiol Rev* **81**, 929–969 (2001).
47. Reynolds, R. P., El-Sharkawy, T. Y. & Diamant, N. E. Lower esophageal sphincter function in the cat: role of central innervation assessed by transient vagal blockade. *American Journal of Physiology-Gastrointestinal and Liver Physiology* **246**, G666–G674 (1984).
48. Kirchgessner, A. L. & Gershon, M. D. Projections of submucosal neurons to the myenteric plexus of the guinea pig intestine: In vitro tracing of microcircuits by retrograde and anterograde transport. *Journal of Comparative Neurology* **277**, 487–498 (1988).
49. Bertrand, P. P., Kunze, W. A., Bornstein, J. C., Furness, J. B. & Smith, M. L. Analysis of the responses of myenteric neurons in the small intestine to

chemical stimulation of the mucosa. *American Journal of Physiology-Gastrointestinal and Liver Physiology* **273**, G422–G435 (1997).
50. Kirchgessner, A. L., Tamir, H. & Gershon, M. D. Identification and stimulation by serotonin of intrinsic sensory neurons of the submucosal plexus of the guinea pig gut: activity- induced expression of Fos immunoreactivity. *J. Neurosci.* **12**, 235–248 (1992).
51. Gershon, M. D. & Kirchgessner, A. L. Identification, characterization and projections of intrinsic primary afferent neurones of the submucosal plexus: activity-induced expression of *c-fos* immunoreactivity. *Journal of the Autonomic Nervous System* **33**, 185–187 (1991).
52. Furness, J. B., Kunze, W. A. A., Bertrand, P. P., Clerc, N. & Bornstein, J. C. Intrinsic primary afferent neuronsof the intestine. *Progress in Neurobiology* **54**, 1–18 (1998).
53. Hendriks, R., Bornstein, J. C. & Furness, J. B. An electrophysiological study of the projections of putative sensory neurons within the myenteric plexus of the guinea pig ileum. *Neuroscience Letters* **110**, 286–290 (1990).
54. Evans, R. J., Derkach, V. & Surprenant, A. ATP mediates fast synaptic transmission in mammalian neurons. *Nature* **357**, 503–505 (1992).
55. Galligan, J. J., LePard, K. J., Schneider, D. A. & Zhou, X. Multiple mechanisms of fast excitatory synaptic transmission in the enteric nervous system. *Journal of the Autonomic Nervous System* **81**, 97–103 (2000).
56. Johnson, P. j., Bornstein, J. c., Yuan, S. y. & Furness, J. b. Analysis of contributions of acetylcholine and tachykinins to neuro-neuronal transmission in motility reflexes in the guinea-pig ileum. *British Journal of Pharmacology* **118**, 973–983 (1996).
57. Hardwick, J. C., Mawe, G. M. & Parsons, R. L. Tachykinin-induced activation of non-specific cation conductance via NK3 neurokinin receptors in guinea-pig intracardiac neurones. *The Journal of Physiology* **504**, 65 (1997).
58. Furness, J. B., Jones, C., Nurgali, K. & Clerc, N. Intrinsic primary afferent neurons and nerve circuits within the intestine. *Progress in Neurobiology* **72**, 143–164 (2004).
59. Costa, M. *et al*. Neurochemical classification of myenteric neurons in the guinea-pig ileum. *Neuroscience* **75**, 949–967 (1996).
60. Brookes, S. J. H., Steele, P. A. & Costa, M. Identification and immunohistochemistry of cholinergic and non-cholinergic circular muscle motor neurons in the guinea-pig small intestine. *Neuroscience* **42**, 863–878 (1991).
61. Tonini, M. & Costa, M. A pharmacological analysis of the neuronal circuitry involved in distension-evoked enteric excitatory reflex. *Neuroscience* **38**, 787–795 (1990).
62. Pompolo, S. & Furness, J. B. Sources of inputs to longitudinal muscle motor neurons and ascending interneurons in the guinea-pig small intestine. *Cell Tissue Res* **280**, 549–560 (1995).

63. Nurgali, K., Furness, J. B. & Stebbing, M. J. Analysis of purinergic and cholinergic fast synaptic transmission to identified myenteric neurons. *Neuroscience* **116**, 335–347 (2003).
64. Natale, M. R. D. *et al.* Morphologies, dimensions and targets of gastric nitric oxide synthase neurons. *Cell and Tissue Research* **388**, 19 (2022).
65. Monro, R. L., Bertrand, P. P. & Bornstein, J. C. ATP and 5-HT are the principal neurotransmitters in the descending excitatory reflex pathway of the guinea-pig ileum. *Neurogastroenterology & Motility* **14**, 255–264 (2002).
66. Pompolo, S. & Furness, J. B. Quantitative analysis of inputs to somatostatin-immunoreactive descending interneurons in the myenteric plexus of the guinea-pig small intestine. *Cell Tissue Res* **294**, 219–226 (1998).
67. Ekblad, E., Winther, C., Ekman, R., Ha ̊kanson, R. & Sundler, F. Projections of peptide-containing neurons in rat small intestine. *Neuroscience* **20**, 169–188 (1987).
68. Holzer, P. & Holzer-Petsche, U. Tachykinins in the gut. Part I. Expression, release and motor function. *Pharmacology & Therapeutics* **73**, 173–217 (1997).
69. Suthamnatpong, N., Hata, F., Kanada, A., Takeuchi, T. & Yagasaki, O. Mediators of nonadrenergic, noncholinergic inhibition in the proximal, middle and distal regions of rat colon. *British Journal of Pharmacology* **108**, 348–355 (1993).
70. Crist, J. R., He, X. D. & Goyal, R. K. Both ATP and the peptide VIP are inhibitory neurotransmitters in guinea-pig ileum circular muscle. *The Journal of Physiology* **447**, 119–131 (1992).
71. Okasora, T., Bywater, R. A. R. & Taylor, G. S. Projections of enteric motor neurons in the mouse distal colon. *Gastroenterology* **90**, 1964–1971 (1986).
72. Wright, E. M. & Loo, D. D. F. Coupling between Na+, Sugar, and Water Transport across the Intestine. *Annals of the New York Academy of Sciences* **915**, 54–66 (2000).
73. Furness, J. B., Alex, G., Clark, M. J. & Lal, V. V. Morphologies and projections of defined classes of neurons in the submucosa of the guinea-pig small intestine. *The Anatomical Record Part A: Discoveries in Molecular, Cellular, and Evolutionary Biology* **272A**, 475–483 (2003).
74. Song, Z.-M., Brookes, S. J. H., Steele, P. A. & Costa, M. Projections and pathways of submucous neurons to the mucosa of the guinea-pig small intestine. *Cell Tissue Res* **269**, 87–98 (1992).
75. Porter, A. J., Wattchow, D. A., Brookes, S. J. & Costa, M. Projections of nitric oxide synthase and vasoactive intestinal polypeptide-reactive submucosal neurons in the human colon. *Journal of Gastroenterology and Hepatology* **14**, 1180–1187 (1999).
76. Crowcroft, P. J., Holman, M. E. & Szurszewski, J. H. Excitatory input from the distal colon to the inferior mesenteric ganglion in the guinea-pig. *The Journal of Physiology* **219**, 443–461 (1971).
77. Szurszewski, J. H. & Weems, W. A. A study of peripheral input to and its control by post-ganglionic neurones of the inferior mesenteric ganglion. *The Journal of Physiology* **256**, 541–556 (1976).

78. Miller, S. M. & Szurszewski, J. H. Colonic mechanosensory afferent input to neurons in the mouse superior mesenteric ganglion. *American Journal of Physiology-Gastrointestinal and Liver Physiology* **272**, G357–G366 (1997).
79. Sharkey, K. A., Lomax, A. E. G., Bertrand, P. P. & Furness, J. B. Electrophysiology, shape, and chemistry of neurons that project from guinea pig colon to inferior mesenteric ganglia. *Gastroenterology* **115**, 909–918 (1998).
80. Muller, P. A. *et al*. Microbiota-modulated CART+ enteric neurons autonomously regulate blood glucose. *Science* **370**, 314–321 (2020).
81. Ward, S. M. & Sanders, K. M. Interstitial cells of Cajal: Primary targets of enteric motor innervation. *The Anatomical Record* **262**, 125–135 (2001).
82. Takaki, M. Gut pacemaker cells: the interstitial cells of Cajal (ICC). *J Smooth Muscle Res* **39**, 137–161 (2003).
83. Spencer, N. J. & Hu, H. Enteric nervous system: sensory transduction, neural circuits and gastrointestinal motility. *Nat Rev Gastroenterol Hepatol* **17**, 338–351 (2020).
84. Browning, K. N. & Travagli, R. A. Central Nervous System Control of Gastrointestinal Motility and Secretion and Modulation of Gastrointestinal Functions. in *Comprehensive Physiology* 1339–1368 (John Wiley & Sons, Ltd, 2014). doi:10.1002/cphy.c130055.
85. Berthoud, H.-R., Jedrzejewska, A. & Powley, T. L. Simultaneous labeling of vagal innervation of the gut and afferent projections from the visceral forebrain with Dil injected into the dorsal vagal complex in the rat. *Journal of Comparative Neurology* **301**, 65–79 (1990).
86. Sanders, K. M., Koh, S. D., Ro, S. & Ward, S. M. Regulation of gastrointestinal motility—insights from smooth muscle biology. *Nat Rev Gastroenterol Hepatol* **9**, 633–645 (2012).
87. Guo, J. J., Browning, K. N., Rogers, R. C. & Travagli, R. A. Catecholaminergic neurons in rat dorsal motor nucleus of vagus project selectively to gastric corpus. *American Journal of Physiology-Gastrointestinal and Liver Physiology* **280**, G361–G367 (2001).
88. Zheng, Z. L., Rogers, R. C. & Travagli, R. A. Selective gastric projections of nitric oxide synthase-containing vagal brainstem neurons. *Neuroscience* **90**, 685–694 (1999).
89. Travagli, R. A., Hermann, G. E., Browning, K. N. & Rogers, R. C. Brainstem Circuits Regulating Gastric Function. *Annual review of physiology* **68**, 279 (2006).
90. Felten, D. L., Felten, S. Y., Carlson, S. L., Olschowka, J. A. & Livnat, S. Noradrenergic and peptidergic innervation of lymphoid tissue. *J Immunol* **135**, 755s–765s (1985).
91. Phillips, R. J. & Powley, T. L. Macrophages associated with the intrinsic and extrinsic autonomic innervation of the rat gastrointestinal tract. *Auton Neurosci* **169**, 12–27 (2012).

92. Gulbransen, B. D., Bains, J. S. & Sharkey, K. A. Enteric Glia Are Targets of the Sympathetic Innervation of the Myenteric Plexus in the Guinea Pig Distal Colon. *The Journal of Neuroscience* **30**, 6801 (2010).
93. Brookes, S. J. H., Spencer, N. J., Costa, M. & Zagorodnyuk, V. P. Extrinsic primary afferent signalling in the gut. *Nat Rev Gastroenterol Hepatol* **10**, 286–296 (2013).
94. Zagorodnyuk, V. P., Chen, B. N., Costa, M. & Brookes, S. J. H. Mechanotransduction by intraganglionic laminar endings of vagal tension receptors in the guinea-pig oesophagus. *The Journal of Physiology* **553**, 575–587 (2003).
95. Lynn, P., Zagorodnyuk, V., Hennig, G., Costa, M. & Brookes, S. Mechanical activation of rectal intraganglionic laminar endings in the guinea pig distal gut. *The Journal of Physiology* **564**, 589–601 (2005).
96. Wang, F. B. & Powley, T. L. Topographic inventories of vagal afferents in gastrointestinal muscle. *J Comp Neurol* **421**, 302–324 (2000).
97. Berthoud, H.-R. & Powley, T. L. Vagal afferent innervation of the rat fundic stomach: Morphological characterization of the gastric tension receptor. *Journal of Comparative Neurology* **319**, 261–276 (1992).
98. Spencer, N. J. *et al*. Identification of capsaicin-sensitive rectal mechanoreceptors activated by rectal distension in mice. *Neuroscience* **153**, 518–534 (2008).
99. Lynn, P. A. & Brookes, S. J. H. Pudendal afferent innervation of the guinea pig external anal sphincter. *Neurogastroenterol Motil* **23**, 871-e343 (2011).
100. Yu, S., Undem, B. J. & Kollarik, M. Vagal afferent nerves with nociceptive properties in guinea-pig oesophagus. *J Physiol* **563**, 831–842 (2005).
101. Song, X. *et al*. Identification of medium/high-threshold extrinsic mechanosensitive afferent nerves to the gastrointestinal tract. *Gastroenterology* **137**, 274–284, 284.e1 (2009).
102. Takaki, M. & Nakayama, S. Effects of capsaicin on myenteric neurons of the guinea pig ileum. *Neuroscience Letters* **105**, 125–130 (1989).
103. Barthó, L., Holzer, P., Lembeck, F. & Szolcsányi, J. Evidence that the contractile response of the guinea-pig ileum to capsaicin is due to release of substance P. *The Journal of Physiology* **332**, 157–167 (1982).
104. Figini, M. *et al*. Substance P and bradykinin stimulate plasma extravasation in the mouse gastrointestinal tract and pancreas. *American Journal of Physiology-Gastrointestinal and Liver Physiology* **272**, G785–G793 (1997).
105. Sann, H., Dux, M., Schemann, M. & Jancsó, G. Neurogenic inflammation in the gastrointestinal tract of the rat. *Neuroscience Letters* **219**, 147–150 (1996).
106. Binshtok, A. M. *et al*. Nociceptors Are Interleukin-1β Sensors. *J. Neurosci.* **28**, 14062–14073 (2008).
107. Andratsch, M. *et al*. A Key Role for gp130 Expressed on Peripheral Sensory Nerves in Pathological Pain. *J. Neurosci.* **29**, 13473–13483 (2009).

108. Li, Y., Ji, A., Weihe, E. & Schäfer, M. K.-H. Cell-Specific Expression and Lipopolysaccharide-Induced Regulation of Tumor Necrosis Factor α (TNFα) and TNF Receptors in Rat Dorsal Root Ganglion. *J. Neurosci.* **24**, 9623–9631 (2004).
109. Barker, N. *et al.* Identification of stem cells in small intestine and colon by marker gene Lgr5. *Nature* **449**, 1003–1007 (2007).
110. Jenny, M. *et al.* Neurogenin3 is differentially required for endocrine cell fate specification in the intestinal and gastric epithelium. *The EMBO Journal* **21**, 6338–6347 (2002).
111. Rehfeld, J. F. A centenary of gastrointestinal endocrinology. *Horm Metab Res* **36**, 735–741 (2004).
112. Engelstoft, M. S., Egerod, K. L., Lund, M. L. & Schwartz, T. W. Enteroendocrine cell types revisited. *Curr Opin Pharmacol* **13**, 912–921 (2013).
113. Gribble, F. M. & Reimann, F. Enteroendocrine Cells: Chemosensors in the Intestinal Epithelium. *Annu Rev Physiol* **78**, 277–299 (2016).
114. Furness, J. B., Rivera, L. R., Cho, H.-J., Bravo, D. M. & Callaghan, B. The gut as a sensory organ. *Nat Rev Gastroenterol Hepatol* **10**, 729–740 (2013).
115. Lin, H. C., Zhao, X. T., Wang, L. & Wong, H. Fat-induced ileal brake in the dog depends on peptide YY. *Gastroenterology* **110**, 1491–1495 (1996).
116. Strader, A. D. & Woods, S. C. Gastrointestinal hormones and food intake. *Gastroenterology* **128**, 175–191 (2005).
117. Kaelberer, M. M. *et al.* A gut-brain neural circuit for nutrient sensory transduction. *Science* **361**, eaat5236 (2018).
118. Buchanan, K. L. *et al.* The preference for sugar over sweetener depends on a gut sensor cell. *Nat Neurosci* **25**, 191–200 (2022).
119. Bohórquez, D. V. *et al.* An enteroendocrine cell-enteric glia connection revealed by 3D electron microscopy. *PLoS One* **9**, e89881 (2014).
120. Allen, N. J. & Lyons, D. A. Glia as architects of central nervous system formation and function. *Science* **362**, 181–185 (2018).
121. Bronner, M. E. & LeDouarin, N. M. Development and evolution of the neural crest: An overview. *Developmental Biology* **366**, 2–9 (2012).
122. Powell, N., Walker, M. M. & Talley, N. J. The mucosal immune system: master regulator of bidirectional gut–brain communications. *Nat Rev Gastroenterol Hepatol* **14**, 143–159 (2017).
123. Rao, M. *et al.* Enteric glia express proteolipid protein 1 and are a transcriptionally unique population of glia in the mammalian nervous system. *Glia* **63**, 2040–2057 (2015).
124. Patyal, P., Fil, D. & Wight, P. A. Plp1 in the enteric nervous system is preferentially expressed during early postnatal development in mouse as DM20, whose expression appears reliant on an intronic enhancer. *Front. Cell. Neurosci.* **17**, (2023).
125. Boesmans, W., Lasrado, R., Vanden Berghe, P. & Pachnis, V. Heterogeneity and phenotypic plasticity of glial cells in the mammalian enteric nervous system. *Glia* **63**, 229–241 (2015).

126. Schneider, R. *et al.* A novel P2X2-dependent purinergic mechanism of enteric gliosis in intestinal inflammation. *EMBO Mol Med* **13**, e12724 (2021).
127. Schneider, R. *et al.* IL-1-dependent enteric gliosis guides intestinal inflammation and dysmotility and modulates macrophage function. *Commun Biol* **5**, 1–16 (2022).
128. Gabella, G. Intramural Ganglia. in *Structure of the Autonomic Nervous System* (ed. Gabella, G.) 117–132 (Springer Netherlands, Dordrecht, 1976). doi:10.1007/978-94-009-5745-9_7.
129. Gulbransen, B. D. & Sharkey, K. A. Purinergic Neuron-to-Glia Signaling in the Enteric Nervous System. *Gastroenterology* **136**, 1349–1358 (2009).
130. Drokhlyansky, E. *et al.* The Human and Mouse Enteric Nervous System at Single-Cell Resolution. *Cell* **182**, 1606-1622.e23 (2020).
131. Elmentaite, R. *et al.* Cells of the human intestinal tract mapped across space and time. *Nature* **597**, 250–255 (2021).
132. Fawkner-Corbett, D. *et al.* Spatiotemporal analysis of human intestinal development at single-cell resolution. *Cell* **184**, 810-826.e23 (2021).
133. Wright, C. M. *et al.* scRNA-Seq Reveals New Enteric Nervous System Roles for GDNF, NRTN, and TBX3. *Cellular and Molecular Gastroenterology and Hepatology* **11**, 1548-1592.e1 (2021).
134. Guyer, R. A. *et al.* Single-cell multiome sequencing clarifies enteric glial diversity and identifies an intraganglionic population poised for neurogenesis. *Cell Reports* **42**, 112194 (2023).
135. Laddach, A. *et al.* A branching model of lineage differentiation underpinning the neurogenic potential of enteric glia. *Nat Commun* **14**, 5904 (2023).
136. Nguyen, T. T., Baumann, P., Tüscher, O., Schick, S. & Endres, K. The Aging Enteric Nervous System. *International Journal of Molecular Sciences* **24**, 9471 (2023).
137. Matheis, F. *et al.* Adrenergic Signaling in Muscularis Macrophages Limits Infection-Induced Neuronal Loss. *Cell* **180**, 64-78.e16 (2020).
138. Janova, H. *et al.* West Nile virus triggers intestinal dysmotility via T cell–mediated enteric nervous system injury. *J Clin Invest* **134**, (2024).
139. Kulkarni, S. *et al.* Adult enteric nervous system in health is maintained by a dynamic balance between neuronal apoptosis and neurogenesis. *Proceedings of the National Academy of Sciences* **114**, E3709–E3718 (2017).
140. De Vadder, F. *et al.* Gut microbiota regulates maturation of the adult enteric nervous system via enteric serotonin networks. *Proceedings of the National Academy of Sciences* **115**, 6458–6463 (2018).
141. Rueckert, H. & Ganz, J. How to Heal the Gut's Brain: Regeneration of the Enteric Nervous System. *International Journal of Molecular Sciences* **23**, 4799 (2022).
142. Belkind-Gerson, J. *et al.* Colitis promotes neuronal differentiation of Sox2+ and PLP1+ enteric cells. *Sci Rep* **7**, 2525 (2017).
143. Laranjeira, C. *et al.* Glial cells in the mouse enteric nervous system can undergo neurogenesis in response to injury. *J Clin Invest* **121**, 3412–3424 (2011).

144. Mueller, J. L. *et al.* Highly neurogenic glia from human and mouse myenteric ganglia generate functional neurons following culture and transplantation into the gut. *Cell Reports* **43**, 114919 (2024).
145. Soret, R. *et al.* Glial Cell-Derived Neurotrophic Factor Induces Enteric Neurogenesis and Improves Colon Structure and Function in Mouse Models of Hirschsprung Disease. *Gastroenterology* **159**, 1824-1838.e17 (2020).
146. Stavely, R. *et al.* Mature enteric neurons have the capacity to reinnervate the intestine with glial cells as their guide. *Neuron* **112**, 3143-3160.e6 (2024).
147. Rao, M. *et al.* Enteric Glia Regulate Gastrointestinal Motility but Are Not Required for Maintenance of the Epithelium in Mice. *Gastroenterology* **153**, 1068-1081.e7 (2017).
148. Grubišić, V. & Parpura, V. Two modes of enteric gliotransmission differentially affect gut physiology. *Glia* **65**, 699–711 (2017).
149. Costa, M., Brookes, S. J. & Hennig, G. W. Anatomy and physiology of the enteric nervous system. *Gut* **47 Suppl 4**, iv15-19; discussion iv26 (2000).
150. Grider, J. R. & Jin, J. G. Distinct populations of sensory neurons mediate the peristaltic reflex elicited by muscle stretch and mucosal stimulation. *J. Neurosci.* **14**, 2854–2860 (1994).
151. Ahmadzai, M. M., Seguella, L. & Gulbransen, B. D. Circuit-specific enteric glia regulate intestinal motor neurocircuits. *Proceedings of the National Academy of Sciences* **118**, e2025938118 (2021).
152. Scavuzzo, M. A. *et al.* Enteric glial hub cells coordinate intestinal motility. *bioRxiv* 2023.06.07.544052 (2023) doi:10.1101/2023.06.07.544052.
153. Bach-Ngohou, K. *et al.* Enteric glia modulate epithelial cell proliferation and differentiation through 15-deoxy-Δ12,14-prostaglandin J2. *The Journal of Physiology* **588**, 2533–2544 (2010).
154. Neunlist, M. *et al.* Enteric glia inhibit intestinal epithelial cell proliferation partly through a TGF-β1-dependent pathway. *American Journal of Physiology-Gastrointestinal and Liver Physiology* **292**, G231–G241 (2007).
155. Van Landeghem, L. *et al.* Enteric glia promote intestinal mucosal healing via activation of focal adhesion kinase and release of proEGF. *American Journal of Physiology-Gastrointestinal and Liver Physiology* **300**, G976–G987 (2011).
156. Van Landeghem, L. *et al.* Regulation of intestinal epithelial cells transcriptome by enteric glial cells: impact on intestinal epithelial barrier functions. *BMC Genomics* **10**, 507 (2009).
157. Bush, T. G. *et al.* Fulminant Jejuno-Ileitis following Ablation of Enteric Glia in Adult Transgenic Mice. *Cell* **93**, 189–201 (1998).
158. Nasser, Y. *et al.* Role of enteric glia in intestinal physiology: effects of the gliotoxin fluorocitrate on motor and secretory function. *American Journal of Physiology-Gastrointestinal and Liver Physiology* **291**, G912–G927 (2006).
159. Prochera, A. *et al.* Enteric glia regulate Paneth cell secretion and intestinal microbial ecology. *eLife* **13**, (2025).
160. Liddelow, S. A. & Barres, B. A. Reactive Astrocytes: Production, Function, and Therapeutic Potential. *Immunity* **46**, 957–967 (2017).

161. Boyen, G. B. T. von *et al.* Proinflammatory cytokines increase glial fibrillary acidic protein expression in enteric glia. *Gut* **53**, 222–228 (2004).
162. Cerantola, S. *et al.* Involvement of Enteric Glia in Small Intestine Neuromuscular Dysfunction of Toll-Like Receptor 4-Deficient Mice. *Cells* **9**, 838 (2020).
163. Clairembault, T. *et al.* Enteric GFAP expression and phosphorylation in Parkinson's disease. *J Neurochem* **130**, 805–815 (2014).
164. McMenamin, C. A., Clyburn, C. & Browning, K. N. High-Fat Diet During the Perinatal Period Induces Loss of Myenteric Nitrergic Neurons and Increases Enteric Glial Density, Prior to the Development of Obesity. *Neuroscience* **393**, 369–380 (2018).
165. Cornet, A. *et al.* Enterocolitis induced by autoimmune targeting of enteric glial cells: A possible mechanism in Crohn's disease? *Proceedings of the National Academy of Sciences* **98**, 13306–13311 (2001).
166. Ma, E. L. *et al.* Bidirectional brain-gut interactions and chronic pathological changes after traumatic brain injury in mice. *Brain, Behavior, and Immunity* **66**, 56–69 (2017).
167. Wunsch, M. *et al.* The enteric nervous system is a potential autoimmune target in multiple sclerosis. *Acta Neuropathol* **134**, 281–295 (2017).
168. Turco, F. *et al.* Enteroglial-derived S100B protein integrates bacteria-induced Toll-like receptor signalling in human enteric glial cells. *Gut* **63**, 105–115 (2014).
169. Esposito, G. *et al.* Palmitoylethanolamide improves colon inflammation through an enteric glia/toll like receptor 4-dependent PPAR-α activation. *Gut* **63**, 1300–1312 (2014).
170. Esposito, G. *et al.* Enteric Glial-Derived S100B Protein Stimulates Nitric Oxide Production in Celiac Disease. *Gastroenterology* **133**, 918–925 (2007).
171. Cirillo, C. *et al.* Increased mucosal nitric oxide production in ulcerative colitis is mediated in part by the enteroglial-derived S100B protein. *Neurogastroenterol Motil* **21**, 1209-e112 (2009).
172. Capoccia, E. *et al.* Enteric glia: A new player in inflammatory bowel diseases. *Int J Immunopathol Pharmacol* **28**, 443–451 (2015).
173. Brown, I. A. M., McClain, J. L., Watson, R. E., Patel, B. A. & Gulbransen, B. D. Enteric glia mediate neuron death in colitis through purinergic pathways that require connexin-43 and nitric oxide. *Cell Mol Gastroenterol Hepatol* **2**, 77–91 (2016).
174. Gulbransen, B. D. *et al.* Activation of neuronal P2X7 receptor-pannexin-1 mediates death of enteric neurons during colitis. *Nat Med* **18**, 600–604 (2012).
175. Mowat, A. M. & Agace, W. W. Regional specialization within the intestinal immune system. *Nat Rev Immunol* **14**, 667–685 (2014).
176. Ibiza, S. *et al.* Glial-cell-derived neuroregulators control type 3 innate lymphoid cells and gut defence. *Nature* **535**, 440–443 (2016).
177. van Baarle, L. *et al.* IL-1R signaling drives enteric glia-macrophage interactions in colorectal cancer. *Nat Commun* **15**, 6079 (2024).

178. Mehrfeld, C., Zenner, S., Kornek, M. & Lukacs-Kornek, V. The Contribution of Non-Professional Antigen-Presenting Cells to Immunity and Tolerance in the Liver. *Front Immunol* **9**, 635 (2018).
179. Barcelos Morais da Silveira, A. *et al.* Enteroglial cells act as antigen-presenting cells in chagasic megacolon. *Human Pathology* **42**, 522–532 (2011).
180. Chow, A. K., Grubišić, V. & Gulbransen, B. D. Enteric Glia Regulate Lymphocyte Activation via Autophagy-Mediated MHC-II Expression. *Cellular and Molecular Gastroenterology and Hepatology* **12**, 1215–1237 (2021).
181. Cryan, J. F., O'Riordan, K. J., Sandhu, K., Peterson, V. & Dinan, T. G. The gut microbiome in neurological disorders. *The Lancet Neurology* **19**, 179–194 (2020).
182. von Boyen, G. B. *et al.* Distribution of enteric glia and GDNF during gut inflammation. *BMC Gastroenterol* **11**, 3 (2011).
183. Braak, H., de Vos, R. A. I., Bohl, J. & Del Tredici, K. Gastric α-synuclein immunoreactive inclusions in Meissner's and Auerbach's plexuses in cases staged for Parkinson's disease-related brain pathology. *Neuroscience Letters* **396**, 67–72 (2006).
184. Challis, C. *et al.* Gut-seeded α-synuclein fibrils promote gut dysfunction and brain pathology specifically in aged mice. *Nat Neurosci* **23**, 327–336 (2020).
185. Pellegrini, C. *et al.* Alteration of colonic excitatory tachykininergic motility and enteric inflammation following dopaminergic nigrostriatal neurodegeneration. *Journal of Neuroinflammation* **13**, 146 (2016).
186. Joachim, C. L., Mori, H. & Selkoe, D. J. Amyloid β-protein deposition in tissues other than brain in Alzheimer's disease. *Nature* **341**, 226–230 (1989).
187. Honarpisheh, P. *et al.* Dysregulated Gut Homeostasis Observed Prior to the Accumulation of the Brain Amyloid-? in Tg2576 Mice. *International Journal of Molecular Sciences* **21**, 1711 (2020).
188. Tasnády, K. R. *et al.* Gastrointestinal Dysfunction and Low-Grade Inflammation Associate With Enteric Neuronal Amyloid-β in a Model for Amyloid Pathology. *Neurogastroenterology & Motility* **n/a**, e15016.
189. Lee, Y. K., Menezes, J. S., Umesaki, Y. & Mazmanian, S. K. Proinflammatory T-cell responses to gut microbiota promote experimental autoimmune encephalomyelitis. *Proceedings of the National Academy of Sciences* **108**, 4615–4622 (2011).
190. Lammert, C. R. *et al.* Cutting Edge: Critical Roles for Microbiota-Mediated Regulation of the Immune System in a Prenatal Immune Activation Model of Autism. *The Journal of Immunology* **201**, 845–850 (2018).
191. Levinthal, D. J. *et al.* Adding to the Burden: Gastrointestinal Symptoms and Syndromes in Multiple Sclerosis. *Multiple Sclerosis International* **2013**, e319201 (2013).
192. Penzol, M. J. *et al.* Functional Gastrointestinal Disease in Autism Spectrum Disorder: A Retrospective Descriptive Study in a Clinical Sample. *Front. Psychiatry* **10**, (2019).

193. Fröhlich, H. *et al.* Gastrointestinal dysfunction in autism displayed by altered motility and achalasia in Foxp1+/− mice. *Proceedings of the National Academy of Sciences* **116**, 22237–22245 (2019).
194. Hosie, S. *et al.* Gastrointestinal dysfunction in patients and mice expressing the autism-associated R451C mutation in neuroligin-3. *Autism Research* **12**, 1043–1056 (2019).
195. James, D. M. *et al.* Intestinal dysmotility in a zebrafish (Danio rerio) shank3a;shank3b mutant model of autism. *Molecular Autism* **10**, 3 (2019).
196. Grubišić, V. *et al.* Enteric glial adenosine 2B receptor signaling mediates persistent epithelial barrier dysfunction following acute DSS colitis. *Mucosal Immunol* **15**, 964–976 (2022).
197. Progatzky, F. & Pachnis, V. The role of enteric glia in intestinal immunity. *Current Opinion in Immunology* **77**, 102183 (2022).
198. Brun, P. *et al.* Toll-Like Receptor 2 Regulates Intestinal Inflammation by Controlling Integrity of the Enteric Nervous System. *Gastroenterology* **145**, 1323–1333 (2013).
199. Geboes, K. *et al.* Major histocompatibility class II expression on the small intestinal nervous system in Crohn's disease. *Gastroenterology* **103**, 439–447 (1992).
200. Kinchen, J. *et al.* Structural Remodeling of the Human Colonic Mesenchyme in Inflammatory Bowel Disease. *Cell* **175**, 372-386.e17 (2018).
201. Kong, L. *et al.* The landscape of immune dysregulation in Crohn's disease revealed through single-cell transcriptomic profiling in the ileum and colon. *Immunity* **56**, 444-458.e5 (2023).
202. Gkountidi, A. O. *et al.* MHC Class II Antigen Presentation by Lymphatic Endothelial Cells in Tumors Promotes Intratumoral Regulatory T cell-Suppressive Functions. *Cancer Immunol Res* **9**, 748–764 (2021).
203. Turesson, C. Endothelial expression of MHC class II molecules in autoimmune disease. *Curr Pharm Des* **10**, 129–143 (2004).
204. Bábíčková, J. *et al.* Sex Differences in Experimentally Induced Colitis in Mice: a Role for Estrogens. *Inflammation* **38**, 1996–2006 (2015).
205. Chassaing, B., Aitken, J. D., Malleshappa, M. & Vijay-Kumar, M. Dextran Sulfate Sodium (DSS)-Induced Colitis in Mice. *Curr Protoc Immunol* **104**, Unit-15.25. (2014).
206. Egan, C. E., Cohen, S. B. & Denkers, E. Y. Insights into inflammatory bowel disease using Toxoplasma gondii as an infectious trigger. *Immunol Cell Biol* **90**, 668–675 (2012).
207. Kovacs, M. A. *et al.* Vascular Endothelial Growth Factor-C Treatment Enhances Cerebrospinal Fluid Outflow during *Toxoplasma gondii* Brain Infection but Does Not Improve Cerebral Edema. *The American Journal of Pathology* **194**, 225–237 (2024).
208. Alonaizan, R., Woods, S., Hargrave, K. E. & Roberts, C. W. An Exaggerated Immune Response in Female BALB/c Mice Controls Initial Toxoplasma gondii

Multiplication but Increases Mortality and Morbidity Relative to Male Mice. *Pathogens* **10**, 1154 (2021).
209. Shin, J.-S. *et al.* Surface expression of MHC class II in dendritic cells is controlled by regulated ubiquitination. *Nature* **444**, 115–118 (2006).
210. Amersfoort, J., Eelen, G. & Carmeliet, P. Immunomodulation by endothelial cells — partnering up with the immune system? *Nat Rev Immunol* **22**, 576–588 (2022).
211. Mestas, J. & Hughes, C. C. W. Of Mice and Not Men: Differences between Mouse and Human Immunology. *The Journal of Immunology* **172**, 2731–2738 (2004).
212. Scantlen, M. D., Majd, H. & Fattahi, F. Modeling enteric glia development, physiology and disease using human pluripotent stem cells. *Neuroscience Letters* **811**, 137334 (2023).
213. Steimle, V., Otten, L. A., Zufferey, M. & Mach, B. Complementation cloning of an MHC class II transactivator mutated in hereditary MHC class II deficiency (or bare lymphocyte syndrome). *Cell* **75**, 135–146 (1993).
214. Fernández-Castañeda, A. *et al.* The active contribution of OPCs to neuroinflammation is mediated by LRP1. *Acta Neuropathol* **139**, 365–382 (2020).
215. Grubišić, V. & Gulbransen, B. D. Astrocyte Cell Surface Antigen 2 and Other Potential Cell Surface Markers of Enteric glia in the Mouse Colon. *ASN Neuro* **14**, 17590914221083203 (2022).
216. Dzierszinski, F. *et al.* Presentation of Toxoplasma gondii Antigens via the Endogenous Major Histocompatibility Complex Class I Pathway in Nonprofessional and Professional Antigen-Presenting Cells. *Infection and Immunity* **75**, 5200–5209 (2007).
217. Gubbels, M.-J., Striepen, B., Shastri, N., Turkoz, M. & Robey, E. A. Class I Major Histocompatibility Complex Presentation of Antigens That Escape from the Parasitophorous Vacuole of Toxoplasma gondii. *Infection and Immunity* **73**, 703–711 (2005).
218. John, B. *et al.* Dynamic Imaging of CD8+ T Cells and Dendritic Cells during Infection with Toxoplasma gondii. *PLOS Pathogens* **5**, e1000505 (2009).
219. Góis, M. B. *et al.* Chronic infection with Toxoplasma gondii induces death of submucosal enteric neurons and damage in the colonic mucosa of rats. *Exp Parasitol* **164**, 56–63 (2016).
220. Sant'Ana, D. de M. G. *et al.* Acute infection with an avirulent strain of *Toxoplasma gondii* causes decreasing and atrophy of nitrergic myenteric neurons of rats. *Acta Histochemica* **119**, 423–427 (2017).
221. Trevizan, A. R. *et al.* Acute Toxoplasma gondii infection alters the number of neurons and the proportion of enteric glial cells in the duodenum in Wistar rats. *Neurogastroenterology & Motility* **31**, e13523 (2019).
222. Dora, D. *et al.* Evidence of a Myenteric Plexus Barrier and Its Macrophage-Dependent Degradation During Murine Colitis: Implications in Enteric Neuroinflammation. *Cell Mol Gastroenterol Hepatol* **12**, 1617–1641 (2021).

223. R Core Team. R: A Language and Environment for Statistical Computing. (2024).
224. Satija, R., Farrell, J. A., Gennert, D., Schier, A. F. & Regev, A. Spatial reconstruction of single-cell gene expression data. *Nat Biotechnol* **33**, 495–502 (2015).
225. Blighe, K Rana S, Lewis, M. EnhancedVolcano: Publication-ready volcano plots with enhanced colouring and labeling. (2023).
226. Sauter, M. *et al.* Protocol to isolate and analyze mouse bone marrow derived dendritic cells (BMDC). *STAR Protoc* **3**, 101664 (2022).
227. Duregotti, E. *et al.* Mitochondrial alarmins released by degenerating motor axon terminals activate perisynaptic Schwann cells. *Proceedings of the National Academy of Sciences* **112**, E497–E505 (2015).
228. Gómez-Casati, M. E., Murtie, J., Taylor, B. & Corfas, G. Cell-specific inducible gene recombination in postnatal inner ear supporting cells and glia. *J Assoc Res Otolaryngol* **11**, 19–26 (2010).
229. Fulton, D., Paez, P. M. & Campagnoni, A. T. The multiple roles of myelin protein genes during the development of the oligodendrocyte. *ASN Neuro* **2**, e00027 (2010).
230. Almeida, M. N., Silvernale, C., Kuo, B. & Staller, K. Bowel symptoms predate the diagnosis among many patients with multiple sclerosis: A 14-year cohort study. *Neurogastroenterology & Motility* **31**, e13592 (2019).
231. Kosmidou, M. *et al.* Multiple sclerosis and inflammatory bowel diseases: a systematic review and meta-analysis. *J Neurol* **264**, 254–259 (2017).
232. Yang, Y. *et al.* Investigating the shared genetic architecture between multiple sclerosis and inflammatory bowel diseases. *Nat Commun* **12**, 5641 (2021).
233. Cekanaviciute, E. *et al.* Gut bacteria from multiple sclerosis patients modulate human T cells and exacerbate symptoms in mouse models. *Proceedings of the National Academy of Sciences* **114**, 10713–10718 (2017).
234. Jangi, S. *et al.* Alterations of the human gut microbiome in multiple sclerosis. *Nat Commun* **7**, 12015 (2016).
235. Duc, D. *et al.* Disrupting Myelin-Specific Th17 Cell Gut Homing Confers Protection in an Adoptive Transfer Experimental Autoimmune Encephalomyelitis. *Cell Rep* **29**, 378-390.e4 (2019).
236. Höftberger, R., Lassmann, H., Berger, T. & Reindl, M. Pathogenic autoantibodies in multiple sclerosis — from a simple idea to a complex concept. *Nat Rev Neurol* **18**, 681–688 (2022).
237. Spear, E. T. *et al.* Altered gastrointestinal motility involving autoantibodies in the experimental autoimmune encephalomyelitis model of multiple sclerosis. *Neurogastroenterology & Motility* **30**, e13349 (2018).
238. Tognatta, R. *et al.* Astrocytes Are Required for Oligodendrocyte Survival and Maintenance of Myelin Compaction and Integrity. *Front Cell Neurosci* **14**, 74 (2020).
239. Constantinescu, C. S., Farooqi, N., O'Brien, K. & Gran, B. Experimental autoimmune encephalomyelitis (EAE) as a model for multiple sclerosis (MS). *Br J Pharmacol* **164**, 1079–1106 (2011).

240. Norton, W. T. & Poduslo, S. E. Myelination in Rat Brain: Method of Myelin Isolation. *Journal of Neurochemistry* **21**, 749–757 (1973).
241. Sutter, P. A. & Crocker, S. J. Glia as antigen-presenting cells in the central nervous system. *Current Opinion in Neurobiology* **77**, 102646 (2022).
242. Falcão, A. M. *et al.* Disease-specific oligodendrocyte lineage cells arise in multiple sclerosis. *Nature Medicine* **24**, 1837–1844 (2018).
243. Pepper, M., Dzierszinski, F., Crawford, A., Hunter, C. A. & Roos, D. Development of a System To Study CD4+-T-Cell Responses to Transgenic Ovalbumin-Expressing Toxoplasma gondii during Toxoplasmosis. *Infect Immun* **72**, 7240–7246 (2004).
244. Pascottini, O. B. *et al. Technical note:* Assessment of neutrophil endocytosis and proteolytic degradation and its relationship with phagocytosis and oxidative burst in dairy cows. *Journal of Dairy Science* **102**, 9396–9400 (2019).
245. Fernández-Castañeda, A. *et al.* The active contribution of OPCs to neuroinflammation is mediated by LRP1. *Acta Neuropathol* **139**, 365–382 (2020).
246. Fain, C. E. *et al.* Discrete class I molecules on brain endothelium differentially regulate neuropathology in experimental cerebral malaria. *Brain* **147**, 566–589 (2024).
247. Vogt, N. M. *et al.* Gut microbiome alterations in Alzheimer's disease. *Sci Rep* **7**, 13537 (2017).
248. Leblhuber, F., Geisler, S., Steiner, K., Fuchs, D. & Schütz, B. Elevated fecal calprotectin in patients with Alzheimer's dementia indicates leaky gut. *J Neural Transm* **122**, 1319–1322 (2015).
249. Heston, M. B. *et al.* Gut inflammation associated with age and Alzheimer's disease pathology: a human cohort study. *Sci Rep* **13**, 18924 (2023).
250. Fasano, A., Visanji, N. P., Liu, L. W. C., Lang, A. E. & Pfeiffer, R. F. Gastrointestinal dysfunction in Parkinson's disease. *The Lancet Neurology* **14**, 625–639 (2015).
251. Hung, L. Y. & Margolis, K. G. Autism spectrum disorders and the gastrointestinal tract: insights into mechanisms and clinical relevance. *Nat Rev Gastroenterol Hepatol* **21**, 142–163 (2024).
252. Madra, M., Ringel, R. & Margolis, K. G. Gastrointestinal issues and Autism Spectrum Disorder. *Child Adolesc Psychiatr Clin N Am* **29**, 501–513 (2020).
253. Levinthal, D. J. *et al.* Adding to the Burden: Gastrointestinal Symptoms and Syndromes in Multiple Sclerosis. *Multiple Sclerosis International* **2013**, 319201 (2013).
254. Pellegrini, C. *et al.* Prodromal Intestinal Events in Alzheimer's Disease (AD): Colonic Dysmotility and Inflammation Are Associated with Enteric AD-Related Protein Deposition. *Int J Mol Sci* **21**, 3523 (2020).
255. Liu, G. *et al.* Amyloid-β mediates intestinal dysfunction and enteric neurons loss in Alzheimer's disease transgenic mouse. *Cell Mol Life Sci* **80**, 351 (2023).
256. Rietdijk, C. D., Perez-Pardo, P., Garssen, J., van Wezel, R. J. A. & Kraneveld, A. D. Exploring Braak's Hypothesis of Parkinson's Disease. *Front Neurol* **8**, 37 (2017).

257. Konings, B. *et al.* Gastrointestinal syndromes preceding a diagnosis of Parkinson's disease: testing Braak's hypothesis using a nationwide database for comparison with Alzheimer's disease and cerebrovascular diseases. (2023) doi:10.1136/gutjnl-2023-329685.
258. Grubišić, V. & Parpura, V. The second brain in autism spectrum disorder: could connexin 43 expressed in enteric glial cells play a role? *Front. Cell. Neurosci.* **9**, (2015).
259. Wang, X. *et al.* The enteric nervous system deficits in autism spectrum disorder. *Front. Neurosci.* **17**, (2023).